R. & M. No. 3226

R. & M. No. 3226

MINISTRY OF AVIATION

AERONAUTICAL RESEARCH COUNCIL
REPORTS AND MEMORANDA

A Wind Tunnel Investigation of the Longitudinal and Lateral Aerodynamic Characteristics of a Canard Aircraft Model

PART I

Tests at $M = 1 \cdot 04$ and $M = 2 \cdot 02$

By P. E. WATTS and L. J. BEECHAM

PART II

Tests at $M = 2 \cdot 47$

By P. E. WATTS and D. A. TREADGOLD

LONDON: HER MAJESTY'S STATIONERY OFFICE
1962
PRICE £1 15s. 0d. NET

A Wind Tunnel Investigation of the Longitudinal and Lateral Aerodynamic Characteristics of a Canard Aircraft Model

PART I

Tests at $M = 1 \cdot 04$ and $M = 2 \cdot 02$

By P. E. WATTS and L. J. BEECHAM

PART II

Tests at $M = 2 \cdot 47$

By P. E. WATTS and D. A. TREADGOLD

COMMUNICATED BY THE DEPUTY CONTROLLER AIRCRAFT (RESEARCH AND DEVELOPMENT), MINISTRY OF AVIATION

*Reports and Memoranda No. 3226**

February, 1959

PART I

Summary. Tests were made in the Royal Aircraft Establishment No. 19 (18 in. × 18 in.) supersonic wind tunnel to measure the overall normal and side forces, rolling, pitching and yawing moments on a typical canard aircraft layout at $M = 1 \cdot 40$ and $M = 2 \cdot 02$. The complete configuration and configuration less fin, with foreplane angles, η, 0 deg and 10 deg were tested for combinations of incidence and sideslip up to $\alpha = \beta = 10$ deg. Additional breakdown tests were made at $M = 1 \cdot 40$, and supplemented by oil flow and vapour screen tests.

The tests have shown that the foreplane has a reduced lifting, but an increased moment, effectiveness due to the download induced on the mainplane. The longitudinal stability increases with incidence and Mach number; neither normal force nor pitching moment is affected significantly by sideslip.

The lateral and directional characteristics are less satisfactory. When sideslip is present the foreplane-wing interaction produces a large negative rolling moment which increases in magnitude with incidence and control setting. There is a reduction in $\partial C_n / \partial \beta$ with application of incidence, and the evidence suggests that this becomes more marked as the Mach number increases.

The tests indicate that further investigation is required into the effect of a free vortex on the load distribution over a lifting surface if satisfactory estimates are to be made of control-wing and control-fin interference.

1. *Introduction.* Interest has recently been focused on the merits of a canard layout for a long range supersonic aircraft since estimates suggest that such a configuration might have advantages in performance and range.

* Previously issued as R.A.E. Reports Aero. 2575 and 2603—A.R.C. 19,218 and 20,888.

The stability and control characteristics have not, however, been previously examined in detail particularly when both incidence and sideslip are present. Earlier guided weapons experience in this field has shown that aerodynamic cross-couplings and non-linearities can occur. A wind-tunnel investigation has been planned to check for the presence of any similar undesirable characteristics on typical aircraft designs, but as a preliminary to this investigation which is extensive in scope it was considered worth while to make a rapid but restricted survey of the problem using one representative plan-form, and one foreplane. It is with these preliminary tests that this Report is concerned.

As originally conceived these tests, which were made in the Royal Aircraft Establishment No. 19 (18 in. × 18 in.) Supersonic Wind Tunnel during the period June to September 1955, were intended to be concerned principally with the behaviour of the complete configuration in sideslip and at incidence. It soon became evident, however, that a much better understanding of the results was likely if certain additional breakdown configurations (*i.e.*, with various model components absent) were tested. These have been tested at the lower speed ($M = 1{\cdot}4$) where interactions and non-linearities can be expected to be more severe. The programme was further extended to produce data, at reduced pressure, up to a polar incidence of 25 deg.

The emphasis throughout the programme reported herein has been on the need for obtaining information quickly and any limitations in the tests must be related to this overriding consideration. To this end the model was designed as simply as possible and adapted to fit an existing force and moment balance. Considerable credit is due to the Design Office and Workshop Staff of R.A.E. for the production of the model within seven weeks of the inception of the design.

The main programme on the stability of canard layouts covering many geometric variants, will, it is hoped, supplement the tests reported here and amplify many of the points raised in the analysis.

Further tests were made on this model in the R.A.E. No. 8 (9 in. × 9 in.) Supersonic Wind Tunnel at $M = 2{\cdot}47$ and are covered in Part II of the Report.

2. *Description of the Model.* The leading dimensions and geometric details of the model are given in Fig. 1 and Table 1 and supplemented by a photograph of the model mounted in the tunnel Fig. 2. In the interest of speed and model adaptability a simplified construction was used. For example, the body was kept cylindrical aft of the ogival nose, the whole being axially symmetric (*i.e.*, no nose droop included); wing and foreplane were of modified double-wedge section, the thickness/chord ratio being 3·5 per cent for the former and 4·5 per cent for the latter.

The components were assembled onto the mandrel of a rear sting balance each being keyed to the next, the whole being locked on to the sting by the threaded nose section. Alignment of the foreplane and wings was achieved by use of a spacing washer of suitable thickness aft of the nose section. The foreplane was made in a separate unit and was clamped to the nose section in such a way (*see* inset of Fig. 1) that any desired control setting could be obtained.

For subsequent breakdown tests the model components removed were replaced by appropriate blanking and spacing pieces.

3. *Test Arrangement and Procedure.* 3.1. *Wind Tunnel.* The R.A.E. No. 19 (18 in. × 18 in.) Supersonic Wind Tunnel is a continuous return flow closed circuit tunnel with a nominal Mach number range of 1·4 to 2·2 with a square working section of 18 in. side at all Mach numbers. For the present tests the stagnation pressure was maintained at 24 in. Hg abs. for $M = 1{\cdot}40$ and

36 in. Hg abs. at $M = 2{\cdot}02$ (corresponding to Reynolds numbers of $0{\cdot}31 \times 10^6$ and $0{\cdot}36 \times 10^6$ per inch respectively) except for a few later tests at $M = 1{\cdot}40$ where stagnation pressures of 16 in. Hg abs. and 54 in. Hg abs. were used for specific additional investigations.

The stagnation temperatures were 26 deg C and 31 deg C at $M = 1{\cdot}40$ and $M = 2{\cdot}02$ respectively, these values being chosen to minimise the effects of temperature on the strain gauge circuits used on the balance. The tunnel humidity was kept below a value of 0·0003 lbs of water per lb of dry air using a dry air interchange system. The tunnel has a vertical quadrant-type incidence gear behind the working section, which enables a polar incidence of $\pm$ 25 deg to be obtained. The required attitude of the model relative to the free stream is obtained by applying a polar incidence and then rolling the model about its longitudinal axis. Both of these angular rotations, each of which can be varied independently from outside the tunnel, are measured by potentiometers and recorded automatically.

3.2. *Wind Tunnel Balance System.* The model was supported by a flexible sting to which were attached Baldwin SR-4 AB-7 resistance gauges. These were arranged in difference bridge circuits, each of four active gauges, to measure pitching and yawing moments, normal and side forces with only small interactions. The rolling moment was measured by a strain-gauge bridge on a separate cantilever. The signals from each bridge were passed to self-balancing indicator units, the readings from which were recorded automatically in both typewritten and punched card form. The test data were reduced to coefficient form using the DEUCE electronic computer (*see* Appendix).

3.3. *Accuracy.* The overall accuracy of the results depends on a number of factors, some of which cannot easily be assessed quantitatively. The more important of these are discussed in the section below.

3.3.1. *Balance accuracy.* One of the main sources of error is the sensitivity of the strain-gauge resistance bridges to temperature variations which may occur when the tunnel is running. The tunnel stagnation temperature was controlled to within one degree C of the nominal value which was chosen to give approximately room temperature at the balance. It was observed, however, that a change of zero occurred between wind on and wind off conditions. As no absolute zero could be obtained, wind on, with the asymmetric conditions (*e.g.*, with foreplane deflected), the zero shift required to correct the results for the symmetric configuration was applied and likewise assumed constant over the incidence range. Separate tests on the same configuration appeared to justify this in as much as although small differences in absolute value were obtained the variations with incidence or sideslip angle were virtually identical.

Further inaccuracies may arise from uncertainty in reading the strain gauge indicator. This is estimated as $\pm$ 1 division in 500 divisions with the same possibility in the wind-off readings. On this basis the accuracy of observation, expressed in coefficient form, is as follows:

$$C_z = \pm 0{\cdot}006 \qquad C_y = \pm 0{\cdot}001$$

$$C_m = \pm 0{\cdot}002 \qquad C_n = \pm 0{\cdot}001$$

In the case of the rolling moment coefficient there is an additional source of error due to friction in the rolling moment balance which leads to a possible error in $C_l = \pm 0{\cdot}0007$.

In certain of the earlier runs there was an additional uncertainty in the yawing moment results due to malfunctioning of the potentiometer indicator. It is difficult to ascribe any quantitative value to this, but attention is drawn to the probable accuracy in the appropriate section in the discussion.

3.3.2. *Accuracy of model attitude setting.* The roll angle was measured using a potentiometer device, and the accuracy was determined by the resolution of the potentiometer and the non-linearity of the winding. The readings should all be within $\pm 0{\cdot}25$ deg of that indicated and in general the error will be well within these limits.

The polar incidence of the model is also measured by a potentiometer device and corrected for sting deflection under load. The final angular reading is accurate to ± 3 minutes of arc. The angular measurements are made relative to a gravity datum, but no flow angle measurements have been made. Tests with the model upright and inverted suggest a stream zero error of $0{\cdot}14$ deg at $M = 1{\cdot}40$ which has been taken into account where possible.

3.3.3. *Accuracy of control setting.* No special control setting jig was available for these tests and the control to body setting had to be measured using a telescope with a protracter eyepiece to check the setting. It is believed that the error was of the order of $\pm 0{\cdot}1$ deg.

3.3.4. *Uniformity of flow in the working section.* The supersonic nozzles for these tests have been calibrated for Mach number but not for flow inclination. The Mach number changes are gradual over the region occupied by the model and are within the following limits:

$$M = 1{\cdot}40 \pm 0{\cdot}010$$

$$M = 2{\cdot}02 \pm 0{\cdot}015$$

The tunnel stagnation pressure was controlled to within $+ 0{\cdot}03$ in. Hg of that required so that the variation of kinetic pressure in the working section was negligible.

4. *Presentation and Procedure.* 4.1. *Data Presentation.* With the balance arrangement used the forces and moments were all measured normal to, and in the plane of, the aircraft wings (the sting rotating with the model). This led to the adoption of a body system of axes defined as follows.

Ox positive forward along the axes of the body. Oy positive to starboard and normal to Ox in the plane of the wing, and Oz perpendicular to Ox, Oy to form a right-hand system of axes. If a set of tunnel axes $Ox_0\, y_0\, z_0$ is chosen to coincide with $Oxyz$ at zero incidence and sideslip then the angles measured in the tunnel are the polar incidence, θ, defined as the angle between Ox and Ox_0, positive for a clockwise rotation about Oy_0 and the roll angle, ϕ, defined as the angle between the plane Oxz_0 and Oxz positive for a clockwise rotation about Ox. All the data have, however, been plotted as functions of incidence angle, α, and sideslip angle, β, as these are believed to show the results to better advantage for an aircraft configuration than plots as functions of θ and ϕ. The angles α and β are defined in terms of θ and ϕ as follows:

$$\sin \alpha = \sin \theta \cos \phi$$

$$\sin \beta = \sin \theta \sin \phi .$$

It should be noted that the definitions of incidence, α and β, adopted differ slightly from those normally used in presenting subsonic wind tunnel results and those used in most American tests. The differences involved in the incidence range considered are however barely significant. The control setting angle, η, was defined as the angle between the chord line of the control and the body axis Ox, and was positive in the same direction as α.

In the reduction of moment and forces to coefficient form the reference area has been taken as that of the gross wing (8·28 in.^{2}); the reference length for the longitudinal moment, C_m is the aerodynamic mean chord (2·40 in.) whilst that for the lateral moments C_l and C_n is the gross wing span (3·50 in.) (*see* also List of Symbols).

For convenience in referring to different configurations the following notation will be used throughout the report:

B	Body
W	Wing
F	Original fin
F'	Modified fin (net area 75 per cent that of original fin)
C	Foreplane control.

Thus $BWCF'(\eta = 0$ deg) represents the complete configuration with modified fin and zero control setting angle.

When slopes of curves are given the values are for $\alpha \to 0$ deg and $\beta \to 0$ deg unless specifically stated to the contrary. It is important to note this fact as some curves show change of slope at quite low angles of incidence and sideslip.

4.2. *Test Procedure and Scope of Tests.* The original programme was arranged to measure the forces and moments for configuration $BWCF$ and BWC with $\eta = 0$ deg and $\eta = 10$ deg at each of the two test Mach numbers. For each run the polar incidence, θ, was varied from -2 deg to $+16$ deg (the maximum attainable without fouling occurring between the sting and the windshield) in small incidence steps at constant roll angle, ϕ, which in turn was varied by 10 deg steps between 0 deg and 90 deg. The indicator readings were plotted, at the time of test, at constant ϕ to determine continuity and to ensure consistency of data. Where necessary additional readings were taken at $M = 1{\cdot}40$ only, the model was tested through a similar routine with the control removed.

In order to help check the validity of the estimate of the fin contribution to the sideslip derivatives the fin shape was modified by removing 25 per cent of the exposed area from the tip (Fig. 1). The remainder of the tests were made with this fin at $M = 1{\cdot}40$ only, where any undesirable aerodynamic cross-couplings were expected to be most severe.

Although the main purpose of the tests was to make a quick investigation of the overall static stability characteristics at supersonic speeds it soon became obvious that a far better understanding of the results would be obtained if further data were available from certain breakdown configurations. To this end some further tests were made on the configuration with wings removed and with foreplane removed. The details of the various test runs are given in Table 2.

Finally certain tests were repeated over a limited incidence range at high stagnation pressure to determine the slopes of the curves near the origin more accurately.

5. *Discussion of Longitudinal Results.* 5.1. *Zero Sideslip.* As mentioned in Section 3.3 the results were subject to an error due to change of zero reading with temperature. The force and moment curves for the configuration with no controls, or with controls undeflected, have been adjusted to pass through the origin and the same correction has been applied to the results from the

corresponding configuration with controls deflected. This may mean that the absolute values of the latter as plotted in the curves discussed in Section 5.1, are slightly in error but the general trends and the conclusions reached are believed to be valid.

5.1.1. *Foreplane off.* The configurations with the foreplane off, BWF and BF', were tested at $M = 1{\cdot}40$ only. The $-C_z$ vs. α plot of Fig. 3 for BF' shows the expected non-linear curve due to the viscous cross flow effects. An estimate of $-C_z$ has been made, and is seen to be considerably higher than the experiment throughout the incidence range. The corresponding C_m vs. α curves of Fig. 4 show reasonable agreement between estimate and experiment although in this case theory is less than experiment. The $-C_z$ vs. α and C_m vs. α curves for BWF are both non-linear. This non-linearity is primarily a body effect as can be seen from the 'derived' wing results of Fig. 5. These derived curves were obtained as the difference $(C_{z\cdot BWF} - C_{z\cdot BF})$ at corresponding incidences and will therefore include the mutual interference of wing and body. Estimates are shown which agree reasonably well with the experimental values. The derived wing centre of pressure moves slightly rearward which is in accord with earlier unpublished tests on a cruciform wing guided weapon with a wing of similar plan-form (tested at zero roll angle). This rearward movement is probably attributable to tip separation effects.

5.1.2. *Wing off.* This section is concerned with the configuration BCF' with foreplane control deflected and undeflected. The $-C_z$ vs. α and C_m vs. α curves are shown in Figs. 3 and 4 and indicate a non-linear variation with incidence. As in the case of BWF when the 'derived' surface curves are considered it is seen that this non-linearity largely disappears, particularly for $\eta = 0$ deg, indicating that this is predominantly a body effect. As the control has a moment arm about the reference position which is large compared with the control chord the accuracy of the estimate of $\partial C_m/\partial\alpha$ is relatively insensitive to the centre of pressure of the control lift and is closely related to the accuracy of the $\partial C_z/\partial\alpha$ estimate, which agrees quite well with experiment, particularly for the $\eta = 0$ deg case. The derived control curve for $\eta \simeq 10$ deg shows a decrease in slope of the $-C_z$ vs. α curve with increasing α, which might be expected as the control-to-air incidence reaches over 20 deg. There is also the unknown effect of the root gap for these larger angles. It will be noted that the control effectiveness shows reasonable agreement with theory especially for the $\eta = 0$ deg case but as will be shown in Section 5.1.3 the increase in lift is not realised when the wings are also present.

5.1.3. *Complete configuration.* The complete configuration $BWCF$ was tested at both Mach numbers, and the $-C_z$ vs. α and C_m vs. α curves are shown in Figs. 3 and 4. The most notable feature is the apparently small effect of the foreplane on $-C_z$ at small incidences as seen by comparison with the results for BWF at $M = 1{\cdot}40$. This is particularly so for the case $\eta = 10$ deg where the results indicate a slightly negative increment. This increment is of the same order as the probable accuracy and may not be significant. It is quite certain, however, that compared with the results for BCF' the foreplane has almost zero lifting effectiveness at small incidences. This is attributed to the download induced on the wing by the control vortices and is discussed in more detail in Section 5.1.4 dealing with foreplane efficiency. It is worth pointing out here, however, that although the lift increase from the foreplane is not realised the moment effectiveness is in fact increased (Fig. 4), and so the interaction is advantageous in this respect. The $-C_z$ vs. α curves of Fig. 3 at $M = 2{\cdot}02$ would suggest that the loss in lift is not so great as that at $M = 1{\cdot}40$.

Attention is also drawn to the C_m vs. $-C_z$ curves of Fig. 6 which give a measure of the static longitudinal stability. The values of $\partial C_m/\partial C_z$ at $-C_z = 0$ and $-C_z = 0{\cdot}5$ are tabulated below.

Condition	$\partial C_m/\partial C_z$	
	$M = 1{\cdot}40$	$M = 2{\cdot}02$
$BWCF$, $\eta = 0$ deg $-C_z = 0$	0·175	0·230
$BWCF$, $\eta = 0$ deg $-C_z = 0{\cdot}5$	0·288	0·280
$BWCF$, $\eta = 10$ deg $-C_z = 0$	0·168	0·227
$BWCF$, $\eta = 10$ deg $-C_z = 0{\cdot}5$	0·314	0·341

$\partial C_m/\partial C_z$ is expressed in fractions of mean aerodynamic chord behind the reference position, *i.e.*, the intersection of the centre-line and the line joining the wing root leading edges. These indicate that at a given Mach number for $C_z = 0$ change of η has little effect on the aerodynamic centre position and that for a given configuration an increase of Mach number causes a rearward movement of the aerodynamic centre. Increase of incidence leads to an increase of stability as evidenced by an increase in the value of $\partial C_m/\partial C_z$.

The change in aerodynamic centre is greater at $\eta = 10$ deg than at $\eta = 0$ deg, but on all cases the changes are fairly gradual. If the corresponding values of $\partial C_m/\partial C_z$ for configuration BWF are considered:

	$-C_z = 0$	$-C_z = 0{\cdot}5$
$\frac{\partial C_m}{\partial C_z}$ for BWF at $M = 1{\cdot}40$	0·40	0·505

it is seen that the change with increasing $-C_z(\alpha)$ is of the same order as that for $BWCF$, $\eta = 0$ deg suggesting that this movement is primarily a body-wing effect. There is further evidence for this in that the C_m vs. $-C_z$ curve for the 'derived' control is linear and the value of $\bar{\eta}_M$ (Fig. 7b) is nearly constant with incidence.

There is as yet no satisfactory method of predicting the change of aerodynamic centre position with incidence for either a body-wing or a complete configuration.

5.1.4. *Foreplane efficiency.* In configurations in which the foreplane is considerably larger than the rear plane, as in the older type of aircraft, it has been customary and convenient to regard the interference load as arising effectively from a change in the incidence (*i.e.*, the mean downwash angle) of the rear surface. In general, however, slender-body theory shows that this interference load may be simply expressed[14] as the foreplane force, reversed in direction, together with a load which is a function of the position, relative to the rear surface, of the vortices associated with that force. In particular, when the foreplane span is less than that of the rear, and the vortices lie in the plane of the rear surface, this latter function becomes zero, and the interference load is equal and opposite to that of the foreplane, *independently of either the non-dimensional or dimensional lift curve slope of the rear surface*[14].

Physically this could be interpreted as implying that any disturbance introduced into the stream by the foreplane is nullified by the wing, and from this point of view there seems no reason to suppose that slender wings are unique in this respect—so that, even with a non-slender configuration the interference force may still be directly related more to the foreplane load than to the lifting effectiveness of the rear surface.

Accordingly in this report foreplane efficiencies are used in which the reference normal force and pitching moment are those of the 'derived' foreplane in the absence of the wing. These are defined as follows:

$$\bar{\eta}_Z = \left(\frac{C_{z.BWC} - C_{z.BW}}{C_{z.BC} - C_{z.B}}\right) \qquad \bar{\eta}_M = \left(\frac{C_{m.BWC} - C_{m.BW}}{C_{m.BC} - C_{m.B}}\right).$$

The interference download is then

$$(1 - \bar{\eta}_Z) \times (\text{derived control force}).$$

Attention is also drawn to the fact that the definitions of $\bar{\eta}_Z$ and $\bar{\eta}_M$ as used here for the $\eta = 10$ deg case are different from those used in Ref. 1 (Fig. 15) where $\bar{\eta}_Z$ for $\eta = 10$ deg was defined as:

$$\frac{\text{Change of lift due to 10 deg control deflection – wings on}}{\text{Change of lift due to 10 deg control deflection – wings off}}.$$

Reference to Fig. 7 shows that the normal force efficiency at $M = 1{\cdot}40$ for $\eta = 0$ deg is zero at $\alpha = 0$ deg and then rises to a maximum value of approximately $0{\cdot}4$ at $\alpha = 10$ deg. The corresponding curve for $\eta = 10$ deg shows a similar trend but with lower absolute values, this result is likely to be of even more significance due to the loss of lift from the foreplane at a trimmed condition which it implies. The value at $\alpha = 0$ deg is shown as negative. Whilst this may be physically possible the absolute value cannot be guaranteed but it is certainly near zero and only rises relatively slowly to about $0{\cdot}4$ at $\alpha = 10$ deg.

It is evident that a lift contribution from the controls for a trimmed condition, an advantage sometimes claimed for the canard layout, is not likely to be obtained in practice at low supersonic speeds. A similar conclusion may be drawn from tests on a cruciform canard configuration[5, 6] at zero roll angle for which the results are equally applicable to a planar configuration.

In contrast to the low values of $\bar{\eta}_Z$ the moment efficiency $\bar{\eta}_M$, (Fig. 7b), shows a value greater than unity. This is because the effective centre of pressure of the download is acting behind the moment reference position and so gives a moment in the same sense as that due to foreplane. The chordwise centre of pressure of the interference force on the wing has been calculated as:

$$\frac{x_{CP}}{\bar{c}} = \frac{(C_{m.BCF} - C_{m.BF}) - (C_{m.BWCF} - C_{m.BWF})}{(C_{z.BCF} - C_{z.BF}) - (C_{z.BWCF} - C_{z.BWF})}$$

$$= \frac{(1 - \bar{\eta}_M)}{(1 - \bar{\eta}_Z)} \left(\frac{C_{m.BCF} - C_{m.BF}}{C_{z.BCF} - C_{z.BF}}\right).$$

It is of interest that this effective centre of pressure position is almost constant with incidence and is little affected by the control to body setting angle, η. Furthermore, this effective centre of pressure position is ahead of that of the net wing in a uniform flow field. This forward position of the effective centre of pressure can be only partially explained by the concentration of the induced load on the inboard section of a swept wing. It is suggested that in addition to a spanwise variation of loading there is also a chordwise variation, with the main concentration near the leading edge. This could arise if the vorticity associated with the induced load, which will be in the opposite

sense to that of the generating foreplane vortices, has the effect of reducing the downwash velocity on the wing towards the trailing edge. On this basis we should expect an increase of the distance of the vortex from the surface (*e.g.*, with incidence) to reduce the induced load but not the chordwise distribution in conformity with the experimental results.

No such chordwise variation is allowed for on the strip theory and influence function theory. Experimental data on the load produced on a surface due to a nearby vortex are lacking but tests are planned at the R.A.E. to investigate this in detail.

Despite the lack of knowledge on the precise mechanism of the flow several theories are available, using varying simplifying assumptions, for estimating the induced loading. A slender body theory has been developed by Owen and Maskell[4] for missile configurations and, although the configuration considered here is not slender the ratio, incremental lift: original lift may be applicable beyond the recognised limits of slender body theory. As mentioned earlier, the slender body theory may be used to predict a down load on the wing equal to the control lift for zero incidence, which agrees with the experimental results. Morikawa[3] also shows this and demonstrates, moreover, that this down load is operative over the wing area ahead of the intersection of the vortices with the leading edges. Other lifting surface theories are available but these involve considerable numerical work and are of doubtful value due to the difficulty of allowing for the distortion of the vortex sheet due to presence of the body. If the foreplane downwash is assumed to remain constant along a chordwise strip of the wing (an assumption which the authors feel may not be justified) then it is possible to use an influence coefficient method[7]. Calculations using this method show reasonable agreement with experiment although in view of the assumptions necessary this should be treated with some reserve.

Another method of approach is that suggested by Nielsen and others which uses a strip theory to evaluate an interference factor

$$i = \frac{L_{W(V)}}{L_{W(\alpha)}} \frac{2\pi\alpha V_0(b/2 - r_w)}{57{\cdot}3K}$$

where

$L_{W(V)}$	Lift on the wing due to foreplane vortices
$L_{W(\alpha)}$	Lift on the wing due to incidence
$b/2$	Gross wing semi-span
r_w	Body radius at wing position
K	Circulation due to foreplane-body combination.

In order to simplify the calculations it is assumed that the model is planar and that the down load is taken entirely on the wings (none on the body). Values of $\bar{\eta}_Z$ and $\bar{\eta}_M$ have been calculated using this method and the results are plotted in Fig. 7. It will be seen that at small incidences the theory overestimated $\bar{\eta}_Z$ by some 30 per cent but that $\bar{\eta}_M$ shows reasonable agreement over the incidence range. This is partly fortuitous as the theoretical method assumes the download to act at the wing centre of pressure. The experimental results of Fig. 7c show that this load acts forward of the wing centre of pressure. Theory thus gives an underestimate of the down load acting at a greater arm than that realised in practice to give an approximately correct answer.

In the absence of any other test results it is difficult to make any specific recommendations but it would seem probable that at low supersonic speeds the slender body theory is valid near zero incidence, although it may not predict the variation with incidence. The limited evidence available

does suggest that for a given control lift the interference down load decreases with increase of Mach number.

5.2. *Combined Incidence and Sideslip.* Earlier work on a cruciform guided weapon layout had suggested that the pitching moment could be considerably affected by sideslip and later work indicated that this was primarily an interference effect on the body. If this were so then there seemed grounds for thinking that with a planar configuration some cross-coupling effects might still occur. Examination of Figs. 8 and 9 for the complete configuration show however that there is no significant effect of sideslip in either $-C_z$ vs. α or C_m vs. α, even with the foreplane deflected. The configuration BWF was also tested to see if there was any effect on the wing body which was countereacted by a possible foreplane interference.

It can be seen from Fig. 10 that there is no significant effect of sideslip on the C_m vs. α and $-C_z$ vs. α curves for this configuration. The results for the configuration without a fin are not presented because of their similarity to those of configuration $BWCF$.

6. *Discussion of Lateral Results.* When considering the lateral data, yawing moment in particular, it should be borne in mind that there are limitations in absolute accuracy and that it is difficult to make a precise quantitative assessment of certain of the results. The trends exhibited however are believed to be genuine and a valuable guide to the sort of effects which may be expected with this type of configuration. All the 'breakdown' tests were made on the configurations with the modified fin and at the lower Mach number only, so that Mach number effects cannot easily be deduced directly from the data given.

6.1. *Side Force and Yawing Moment Results at Zero Incidence.* 6.1.1. *Foreplane off.* The $-C_y$ vs. β and C_n vs. β results for configuration BWF are shown in Figs. 11 and 12. At $\alpha = 0$ deg there is little difference between these results and those for $BWCF$, $\eta = 0$. The slightly larger values of C_n for BWF in Fig. 12 are of doubtful significance. The non-linearity of the curves is primarily due to the body effect and is discussed together with the estimates in Section 6.1.3.

6.1.2. *Wing off.* The most significant feature of the $-C_y$ vs. β curves for the configuration BCF' at $\alpha = 0$ deg is the marked effect of deflecting the canard control. Deflection of the control from $\eta = 0$ deg to $\eta = 10$ deg causes an increase of both $-C_y$ and C_n (Figs. 11 and 12). This increment reaches a maximum near $\beta = 6$ deg and then reduces with increasing β. The effect is perhaps more clearly seen in the results for the derived* fin of Fig. 13 which shows the $\Delta(-C_y)$ vs. β curve to be linear over the sideslip range tested whilst that for $\eta = 10$ deg has an initial increase in slope of over 30 per cent which however decreases with increase in β. The main cause of this increase is the induced sidewash at the fin surface due to the trailing vortices generated by the foreplane. An attempt at estimating the magnitude of this effect is given in Appendix II.

This approach which involves certain simplifying assumptions consists essentially in calculating a mean side velocity at the fin due to the vortices and hence finding an incremental $(-\partial C_y/\partial\beta)$.

It will be seen that the theory gives a value of $\Delta(-\partial C_y/\partial\beta)$ which is rather lower than the experimental value. It is probably not worth while at this stage making any more refined approach

* The derived fin results are given as $(C_{y\cdot BCF} - C_{y\cdot BWC})$. It was necessary to use the results for BWC as those for BC were not satisfactory. At $\alpha = 0$ deg but with the symmetric mid-wing position and relatively small values of β there should be no significant effect of the wing on the C_y and C_n results. For $\alpha \neq 0$ deg this argument is not necessarily valid.

as the results with wings on, as discussed in the next section, show a masking of this foreplane effect by the wings.

6.1.3. *Complete configuration.* Reference to Figs. 11 and 12 shows that at both Mach numbers the effect of deflecting the foreplane control is negligibly small on both C_y and C_n for configuration *BWCF*. This result was contrary to expectation especially in view of the theoretical results (which were obtained prior to the tests). For $\alpha = 0$ deg it is not difficult to find an explanation. Examination of the schlieren photograph of Fig. 35 shows that for $\alpha = \beta = 0$ deg and $\eta = 10$ deg a strong vortex pair originates from the foreplane surface and streams back to the wing. Behind the wing however, there is no sign of these two strong vortices. The obvious explanation is that these two vortices have induced a down load on the wing which gives rise to vorticity of equal and opposite strength which in turn cancels out the upstream vorticity. There is thus zero vorticity behind the wing and hence there can be no vortex effect on the fin loading. For conditions of $\alpha = \beta \simeq 0$ deg it would seem likely that for most canard configurations with a central fin this result will be quite general and so the fin estimates should be based on those for a fin with no foreplane vortex field considered.

Also shown in Figs. 13 and 14 are the results for the derived fin at both Mach numbers together with estimates based on the net fin and assuming no root loss. This method, which amounts to considering the fin as effectively one half of a surface symmetrical about the root chord, is seen to give values in good agreement with experiment at the higher Mach number where an accurate estimate is most necessary, but to under estimate somewhat at the lower speed. An allowance for the side load carried over on to the body would improve the agreement but no satisfactory factor has so far been obtained although theoretical work on this is under way.

6.2. *Side Force and Yawing Moment Results with Combined Incidence and Sideslip.* 6.2.1. *Foreplane off.* The $-C_y$ vs. β and C_n vs. β results for configuration *BWF* are given in Fig. 15. These indicate that there is a small increase in both $(-C_y)$ and C_n with increase in α. There is some doubt about the absolute magnitude of these results particularly for C_n but the trend may be accepted. The increase is not likely to have much effect on the stability being always less than 10 per cent of the value at $\alpha = 0$ deg. Part of the increase in $(-C_y)$ is accounted for by the increase of $(-\partial C_y/\partial\beta)$ with α from the non-linear body force. For convenience of comparison the experimentally derived curves of $-C_y$ vs. β at various α for the body alone are also given in Fig. 15. There is theoretically a contribution to $\partial C_y/\partial\beta$ from the wing, proportional to α^2, due to tip suction effects, but the extent to which this is present is not known.

6.2.2. *Wing off.* The only configuration with wings off for which satisfactory lateral results are available for the model at incidence is *BCF'*, $\eta = 0$ deg. The results are given in Figs. 16 and 17 and show a marked decrease in both $(-C_y)$ and C_n with increase in α. This corresponds to almost complete loss of fin effectiveness at small β for α greater than 10 deg. This loss of fin effectiveness is thought to arise principally from the sidewash induced at the fin by the foreplane vortices and will be a function of the height at which the vortices pass the fin.

An attempt has been made to estimate this effect by calculating the mean side velocity at the fin due to the vortex and then using a strip theory to calculate the incremental value of $(-\partial C_y/\partial\beta)$. It is realised that this involves certain simplifications but it can be seen from Fig. 18 that it predicts the trend with α although it considerably under estimates the magnitude of the effect. It has been assumed that the vortices trail in a stream-wise direction and with constant spacing equal to the foreplane span. Reference to Fig. 35 shows that this assumption about the spacing is justifiable

at $\alpha = 0$ deg but there is no means of checking this when $\alpha > 0$ deg and it is suggested that as the vortices move above the body with increasing α they may move towards each other. However, even if the limiting value of the theoretical vortex spacing as given by slender body theory (Ref. 4) of $(\pi/4) \times$ span of the lifting surface is assumed to apply for $\alpha > 5$ deg it can be seen from Fig. 18 that the agreement between theory and experiment, although better, is still not satisfactory. As yet no explanation can be given for this discrepancy. The effect of the foreplane vortices at varying α on the value of $\partial C_y/\partial\beta$ due to the body has been investigated and found to be small.

It is also of interest to note that the slope of the C_y vs. β curve, Fig. 16, is little affected for $\beta > 5$ deg (although the absolute magnitude of $(-C_y)$ is reduced). This may be partially explained by the fact that with the larger angles of sideslip the vortex moves near to the fin so that its path will be distorted from the stream-wise direction assumed.

Unfortunately there are no results for BCF', $\eta = 10$ deg for $\alpha \neq 0$ deg but one would expect a greater loss in $(-\partial C_y/\partial\beta)$ at the higher values of α and an increase at the small α.

Due to shortage of time no tests were made on BCF' at $M = 2{\cdot}02$ and so it was not possible to state the effect of Mach number on these fin results. Apart from geometry which is unchanged, the effect noted above is proportional to the foreplane load, or, for a given foreplane setting, proportional to the foreplane lift-curve slope; as this decreases with increase of Mach number the variation of $(-\partial C_y/\partial\beta)$ with α from this cause could also be expected to decrease.

6.2.3. *Complete configuration.* For convenience of comparison with the results just discussed (for BCF', $\eta = 0$ deg) the results for $BWCF'$, $\eta = 0$ deg are also plotted in Figs. 16 and 17. These results are believed to be more reliable than some of the earlier C_y and C_n data for $BWCF$.

It is readily seen that compared with the BCF' results there are much smaller changes in the values of $-C_y$ and C_n with increase of α. Without a detailed knowledge of the wing afterflow any explanation must necessarily be speculative but it is suggested that since the vortex paths are deflected by the wing towards the body axis (*see* Fig. 34) they will pass the fin at a station nearer the root than for the corresponding incidence, wing off. Using the method of Appendix II it can be seen, Fig. 18, that an estimate using these modified heights shows a smaller reduction in $(-\partial C_y/\partial\beta)$ than with wings off. There is however a change in circulation from the wing due to the induced down load which would act in such a way as to counteract the effect mentioned above. The interaction would be reduced if the span of the foreplane vortices increased during passage over the wing, but limitations of the schlieren system did not permit any such change of spacing to be observed.

Recent subsonic tests have shown that there is an increase in the span of vortices on passing close to a flat surface, and it is probable that there is a supersonic counterpart of this effect.

There is evidence to suggest that the directional stability at incidence deteriorates as Mach number increases. This is shown in Figs. 20 and 21 where there is a noticeably greater deviation from the datum ($\alpha = 0$ deg) at $M = 2{\cdot}02$ than at $M = 1{\cdot}40$ as incidence is applied. These data were obtained early in the programme and were thought to be possibly less reliable than the main body of data presented herein; for that reason only the datum curve has been drawn. However, subsequent tests on this model at $M = 2{\cdot}47$, in Part II of this report, confirm the trend shown and suggest moreover that adequate inherent directional stability may be difficult to provide at these speeds.

6.3. *Rolling Moment Results at Zero Incidence.* 6.3.1. *Foreplane Off.* Since there is no dihedral angle and the wing is mounted centrally on the body, the value of C_l at $\alpha = 0$ deg is zero for

configuration BW, Fig. 23. The results for BWF also given in Fig. 23 indicate that at $\alpha = 0$ deg the rolling moment present is that due to the fin and the value measured coincides with that obtained by differencing the C_l results for $BWCF$ and BWC with $\eta = 0$ deg as shown in Fig. 31.

6.3.2. *Wing off.* The only source of rolling moment with no wing present at $\alpha = 0$ deg is that due to the fin. As for the fin contribution for BWF the curve of C_l vs. β for BCF' is almost identical with that from $(BWCF' - BWC)$ as plotted in Fig. 31. In conformity with the C_y and C_n results for BCF' at $\alpha = 0$ deg it will be seen, Fig. 23, that the deflection of the foreplane at $\eta = 10$ deg causes an increase in $\partial C_l/\partial\beta$ of approximately 40 per cent. As indicated in Section 6.1.2 this is due to the effect of the induced sidewash from the foreplane vortices acting on the fin. The method adopted for estimating the effect of vortices is not likely to be very effective for C_l as the velocity distribution over the fin is not considered. The fin centre of pressure as derived from ΔC_l and ΔC_y results for BCF', $\eta = 0$ deg and $\eta = 10$ deg is given in Fig. 19. For comparison the centre of area of the net fin and the gross fin (extended to body centre-line) are also shown. It will be seen that the fin centre of pressure position is almost independent of β and is moved upwards slightly by presence of the vortices. The proximity of the fin centre of pressure position to the centroid of area means that using the centroid of area may give a quick and convenient way of estimating the fin contribution to the aircraft $\partial C_l/\partial\beta$. The only other result is that for BF' which agrees closely with that for BCF', $\eta = 0$ deg.

6.3.3. *Complete configuration.* In contrast with the C_y and C_n results for $BWCF$ at $\alpha = 0$ deg the effect of deflecting the foreplane to $\eta = 10$ deg is quite marked on C_l. In Fig. 23 the C_l vs. β results are shown for $BWCF$ with $\eta = 0$ deg and $\eta = 10$ deg; by comparison with the results for BCF' it can be seen that there is a large additional rolling moment due to the interaction of the foreplane vortices of the same order of magnitude as that due to the fin. The magnitude of this incremental C_l is shown more clearly in Fig. 24 where ΔC_l due to the foreplane interaction is plotted for both Mach numbers. The most interesting feature is that the result is the same for (BWC, $\eta = 10$ deg $- BWC$, $\eta = 0$ deg) as for ($BWCF$, $\eta = 10$ deg $- BWCF$, $\eta = 0$ deg) which means that all the change in C_l is due to the load induced on the wing by the foreplane vortices. This is consistent with the explanation given for the C_y and C_n results in Section 6.1.3.

If, when the aircraft is sideslipped, the centre of pressure of this induced down load can be regarded as unaltered relative to the foreplane (*i.e.*, that the wing changes position within the downwash field but does not affect the field) then rolling moment would be related to the foreplane load, ΔC_z, as follows

$$\frac{\partial \Delta C_l}{\partial \beta} = \Delta C_z (1 - \bar{\eta}_z) \frac{l_c}{b}$$

where l_c is distance from foreplane centre of pressure to effective centre of pressure of the induced down load.

When this is applied there is qualitative agreement, Fig. 24, but the rolling moment is under estimated by some 30 per cent at $M = 1{\cdot}40$. The inference is thus that there is also some change in distribution but the effect on the force as distinct from the rolling moment is small.

It is hoped that tests planned to investigate the relations between vortex strength and position and the induced loading will shed more light on this.

6.4. *Rolling Moment Results with Combined Incidence and Sideslip.* The rolling moment results for conditions of combined incidence and sideslip are presented both as plots of C_l vs. β for constant

values of α, Figs. 25 to 31, and as plots of $\partial C_l/\partial\beta$ vs. α Figs. 32 and 33 where the slope is measured near $\beta = 0$ deg. In some cases $\partial C_l/\partial\beta$ is nearly constant over the whole of the measured range of β but for other configurations it varies considerably and this should be borne in mind when considering the plotted values of $\partial C_l/\partial\beta$.

6.4.1. *Foreplane off.* The two main configurations considered under this heading are *BW* and *BWF* and the C_l vs. β curves are given in Fig. 25. It will be seen that for *BW* there is a steady increase in slope with increasing α, *see* also Fig. 32. It is difficult to make a direct comparison of the *BW* and *BWF* curves due to a difference in scale but if the $\partial C_l/\partial\beta$ curves are compared it will be seen that the variation with α is similar for both, the main difference being that the curve for *BWF* is displaced bodily by an amount corresponding to the value of $(\partial C_l/\partial\beta)_{\alpha=0}$ for the fin. The curve for *BWF* is not as linear as that for *BW* but this is not thought to be very significant due to the difficulty in determining accurately the slope of the C_l vs. β curves which are themselves cross-plots of the original data. The curve of $\partial C_l/\partial\beta$ for results from configuration *BF'* is also shown in Fig. 32 and shows no change with α. This result might be expected and agrees with the results for *BW* and *BWF* which suggest that nearly all the change in $\partial C_l/\partial\beta$ with α is due to the wings. It is quite difficult to predict the wing contribution to $\partial C_l/\partial\beta$ due to incidence and for wings with streamwise tips the sign of $\partial C_l/\partial\beta$ obtained depends on the assumptions about the flow at the tip as to whether the Kutta condition is fulfilled or not[8]. For the wing shape used in these tests there are no satisfactory estimates and the only method available[9, 10] requires considerable computational effort to give a result which is of questionable value. Certain values of $\partial C_l/\partial\beta$ have been worked out in Refs. 9 and 10 for other plan-forms and the experimental value of $\partial C_l/\partial\beta$ obtained from the present tests is of the same order as would be given by a gross interpolation on these theoretical curves. The theoretical prediction of $\partial C_l/\partial\beta$ due to a wing travelling at supersonic speeds is one line of investigation which could profitably be extended.

One feature to note is that at $\alpha = 10$ deg the experiments show a value of C_l from the wing greater than that contributed by the modified fin alone at the same incidence. Despite the complex flow field, however, the fin and wing contributions may be considered as almost directly additive.

6.4.2. *Wing off.* As already noted, the result for configuration *BF'* shows C_l to be independent of α. Since the body vortices are symmetrically disposed and of relatively low strength at the incidences considered this effect would be expected as there are no other reasons for a change in fin contribution to C_l with varying α. The C_l vs. β results for *BCF'*, $\eta = 0$ deg are given in Fig. 26 with the corresponding curves of $\partial C_l/\partial\beta$ in Fig. 32. It will be seen that a significant feature of the results is the small increase in $\partial C_l/\partial\beta$ followed by a decrease as α is increased. There is thus some effect of the foreplane vortices on the fin load distribution and the trend of the results is consistent with that noted in Section 6.2.2 on $-C_y$ vs. β and C_n vs. β for the same configuration. The approximate method suggested for predicting the change in $-C_y$ for the fin has not been developed to include the effect of the pressure distribution across the fin but qualitatively there is reasonable agreement with the shape of the $-C_y$ and C_n curves. Unfortunately no results were obtained for the *BCF'*, $\eta = 10$ deg, and so the effect of stronger vortices when incidence is present cannot be determined; it would be expected to give an increased value of $\partial C_l/\partial\beta$ near $\alpha = 0$ deg and then a greater decrease above $\alpha = 5$ deg.

6.4.3. *Complete configuration.* The C_l vs. β results for the complete configuration and for configuration *BWC* are shown in Figs. 27 to 29, and the related $\partial C_l/\partial\beta$ results in Fig. 33. Little

comment is needed on the C_l vs. β results except perhaps that these are surprisingly linear, particularly at $M = 1{\cdot}40$. Attention will therefore be given to the $\partial C_l/\partial\beta$ results. It has already been noted in Section 6.3.3 that at $\alpha = 0$ deg there is a marked increase in $\partial C_l/\partial\beta$ due to the foreplane vortices. This effect persists at incidence, but the increment due to 10 deg control deflection becomes less. This is consistent with the recovery of normal force efficiency, $\bar{\eta}_z$, as the incidence is increased (Section 5.1.4 and Fig. 7). The magnitude of the effect is best seen from the curves for BWC, $\eta = 0$ deg, and BWC, $\eta = 10$ deg, of Fig. 33 where those for BW are included for comparison. It is worth noting the relative magnitude of the wing-alone contribution and that arising from the effect of the foreplane vortices on the wing since any canard aircraft is likely to fly with several degrees of foreplane deflection in the trimmed condition.

When the complete configuration, $BWCF$, is considered it can be seen that the shape of the $\partial C_l/\partial\beta$ curve is similar to corresponding curves for configuration BWC. This is consistent with the effect noted already of a fin contribution which is invariant with α. Again attention is drawn to the fact that the various contributions to $\partial C_l/\partial\beta$ are almost directly additive, and with foreplane deflection to trim, in the same sense, *viz.*, negative. Such large negative values of $\partial C_l/\partial\beta$ may be undesirable from the point of view of roll: yaw ratio[11].

From the results for BWC and $BWCF$ it is possible to gain some idea of the Mach number effects. One of the most striking features is the increasing relative significance of the effect of the vortices. At the higher Mach number the value of $\partial C_l/\partial\beta$ at $\alpha = 0$ deg due to $\eta = 10$ deg is greater than that due to the fin (*cf.* results at $M = 1{\cdot}40$).

The main effect of increasing Mach number is a decrease in the magnitude of the rolling moment due to sideslip from each cause. However, the implications of this reduction in $\partial C_l/\partial\beta$ on the aircraft motion cannot be determined without considering also the variation with Mach number of the other aerodynamic derivatives, and it would therefore seem advisable to make some form of stability calculations to determine the significance of these values of $\partial C_l/\partial\beta$.

In order to illustrate the magnitude of the induced rolling moments in terms of control deflection the following sample calculation has been made assuming an outboard, semi-span, trailing edge aileron of chord 15 per cent that of the wing. For a trimmed incidence with $\eta = 10$ deg and a sideslip of $\beta = 5$ deg at $M = 1{\cdot}40$ it is estimated using the method of Ref. 12 that 15 deg of aileron deflection would be required to balance this induced rolling moment. This is a conservative estimate assuming a full linear theory value for the control with no reduction for thickness effects and no loss due to aeroelasticity.

If it should be found necessary to limit the value of $\partial C_l/\partial\beta$ one possibility of achieving this would be wing anhedral. For the sake of illustration assume that the value of $\partial C_l/\partial\beta$ is satisfactory for the condition with foreplane undeflected and that it is necessary to counteract the incremental value of $\partial C_l/\partial\beta$ due to 10 deg foreplane. Calculations show that an anhedral angle of the order of 15 deg would be required. These calculations were made using the method of Ref. 13. Whilst this method is likely to give an underestimate of the contribution to $\partial C_l/\partial\beta$ from anhedral yet it does help to emphasise further the magnitude of the effects likely to be encountered with such canard layouts.

As already mentioned the configurations $BWCF'$, $\eta = 0$ deg and $\eta = 10$ deg, were tested up to the highest polar incidences attainable in the tunnel (25 deg) in order to check on the magnitude of the rolling moments induced in such cases. The C_l vs. β results are shown in Fig. 30 and are slightly more reassuring in that they indicate that the large induced rolling moments do not go on increasing indefinitely with increase of α, but reach a maximum value and then decrease. The

variation of C_l with β is markedly non-linear at the higher values of β resulting in a decrease in $\partial C_l/\partial\beta$ at these larger values of β. Although in general the magnitude of $\partial C_l/\partial\beta$ is greater for the configuration with $\eta = 10$ deg it is interesting to note that for $\alpha = 20$ deg the value of $\partial C_l/\partial\beta$ is less than that for $\alpha = 0$ deg. As yet no satisfactory explanation can be given for these effects.

Considered overall it is probable that, although the rolling moment produced by the foreplane-wing interaction can be severe, provided due allowance is made in the early stages of the design, adequate control and stability should be feasible for a canard configuration up to high incidences.

7. *Flow Visualisation Tests.* In order to help in the understanding of some of the phenomena already discussed it was decided to make some flow visualisation studies of flow around the model. Schlieren photographs were obtained during the course of the force and moment tests as the schlieren system forms part of the standard tunnel equipment.

Another technique used was the vapour screen which has been developed mainly in the U.S.A. For this the air in the tunnel has a high humidity and a narrow beam of light is used to illuminate a thin section of the tunnel perpendicular to the free-stream direction. It is particularly valuable for demonstrating vortex flow as the vortices appear as small black discs in the white background.

Finally tests were made using a thick gear oil mixed with titanium oxide powder and spread on the model surface. With the tunnel running the oil film forms a pattern corresponding to the surface flow on the model. This technique has been used fairly extensively at subsonic speeds, but has only recently been used in a supersonic wind tunnel.

Brief comments are made on some of the results obtained by the above mentioned techniques.

7.1. *Schlieren Photographs.* Fig. 35a shows a model viewed in plan with $\alpha = \beta = 0$ deg and $\eta = 10$ deg. As already mentioned there are strong vortices from the foreplane which trail in a stream-wise direction as far as the leading edge of the wing. Behind the wing there is no sign of this concentrated vorticity but only evidence of weak, more distributed, vorticity indicating cancellation of the foreplane vorticity by the wing. This figure should be viewed in conjunction with the oil flow picture of Fig. 40 which shows the surface pattern for the same model conditions. Fig. 35b shows a similar set-up but with $\beta = 5$ deg and is included to show that the vortices trail in a stream direction until they reach the wing, and thus there is still virtually complete cancellation of the control vorticity.

In Fig. 36a the model with $\eta = 10$ deg is shown as $\alpha \simeq 11$ deg, $\beta \simeq 9$ deg. The control vortices are indicated and are seen to move well above the wing but their lateral position relative to the wing cannot be estimated with any accuracy. Attention is also drawn to the complex flow pattern at the rear of the model. Fig. 36b shows for comparison the model at a similar incidence, but with foreplane removed. The quality of this schlieren picture is poor, but it suffices to show the body vortices which are present at such incidences. These vortices are almost suppressed by the presence of the foreplane; further comment on this is made in Section 7.3.

The next series of schlieren photographs are those for $\beta = 0$ deg with $\alpha = 5$ deg, $7{\cdot}5$ deg and 10 deg, and are included mainly to show the paths of the foreplane vortices when passing over the wing. From a sequence of these photographs the vortex paths for $\eta = 0$ deg and $\eta = 10$ deg at $M = 2{\cdot}02$ have been plotted in Fig. 34. It may be seen that on passing through the wing leading edge shock the vortex path is inclined away from its initial free stream direction to flow parallel to the wing surface. This may mean a significant change in the height at which the vortex passes

the fin. There are also indications that the vortex path is deflected back towards the free stream direction behind the wing. It is felt that deflection of the vortex paths may not have been fully realised, and is of considerable practical importance particularly if the fin be set some way behind a large chord wing.

7.2. *Vapour Screen Photographs.* It is preferable where space permits and equipment is suitable to take these vapour screen pictures from a viewpoint directly upstream or downstream of the model. This enables quantitative measurements of the disposition of the vortex cores to be made. This was unfortunately not feasible in the present case for which the oblique viewpoint, Fig. 39, with a corresponding lack of perspective, was necessary.

The photographs are shown in Figs. 38 and 39. Fig. 38 shows the configuration $BWCF'$ ($\eta = 10$ deg, $M = 1{\cdot}40$) at a polar incidence of 10 deg for roll angles 0 deg to 80 deg. The main feature to which attention is drawn is the movement of the control vortices relative to the wing and their almost complete disappearance at the highest roll angle in which position the foreplane and wing are nearly aligned stream-wise. The appearance of body vortices at this altitude should be noted. It is also interesting to note that for small ϕ when the wing has a relatively large incidence there are two quite marked wing vortices.

For comparison the corresponding photographs of the model with the foreplane removed are shown in Fig. 39a and b for $\phi = 0$ deg and $\phi = 90$ deg respectively. Here it will be seen that at $\phi = 0$ deg there are two clearly defined vortices from the wing tips and a further two, much weaker, on the leeward of, and close to, the body. At $\phi = 90$ deg the wing vortices have disappeared since the wings are no longer providing lift and the body vortices have moved further away from the body showing that the wing has a significant effect on their position. It may also have affected their strength by preventing the feeding vortex sheets from functioning over that part of the body carrying the wing.

7.3. *Oil Flow Photographs.* These photographs give a useful guide to the surface flow. Although they vary somewhat in quality it is hoped that the main features will be discernable from the reproductions presented.

The first two photographs Figs. 40a and b are for $BWCF'$, $\eta = 10$ deg with $\alpha \simeq 0$ deg so as to make the wing leading edge split the vortices from the foreplane. Aft of the intersection of the vortices with the wing leading edges the vortex paths are altered considerably, those on the upper surface diverging, and those on the lower surface converging. Judged from the obliquity of the herring-bone pattern to the free-stream direction there is some indication that the vortex strengths are decreasing with distance along the chord. Whilst it is not possible to be dogmatic from this rather limited evidence it does appear to support the view that the majority of the down load is induced near the leading edge of the wing.

The pictures for BWF at $\alpha = 10$ deg $\beta = 0$ deg are shown in Fig. 41. Fig. 41a shows the suction surface of the wing, and the main feature to note is the line marked out by the shock wave from the root leading edge and the indication of vorticity shed from the wing tip. Also to be noted in this view is the 'secondary' separation line along the body. Fig. 41b shows the pressure surface of the same model on which there is an indication of outflow near the wing tip. It can be seen that the presence of the wing interrupts the smooth flow of the air around the body. Also worthy of note is the remarkable symmetry of the flow pattern. Corresponding to these figures is the side view (port)

of Fig. 41c which shows the main separation line on the forebody which is associated with the body vortices already noted in Section 7.2. It can be seen that this separation is markedly affected by the presence of the wing.

The photographs of Fig. 42 show the model at the same incidence ($\alpha = 10$ deg) but with the foreplane added ($\eta = 0$ deg). The flow pattern on the suction surface is very similar except that the body separation, having been forced further round the body by the presence of the foreplane, has a more marked effect on the body wing junction, and there is a small separation region as indicated by the accumulation of oil at the root. This photograph shows rather more clearly than 41a the effect of the wing tip vortices. The flow pattern on the pressure surface of the wing, Fig. 42b, is very similar to that of 41b. On the body ahead of the wing, however, the component of the flow across the body is less, and the separation line further around the body, than in the case with the foreplane absent; but these effects indicate a reduction in the body vorticity (*see* Section 7.2).

In Fig. 43 the configuration *BWF* is shown at $\theta = 15$ deg and $\phi = 60$ deg (corresponding to $\alpha \simeq 7{\cdot}5$ deg and $\beta \simeq 13$ deg). The patterns are much more complex, and not so easily interpreted. On the starboard wing of the suction surface the traces of the root shock wave and the tip vortex are still apparent, but they have moved round in a sense consistent with that of β. On the port wing the pattern is masked by the trace of a strong vortex, probably the nearer of the two shed by the body. The tip vortex is no longer evident due to an angular movement arising from the sideslip angle. Both of these could be important factors in the determination of $\partial C_l/\partial\beta$. The separation line is clearly seen on the body. The pressure surface Fig. 43b is not greatly affected by the sideslip, although there is evidence of increased outflow towards the tip on the port (upper) wing. Figs. 43c and d show the corresponding side views, and the main feature to note is the change in position of the separation line as compared with Fig. 41c.

Finally the curves of Fig. 44 show the pattern obtained with the model at the same altitude as for Fig. 43 ($\alpha \simeq 7{\cdot}5$ deg $\beta \simeq 13$ deg) but now with the foreplane on. The body vortex trace is no longer evident across the suction surface of the port wing which again suggests that the foreplane tends to suppress the development of the body vortices. The side view photographs 44c and d also support this. In other respects the flow over the wing surfaces, both suction and pressure, are similar to those with the foreplane absent.

8. *Conclusions.* The main features arising from the tests on an interim canard model at $M = 1{\cdot}40$ and $M = 2{\cdot}02$ are summarised below. Care should be taken in trying to make quantitative generalisations from the results particularly at the higher angles of incidence and sideslip.

(1) Due to the down load induced on the wing by the foreplane vortices the lift effectiveness of the foreplane at $M = 1{\cdot}40$ is zero at small incidences, and rises to approximately $0{\cdot}4$ at $\alpha = 10$ deg. This result is little affected by change of foreplane setting. There is reason to believe the effectiveness will improve with increase of Mach number.

(2) The effective centre of pressure of the induced down load is well ahead of that for the wing alone in uniform flow, and is almost constant with incidence. As a result, with the moment centre chosen, the moment effectiveness is greater than $1{\cdot}2$ for all attitudes at $M = 1{\cdot}40$. No corresponding results are available at $M = 2{\cdot}02$.

(3) For the foreplane settings used and the particular moment reference chosen the aircraft is longitudinally stable at all incidences; the stability increases with increase of incidence, and is greater at $M = 2{\cdot}02$ than at $M = 1{\cdot}40$ (*see* table in Section 5.1.3 for details).

(4) Sideslip causes no significant change in the curve of either normal force or pitching moment against incidence.

(5) For the original configuration the value of $\partial C_n/\partial\beta$ shows the expected decrease with increase of Mach number, and agrees reasonably well with estimates at the higher Mach number.

(6) For the complete configuration ($BWCF'$) there is a reduction in $\partial C_n/\partial\beta$ with increase in α over the range of incidence tested amounting to 20 per cent at $M = 1{\cdot}40$ and even more at $M = 2{\cdot}02$. This indicates that there may possibly be difficulties in obtaining sufficient static directional stability at the higher Mach number.

(7) At $M = 1{\cdot}40$ with the wing removed there is a marked effect of the foreplane vortices on the fin effectiveness leading to an almost complete loss of $(\partial C_n/\partial\beta)_F$ at $\alpha = 10$ deg.

(8) The rolling moments acting on the model when both incidence and sideslip are present arise from three main causes which are, to a close approximation, directly additive, *viz.*,

(*a*) A fin contribution which is almost independent of α.

(*b*) A wing contribution which is a linear function of α, and gives $\partial C_l/\partial\beta$ negative for a positive α.

(*c*) A contribution due to the foreplane interference on the wing in the same sense as that due to the wing alone, and increasing non-linearly with α. At $\alpha = 0$ deg, for $\eta = 10$ deg, this contribution is of similar magnitude to that due to the fin.

It is felt that these large negative values of $\partial C_l/\partial\beta$ need careful consideration when calculating the lateral stability particularly as the typical aileron power to correct these induced moments is of the order of three degrees of aileron per one degree of sideslip.

(9) Schlieren, vapour screen and oil film tests at $M = 1{\cdot}40$ help towards an understanding of some of the flow phenomena, but it is recommended that a more complete investigation be made soon of the effect of a vortex on the pressure distribution on the lifting surface.

LIST OF SYMBOLS

The various configurations are denoted by the following letters used in combination.

B	Body
C	Foreplane control surface
F	Original fin
F'	Modified fin (0·75 area of original net fin)
W	Wing

If used as a subscript to a coefficient it denotes the force or moment on that particular configuration.

$Oxyz$	Right-hand system of axes fixed in the aircraft
$Ox_0y_0z_0$	Right-hand system of axes fixed in the tunnel with Ox_0 along the direction of the relative wind
b	Gross span = 3·50 inches
c	Local chord
$\bar{\bar{c}}$	Aerodynamic mean chord $\int_{-b/2}^{b/2} \frac{c^2 dy}{S_w}$
C_y	Side-force coefficient
	$= \frac{Y}{qS_W}$
C_z	Normal-force coefficient
	$= \frac{Z}{qS_W}$
C_l	Rolling-moment coefficient (measured about Ox)
	$= \frac{L}{qS_W b}$
C_m	Pitching-moment coefficient (measured about wing root leading edge)
	$= \frac{M}{qS_W \bar{\bar{c}}}$
C_n	Yawing-moment coefficient (measured about wing root leading edge)
	$= \frac{N}{qS_W b}$
h_F	Height of the fin (above upper surface of the body)
h, h_1 and h_2	Heights on the fin (*see* Appendix II)

$\bar{h}_\alpha$		Centre of pressure position
	$=$	C_m/C_z
$\bar{h}_z$		Height of centre of pressure of fin force above the body centre-line
l		Distance from foreplane hinge line to fin centre of pressure
l_c		Distance from foreplane centre of pressure to centre of pressure of down load on the wing
K		Circulation due to vortex
M		Mach number
q		Kinetic pressure
	$=$	$\frac{1}{2}\rho V^2$
V		Free stream velocity
R		Non-dimensional fin height (*see* Appendix II)
	$=$	h_F/s
$2s$		Foreplane vortex spacing
S_W		Gross wing area
S_F		Net fin area
x		Non-dimensional height (*see* Appendix II)
	$=$	h_2/s
α		Incidence of wing, $\sin^{-1}$ (sin θ cos ϕ), in degrees
β		Sideslip of wing, $\sin^{-1}$ (sin θ sin ϕ), in degrees
θ		Polar incidence, angle between Ox and Ox_0
ϕ		Roll angle, angle between Oxz_0 and Oxz
η		Foreplane setting angle, angle between chord line of control and Oxy
λ		Taper ratio—tip chord ÷ root chord
Γ		Dihedral angle of the wing, degrees
$\bar{\eta}_M$		Foreplane moment efficiency (*see* Section 5.1.4)
$\bar{\eta}_Z$		Foreplane force efficiency (*see* Section 5.1.4)

REFERENCES

No.	*Author*	*Title, etc.*
1	J. R. Anderson	A note on the use of strain gauges in wind tunnel balances. NATO/AGARD Memo. AG10/M6. R.A.E. Tech. Note Aero. 2290. January, 1954.
2	W. C. Pitts, J. N. Neilsen and G. E. Kaattari	Lift and center of pressure of wing-body-tail combinations at subsonic, transonic and supersonic speeds. N.A.C.A. Report 1307. 1957.
3	G. Morikawa	Supersonic wing-body-tail interference. *J. Ae. Sci.* Vol. 19. No. 5 p. 333. May, 1952.
4	P. R. Owen and E. C. Maskell ..	Interference between the wings and the tail plane of a slender wing-body-tailplane combination. A.R.C. 14,483. October, 1951.
5	M. L. Spearman and C. Driver ..	Wind tunnel investigation at a Mach number of 2·01 of the aerodynamic characteristics in combined pitch and sideslip of some canard-type missiles having cruciform wings and canard surfaces with 70 deg delta planforms. N.A.C.A. Research Memo. L54F09. TIB/4359. August, 1954.
6	M. L. Spearman and R. B. Robinson	Aerodynamic characteristics at a Mach number of 2·01 of two cruciform missile configurations having 70 deg delta wings with length-diameter ratios of 14·8 and 17·7 with several canard controls. N.A.C.A. Research Memo. L54G20. TIB/4383. August, 1954.
7	H. L. Alden and L. H. Schindel ..	The lift, rolling moment and pitching moment on wings in non-uniform supersonic flow. *J. Ae. Sci.* Vol. 19. No. 1 p.7. January, 1952.
8	A. L. Jones and A. Alksne	A summary of lateral stability derivatives calculated for wing planforms in supersonic flow. N.A.C.A. Report 1052. 1951.
9	K. Margolis, W. L. Sherman and M. E. Hannah	Theoretical calculations of the pressure distribution, span loading and rolling moment due to sideslip at supersonic speeds for thin sweptback tapered wings with supersonic trailing edges and wing tips parallel to the axis of wing symmetry. N.A.C.A. Tech. Note 2898. February, 1953.
10	W. L. Sherman and K. Margolis ..	Theoretical calculations of the effects of finite sideslip at supersonic speeds on the span loading and rolling moment for families of thin sweptback tapered wings at angles of attack. N.A.C.A. Tech. Note 3046. November, 1953.
11	H. H. B. M. Thomas and J. Neumark	Interim note on stability and response characteristics of supersonic aircraft (linear theory). R.A.E. Tech. Note No. Aero 2412, November, 1955.

REFERENCES—*continued*

No.	*Author*	*Title, etc.*
12	K. L. Goin	Equations and charts for the rapid estimation of hinge moment and effectiveness parameters for trailing edge controls having leading and trailing edges swept ahead of the Mach lines. N.A.C.A. Report 1041. (Supersedes N.A.C.A. Tech. Note 2221, 1951.)
13	P. E. Purser	An approximation to the effect of geometric dihedral on the rolling moment due to sideslip for wings at transonic and supersonic speeds. N.A.C.A. Research Memo. L52B01. TIB/3081. April, 1952.
14	A. H. Sacks	Vortex interference on slender airplanes. N.A.C.A. Tech. Note 3525. November, 1955.

TABLE 1

Model Details

Wing	
Plan-form	Cropped delta
Leading-edge sweep angle	30 deg
Section	Modified double wedge
Thickness/chord ratio	0·035
Leading edge and trailing edge included angle in streamwise direction	6 deg 41 min
Gross span b	3·50 in.
Root chord C_R	2·73 in.
Root chord at centre-line of body	2·87 in.
Tip chord C_T	1·86 in.
Taper ratio—gross wing λ_G	0·65
Taper ratio—net wing λ_N	0·68
Gross area	8·28 sq in.
Net area	6·89 sq in.
Aspect ratio—gross wing	1·48
Aspect ratio—net wing	1·31
Control	
Plan-form	Cropped delta
Leading-edge sweep angle	20 deg
Section	Modified double wedge
Thickness/chord ratio	0·045
Leading edge and trailing edge included angle in streamwise direction	8 deg 35 min
Gross span	1·63 in.
Root chord at centre-line of body	0·88 in.
Tip chord	0·583 in.
Taper ratio—gross control	0·66
Taper ratio—net control	0·71
Gross area	1·19 sq in.
Net area	0·82 sq in.
Aspect ratio—gross control	2·24
Aspect ratio—net control	1·73
Fin	
Plan-form	Cropped delta
Section	Modified double wedge
Thickness/chord ratio	0·035
L.E. and T.E. included angle	6 deg 41 min
Height (from centre-line of body)	1·45 in.
Net height	1·20 in.
Root chord	1·00 in.
Tip chord	0·563 in.
Net area	1·54 sq in.
Net aspect ratio	1·54
Net taper ratio	0·56

TABLE 1—*continued*

Modified fin	
Net height	0·828 in.
Tip chord	0·699 in.
Net area	0·702 sq in.
Net taper ratio	0·70
Body	
Overall length l	9·0 in.
Diameter	0·5 in.
Length/diameter ratio	18·0
Nose shape	Modified ogive
Nose fineness ratio	5·0:1

Moment reference position is at intersection of the centre-line and the line joining the wing root leading edges (4·77 in. behind nose tip).

TABLE 2

List of Runs

Run No.	Configuration	Mach number	Stag Pressure Hg in.	Remarks
1 and 2	*BWCF*, $\eta = 0°$	2·02	36	$-2° < \alpha < 12°$, $0° < \beta < 10°$
3	*BWCF*, $\eta = 9{\cdot}7°$	2·02	36	$-2° < \alpha < 12°$, $0° < \beta < 10°$
4	*BWC*, $\eta = 0°$	2·02	36	$-2° < \alpha < 12°$, $0° < \beta < 10°$
5	*BWC*, $\eta = 9{\cdot}9°$	2·02	36	$-2° < \alpha < 12°$, $0° < \beta < 10°$
6	*BWCF*, $\eta = 9{\cdot}9°$	1·40	24	$-2° < \alpha < 12°$, $0° < \beta < 10°$
7	*BWC*, $\eta = 9{\cdot}9°$	1·40	24	$-2° < \alpha < 12°$, $0° < \beta < 10°$
8	*BWC*, $\eta = 0°$	1·40	24	$-2° < \alpha < 12°$, $0° < \beta < 10°$
9	*BWCF*, $\eta = 0°$	1·40	24	$-2° < \alpha < 12°$, $0° < \beta < 10°$
10	*BWF*	1·40	24	$-2° < \alpha < 12°$, $0° < \beta < 10°$
11	*BWCF'*, $\eta = 0°$	1·40	24	$-2° < \alpha < 12°$, $0° < \beta < 10°$
12	*BCF'*, $\eta = 0°$	1·40	24	$-2° < \alpha < 12°$, $0° < \beta < 10°$
13	*BF'*	1·40	24	$\alpha = 0$, $-2° < \beta < 14°$ $\beta = 0$, $-2° < \alpha < 14°$
14	*BCF'*, $\eta = 0°$	1·40	24	$\alpha = 0$, $-2° < \beta < 14°$ $\beta = 0$, $-2° < \alpha < 14°$
15	*BCF'*, $\eta = 9{\cdot}9°$	1·40	24	$\alpha = 0$, $-2° < \beta < 14°$ $\beta = 0$, $-2° < \alpha < 14°$
16	*BW*	1·40	24	C_m, C_n, C_y and C_z not recorded.
17	*BF'*	1·40	24	C_m, C_n, C_y and C_z results doubtful.
18	*BWCF'*, $\eta = 0°$	1·40	16 and 54	$-2° < \alpha < 24°$, $0° < \beta < 20°$
19	*BCF'*, $\eta = 0°$	1·40	54	$\beta = 0°$, $-1° < \alpha < 5°$ $\alpha = 0°$, $-1° < \beta < 5°$
20	*BCF'*, $\eta = 9{\cdot}9°$	1·40	54	$\beta = 0°$, $-1° < \alpha < 5°$ $\alpha = 0°$, $-1° < \beta < 5°$
21	*BWCF'*, $\eta = 9{\cdot}9°$	1·40	54	$\beta = 0°$, $-1° < \alpha < 5°$ $\alpha = 0°$, $-1° < \beta < 5°$
22	*BWCF'*, $\eta = 9{\cdot}9°$	1·40	16	$-2° < \alpha < 24°$, $0° < \beta < 20°$
23	*BWF'*	1·40	54	$\beta = 0°$, $-1° < \alpha < 5°$ $\alpha = 0°$, $-1° < \beta < 5°$
24	*BF'*	1·40	54	$\beta = 0°$, $-1° < \alpha < 5°$ $\alpha = 0°$, $-1° < \beta < 5°$

APPENDIX I

Calibration and Data Reduction Formulae

The static loading calibrations gave the following data reduction formulae for use in the DEUCE computer. The coefficients are based on values of $\frac{1}{2}\rho V^2$ corresponding to a stagnation pressure of $P_0 = 36$ in. Hg at $M = 2{\cdot}02$ and $P_0 = 24$ in. Hg at $M = 1{\cdot}40$.

At $M = 1{\cdot}40$

$$C_z = \quad 0{\cdot}02904R_Z - 0{\cdot}00001R_M - 0{\cdot}00024R_Y - 0{\cdot}00007R_N$$

$$C_m = \quad 0{\cdot}00190R_Z + 0{\cdot}00987R_M + 0{\cdot}00126R_Y + 0{\cdot}00075R_N$$

$$C_y = -0{\cdot}00129R_Z + 0{\cdot}00013R_M + 0{\cdot}00693R_Y + 0{\cdot}00001R_N$$

$$C_n = -0{\cdot}00117R_Z + 0{\cdot}00012R_M - 0{\cdot}00043R_Y + 0{\cdot}00660R_N$$

$$C_l = \quad 0{\cdot}0007R_L$$

At $M = 2{\cdot}02$

$$C_z = \quad 0{\cdot}02358R_Z - 0{\cdot}00001R_M - 0{\cdot}00020R_Y - 0{\cdot}00006R_N$$

$$C_m = \quad 0{\cdot}00154R_Z + 0{\cdot}00801R_M + 0{\cdot}00102R_Y + 0{\cdot}00061R_N$$

$$C_y = -0{\cdot}00104R_Z + 0{\cdot}00011R_M + 0{\cdot}00563R_Y + 0{\cdot}00001R_N$$

$$C_n = -0{\cdot}00095R_Z + 0{\cdot}00009R_M - 0{\cdot}00035R_Y + 0{\cdot}00536R_N$$

$$C_l = \quad 0{\cdot}000568R_L$$

The sting deflections due to bending under aerodynamic loading were also computed on DEUCE according to the following formulae:

$$\Delta\alpha = -0{\cdot}051406R_Z + 0{\cdot}00786R_M + 0{\cdot}00146R_Y + 0{\cdot}00074R_N$$

$$\Delta\beta = \quad 0{\cdot}00372R_Z - 0{\cdot}00039R_M - 0{\cdot}01213R_Y - 0{\cdot}00768R_N$$

where R_Y, R_Z, R_L, R_M and R_N are the changes of reading on the strain-gauge indicator units due to application of aerodynamic loads.

APPENDIX II

A Strip Theory Estimate of the Additional Fin Effectiveness in the Presence of Foreplane Vortices

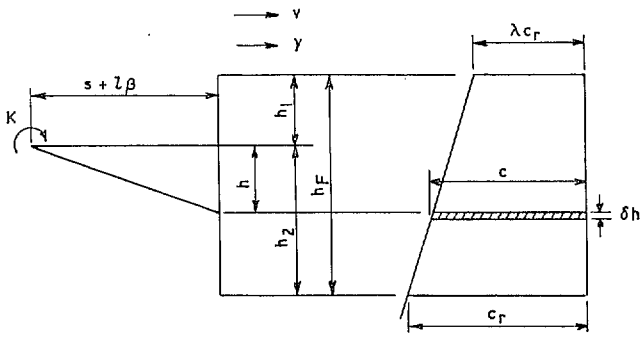

$\delta S_F \equiv c\delta h$

Vortex spacing $= 2s$

Let the velocity normal to the element of fin area δS_F be v. Then mean sidewash velocity, $\bar{v} = \dfrac{1}{S_F}\int v\, dS_F$ from one vortex.

$$\text{Side-force coefficient (strip theory)} = \frac{\bar{v}}{U}\left(\frac{\partial C_y}{\partial \beta}\right)_F$$

$$\frac{\Delta\, \partial C_y}{\partial \beta} \text{ from one vortex} = \frac{1}{U}\frac{\partial \bar{v}}{\partial \beta}\left(\frac{\partial C_y}{\partial \beta}\right)_F$$

At $\beta = 0$ the contribution from the other vortex is equal and additive

therefore

$$\frac{\left(\dfrac{\partial C_y}{\partial \beta}\right)_{\text{vortices present}}}{\left(\dfrac{\partial C_y}{\partial \beta}\right)_{\text{vortices absent}}} = 1 + \frac{2}{U}\left(\frac{\partial \bar{v}}{\partial \beta}\right)_{\beta=0}$$

$$= 1 + \frac{2}{S_F U}\left[\frac{\partial}{\partial \beta}\int_{-h1}^{h2} v(h)c(h)\, dh\right]_{\beta=0}$$

$$= 1 + \frac{2}{S_F U}\int_{-h1}^{h2} c(h)\left(\frac{\partial v}{\partial \beta}\right)_{\beta=0} dh \qquad (1)$$

since h is assumed independent of β.

Now

$$v = \frac{-Kh}{2\pi[h^2 + (s+l\beta)^2]}$$

therefore

$$\left(\frac{\partial v}{\partial \beta}\right)_{\beta=0} = \frac{Ksl}{\pi}\,\frac{h}{[h^2 + s^2]^2}.$$

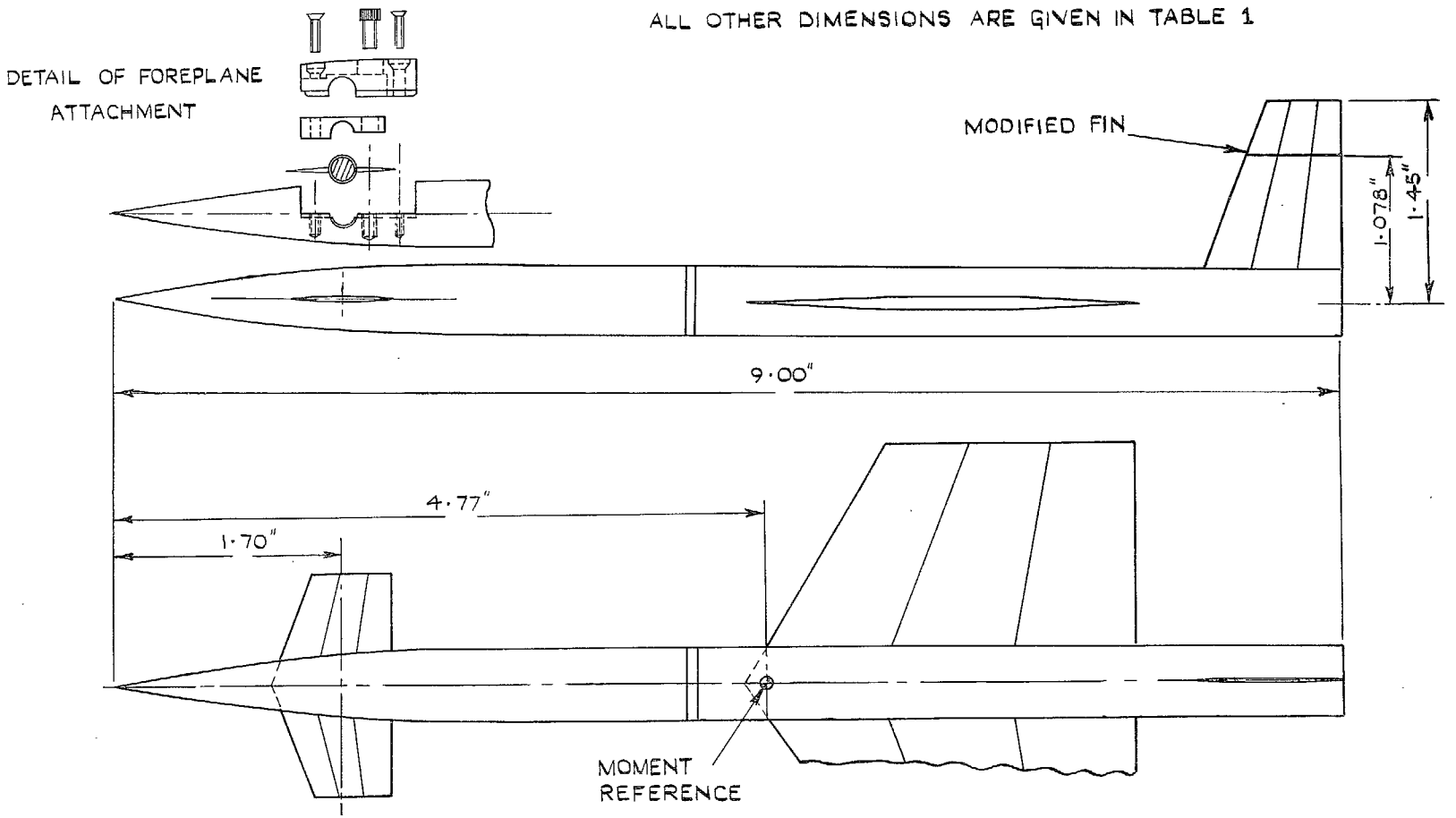

FIG. 1. Outline drawing of wind tunnel model.

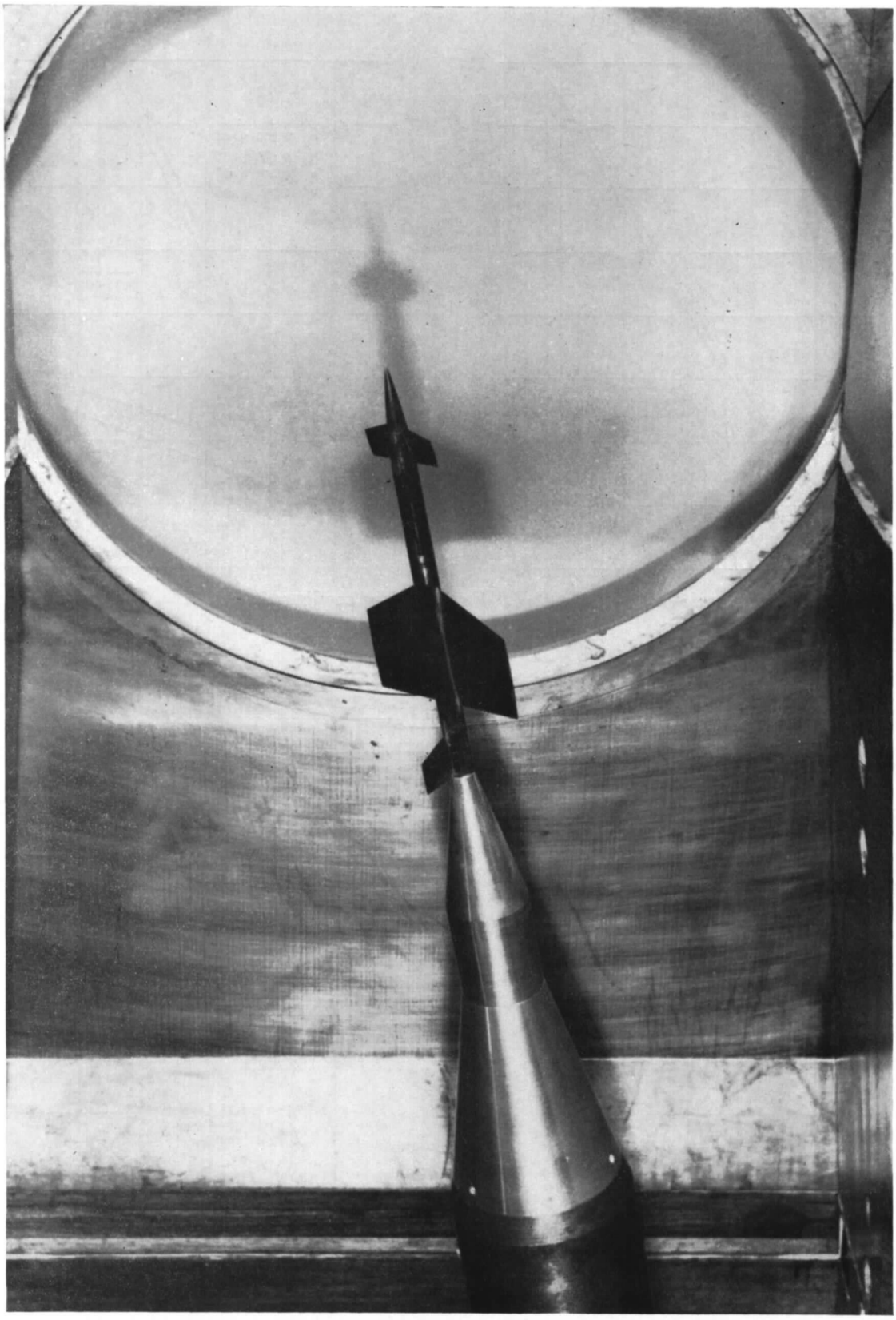

FIG. 2. Model mounted on balance in tunnel.

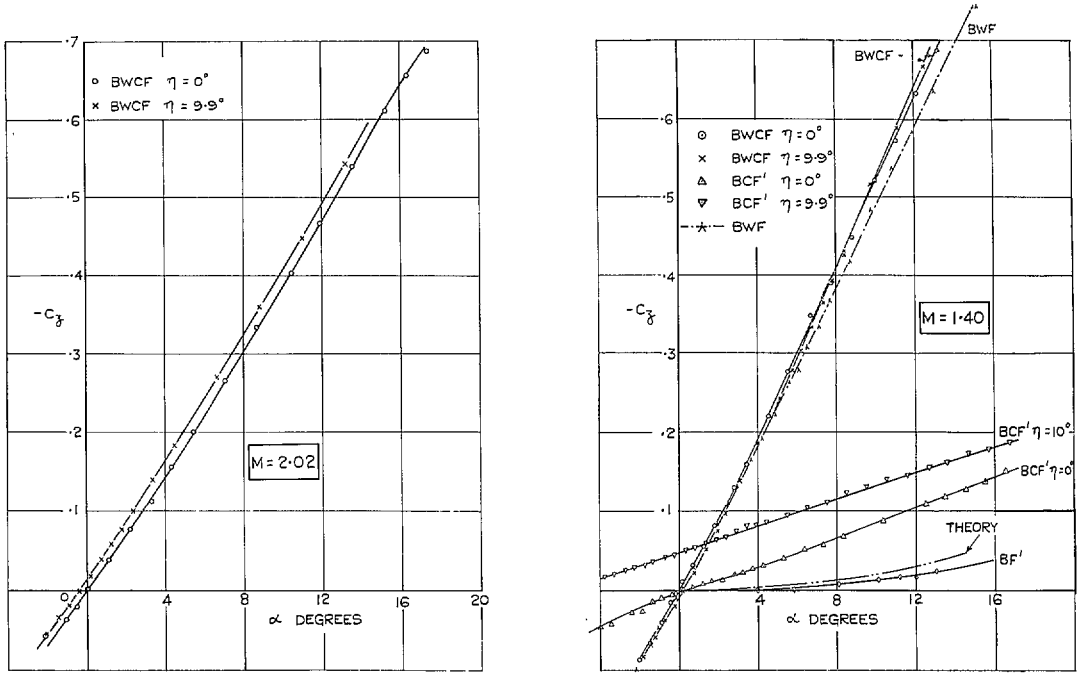

FIG. 3. Variation of $-C_z$ with α at $\beta = 0$ deg for various configurations at $M = 1{\cdot}40$ and $2{\cdot}02$.

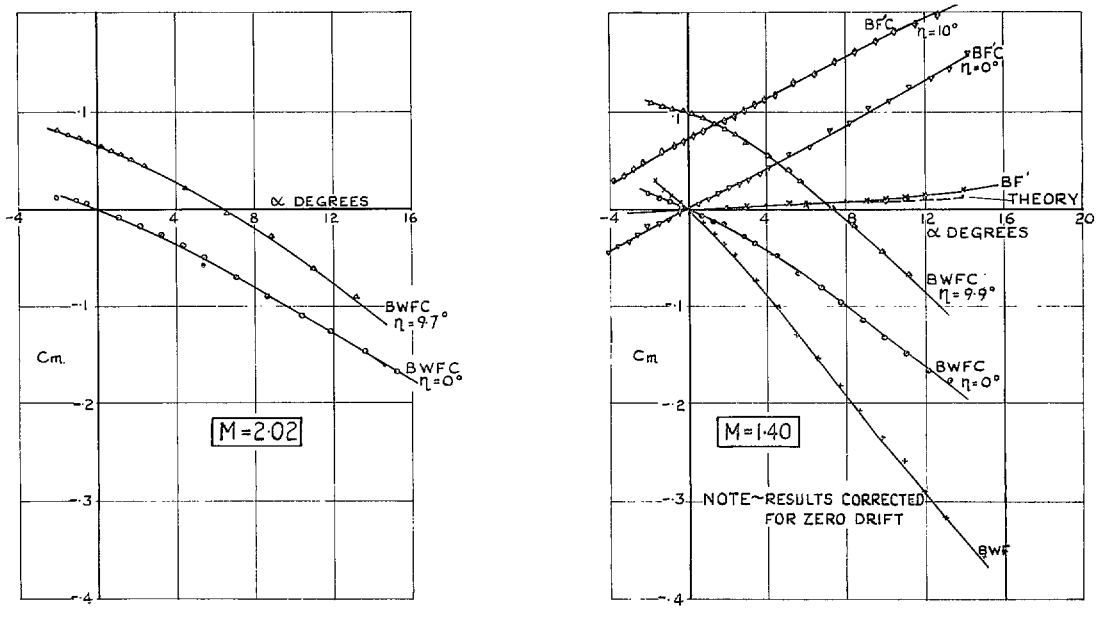

FIG. 4. Variation of C_m with α at $\beta = 0$ deg for various configurations at $M = 1{\cdot}40$ and $M = 2{\cdot}02$.

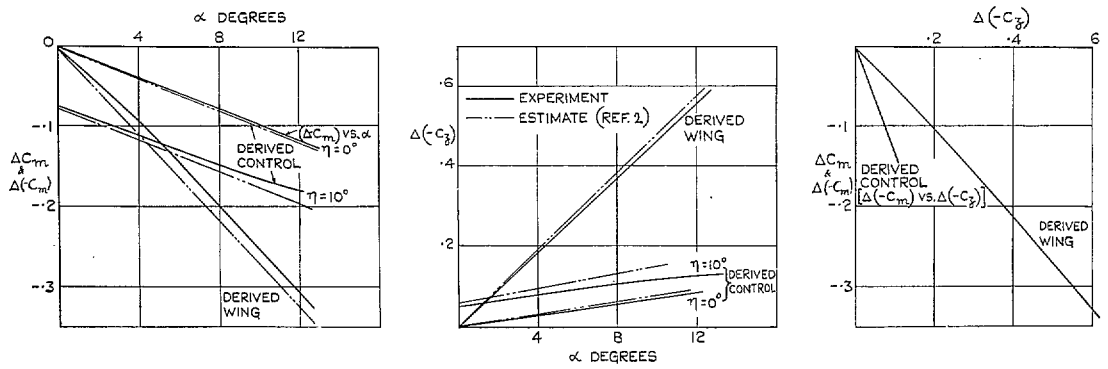

FIG. 5. Variation of $\Delta(-C_z)$ vs. α, ΔC_m vs. α and ΔC_m vs. $\Delta(-C_z)$ for derived wing and derived control, $M = 1{\cdot}40$.

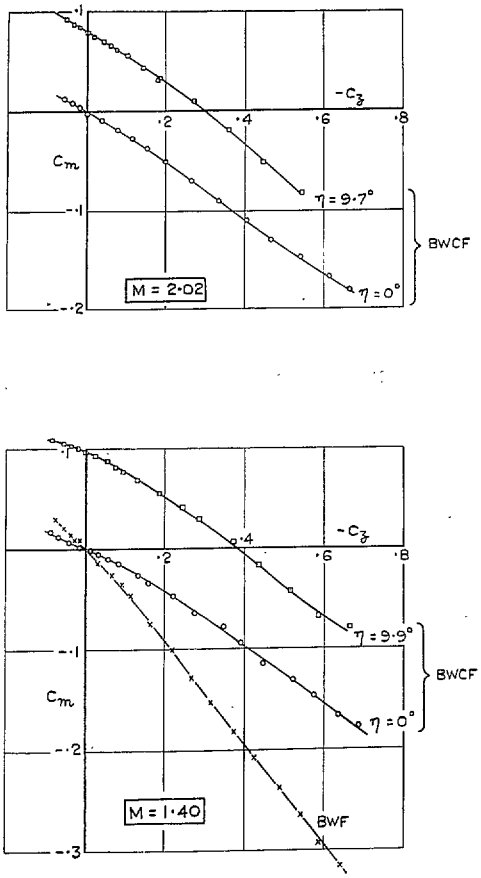

FIG. 6. Variation of C_m with $-C_z$ for configuration *BWCF*, $\eta = 0$ deg and $\eta \simeq 10$ deg at $M = 1{\cdot}40$ and $M = 2{\cdot}02$.

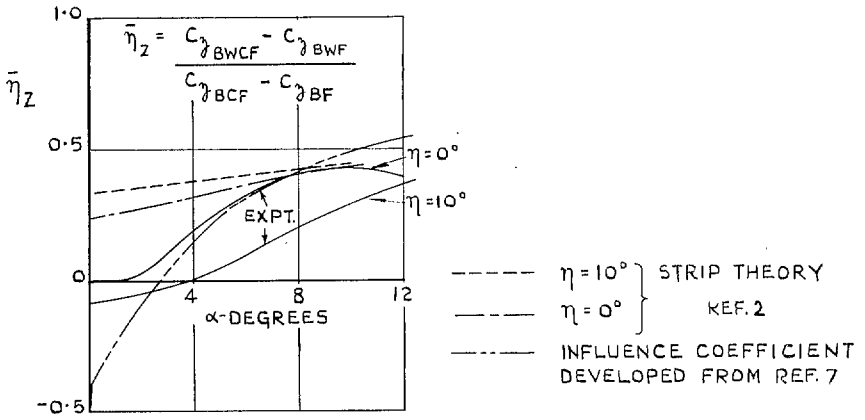

(a). FOREPLANE NORMAL FORCE EFFICIENCY.

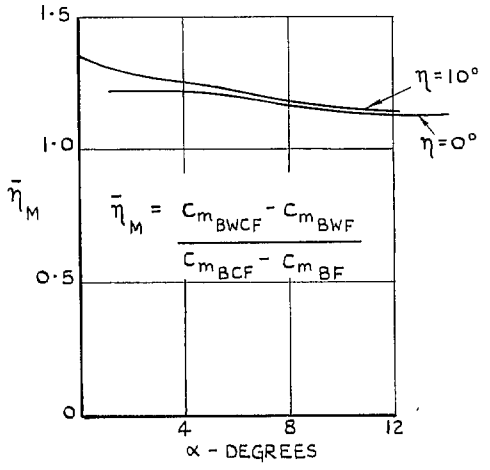

(b). FOREPLANE PITCHING MOMENT EFFICIENCY.

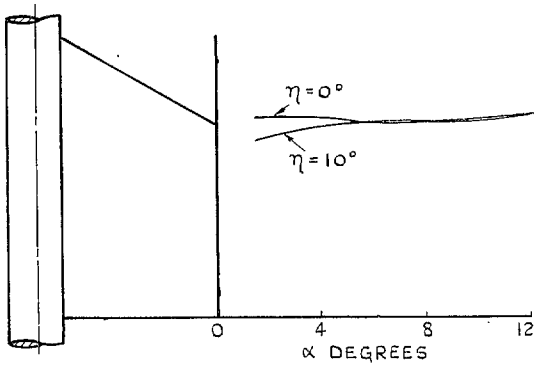

(c). CHORDWISE C.P. OF INTERFERENCE FORCE.

FIG. 7a to c. Interference effects between foreplane and wing at $M = 1{\cdot}40$.

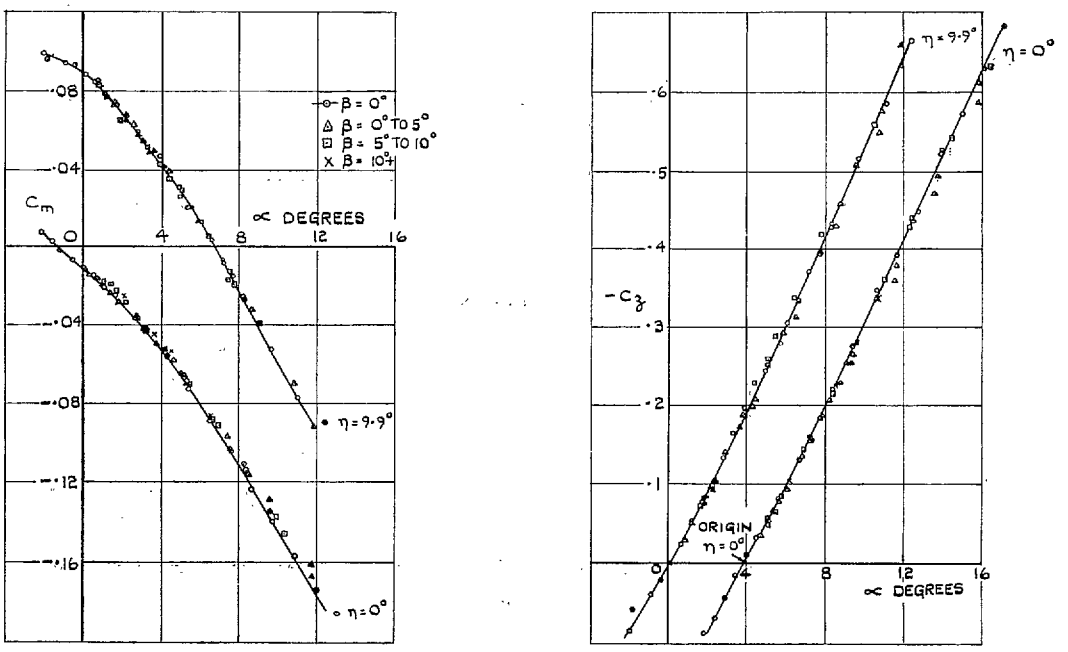

FIG. 8. Effect of β on C_m vs. α and $-C_z$ vs. α for configuration *BWCF*, $\eta = 0$ deg and $\eta = 9{\cdot}9$ deg at $M = 1{\cdot}40$.

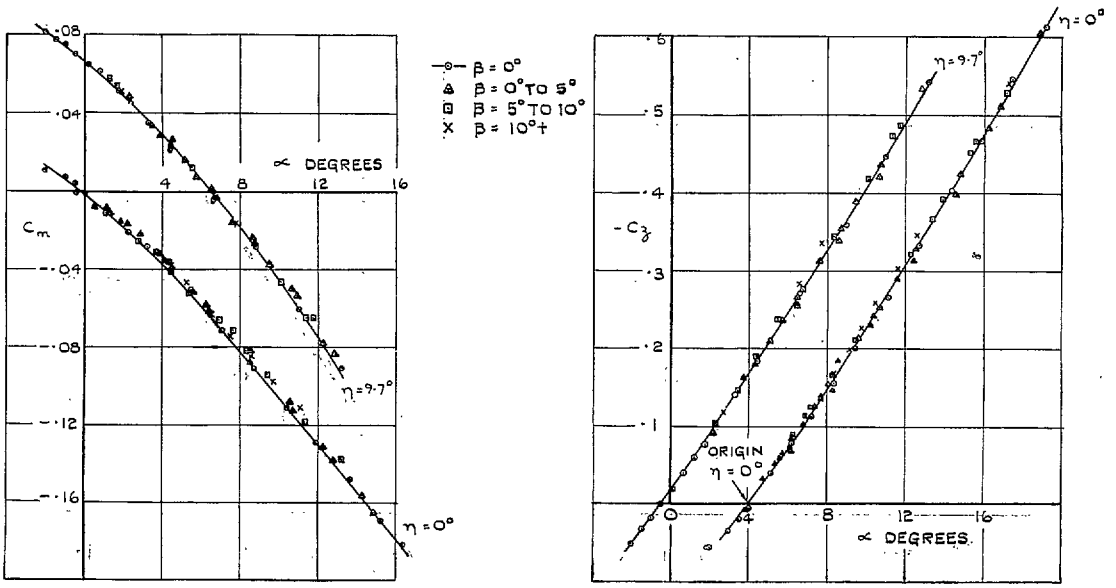

FIG. 9. Effect of β on C_m vs. α and $-C_z$ vs. α for configuration *BWCF* $\eta = 0$ deg and $\eta = 9{\cdot}7$ deg at $M = 2{\cdot}02$.

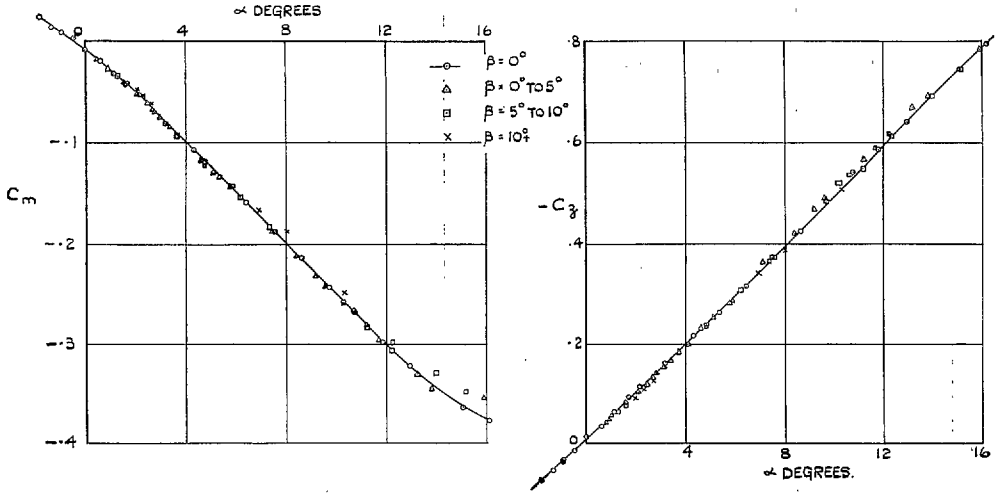

FIG. 10. Effect of β on C_m vs. α and $-C_z$ vs. α for configuration *BWF* at $M = 1{\cdot}40$.

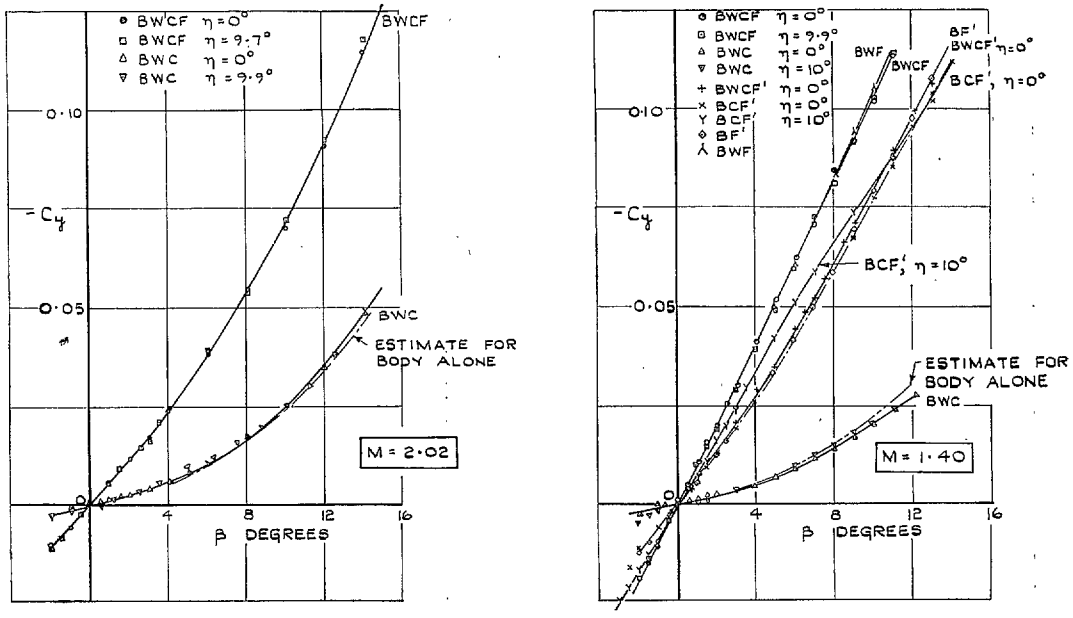

FIG. 11. Variation of $-C_y$ with β at $\alpha = 0$ deg for various configurations at $M = 1{\cdot}40$ and $M = 2{\cdot}02$.

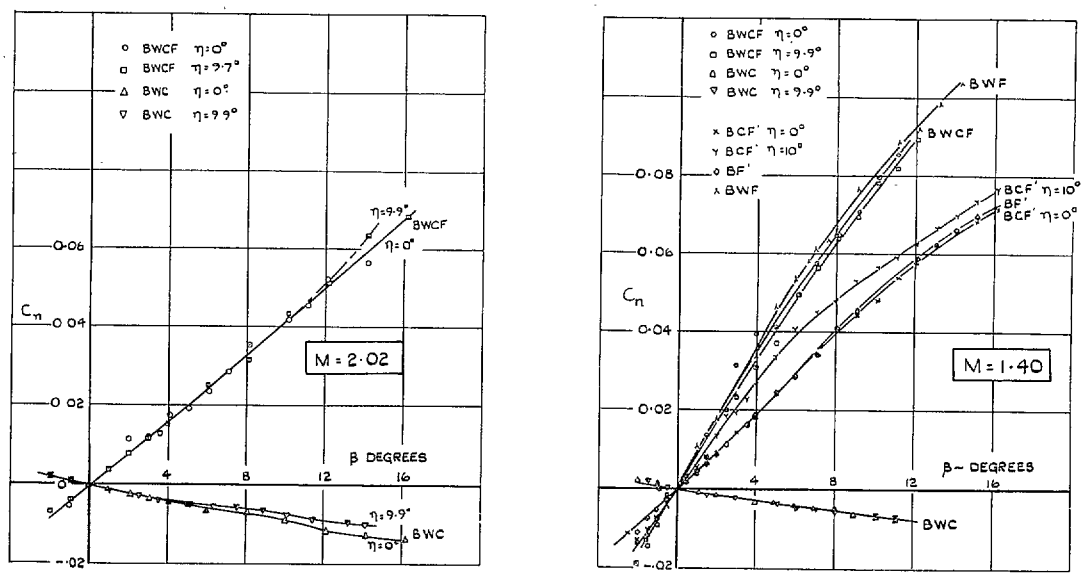

FIG. 12. Variation of C_n with β at $\alpha = 0$ deg for various configurations at $M = 1{\cdot}40$ and $M = 2{\cdot}02$.

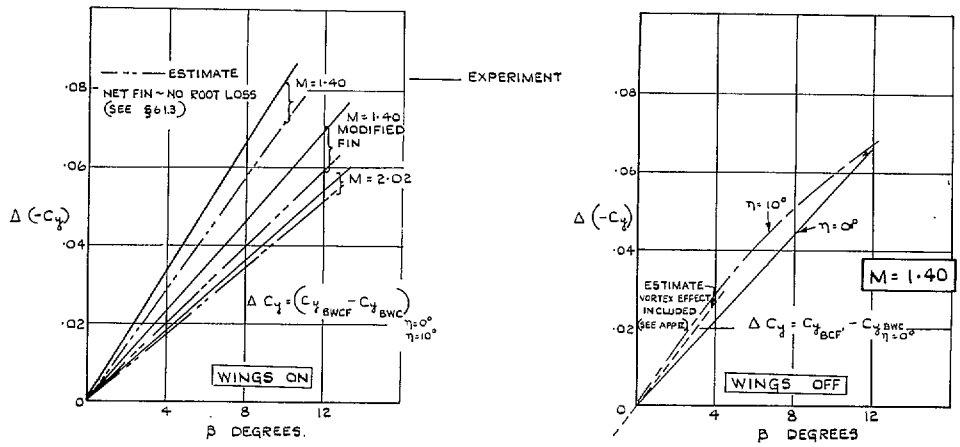

FIG. 13. Variation of $\Delta(-C_y)$ with β for 'derived' fin at $\alpha = 0$ deg.

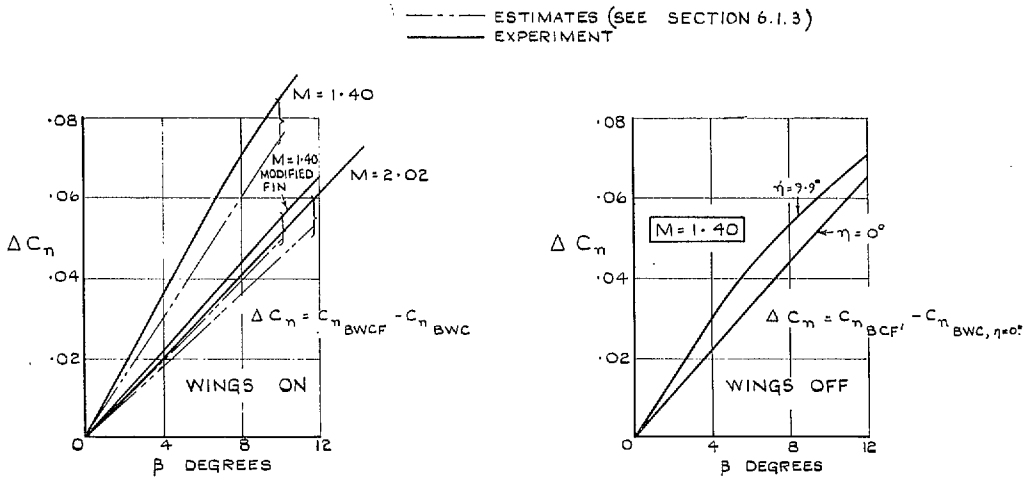

FIG. 14. Variation of ΔC_n with β for 'derived' fin at $\alpha = 0$ deg.

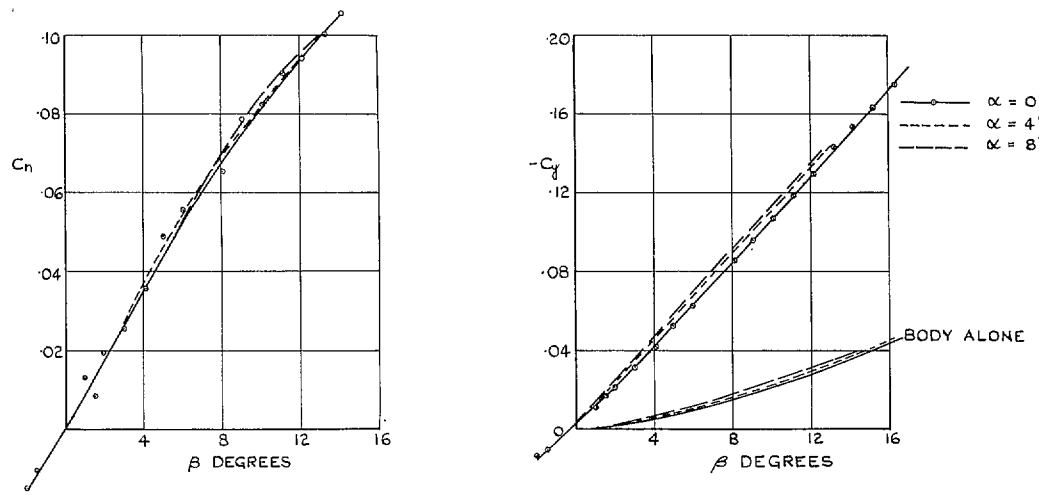

FIG. 15. Effect of α on C_n vs. β and $-C_y$ vs. β for configuration BWF at $M = 1{\cdot}40$.

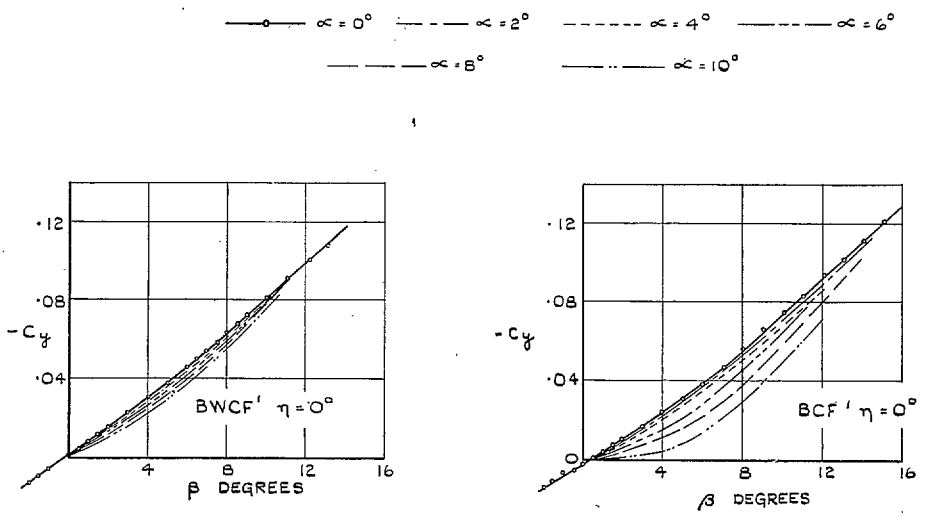

FIG. 16. Effect of α on $-C_y$ vs. β for configurations *BWCF'* and *BCF'*, $\eta = 0$ deg, at $M = 1{\cdot}40$.

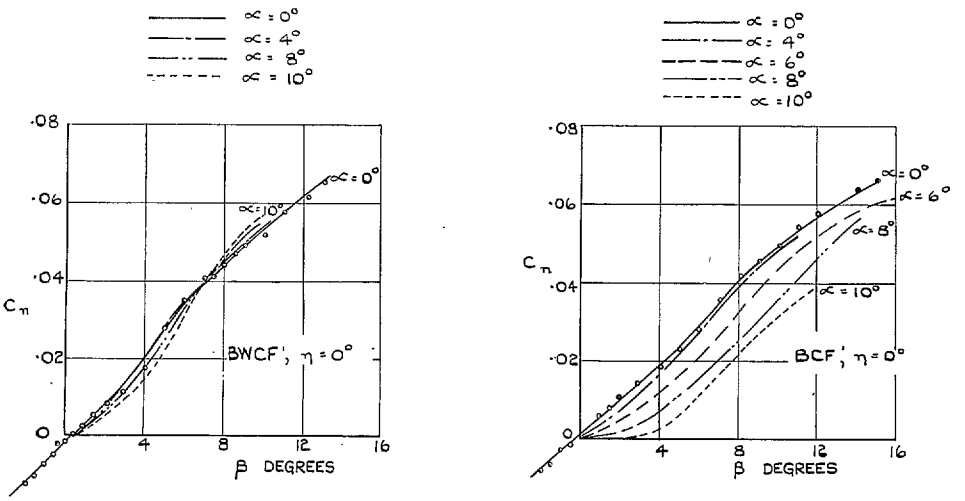

FIG. 17. Effect of α on C_n vs. β for configurations *BWCF'* and *BCF'*, $\eta = 0$ deg at $M = 1{\cdot}40$.

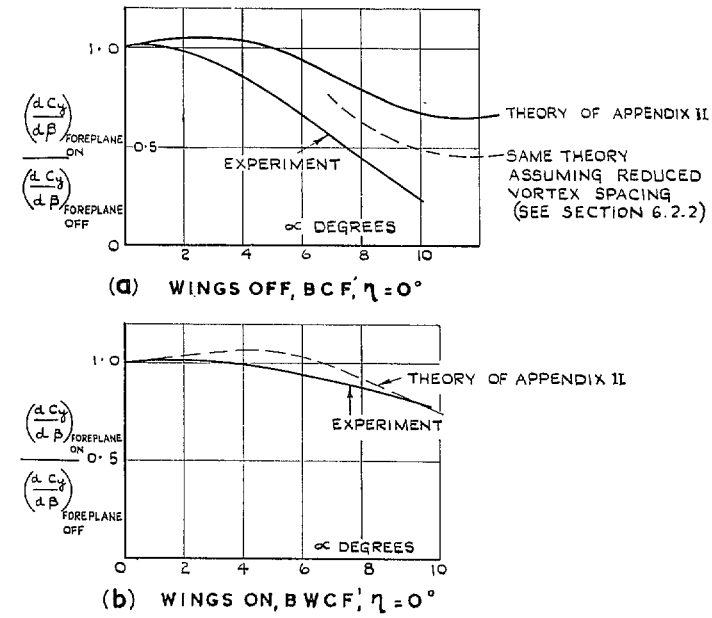

FIG. 18a and b. Effect of foreplane vortices on $\partial C_y/\partial\beta$ at $M = 1{\cdot}40$.

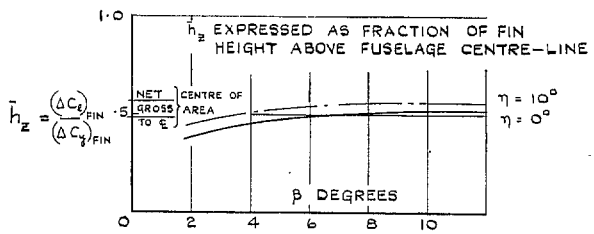

FIG. 19. Variation of fin vertical centre of pressure $\bar{h}_z$ for BCF' at $\alpha = 0$ deg, $M = 1{\cdot}40$.

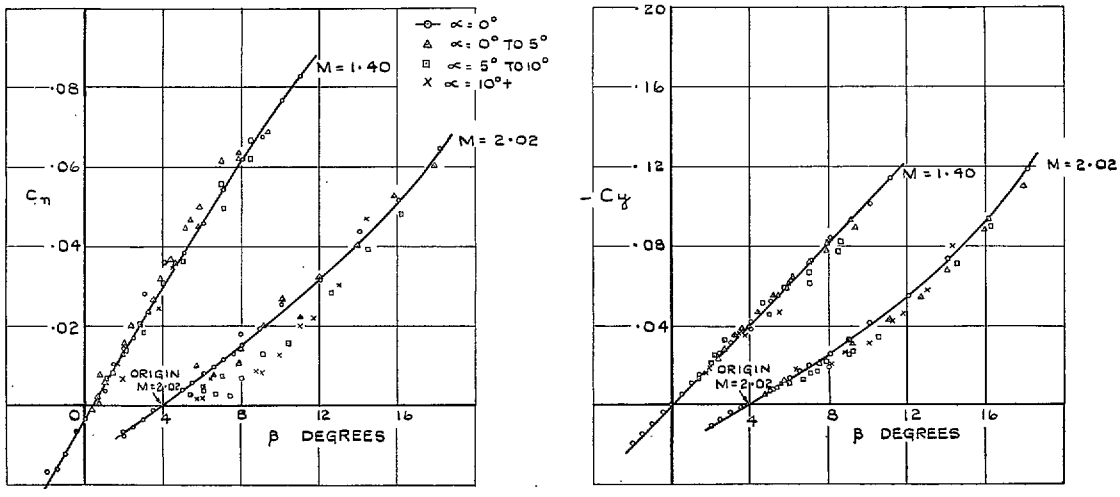

FIG. 20. Variation of $-C_y$ vs. β and C_n vs. β ($\alpha \neq 0$ deg) for configuration $BWCF$, $\eta = 9{\cdot}9$ deg at $M = 1{\cdot}40$ and $M = 2{\cdot}02$.

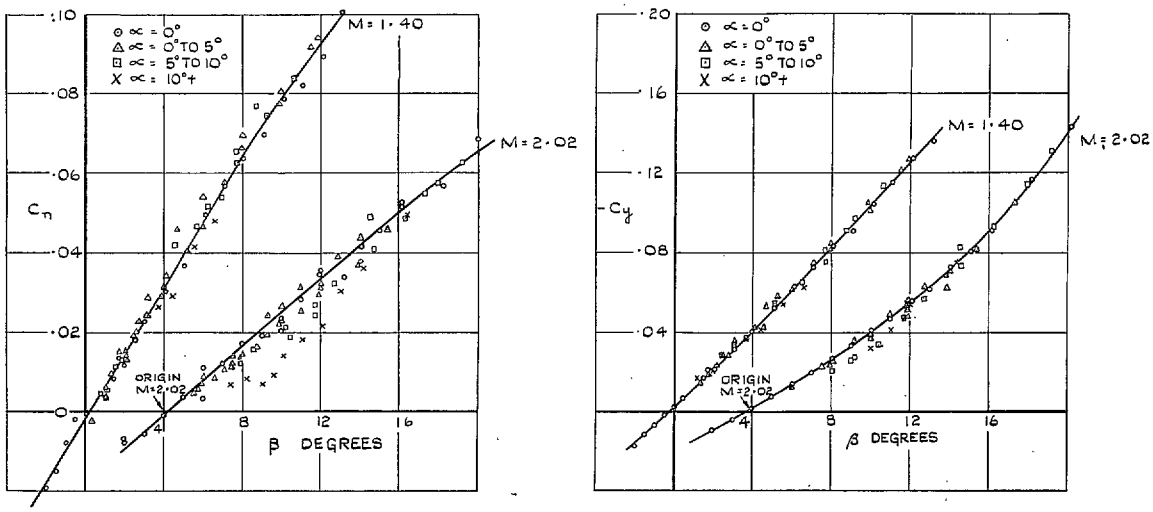

FIG. 21. Variation of $-C_y$ vs. β and C_n vs. β ($\alpha \neq 0$ deg) for configuration $BWCF$, $\eta = 0$ deg at $M = 1{\cdot}40$ and $M = 2{\cdot}02$.

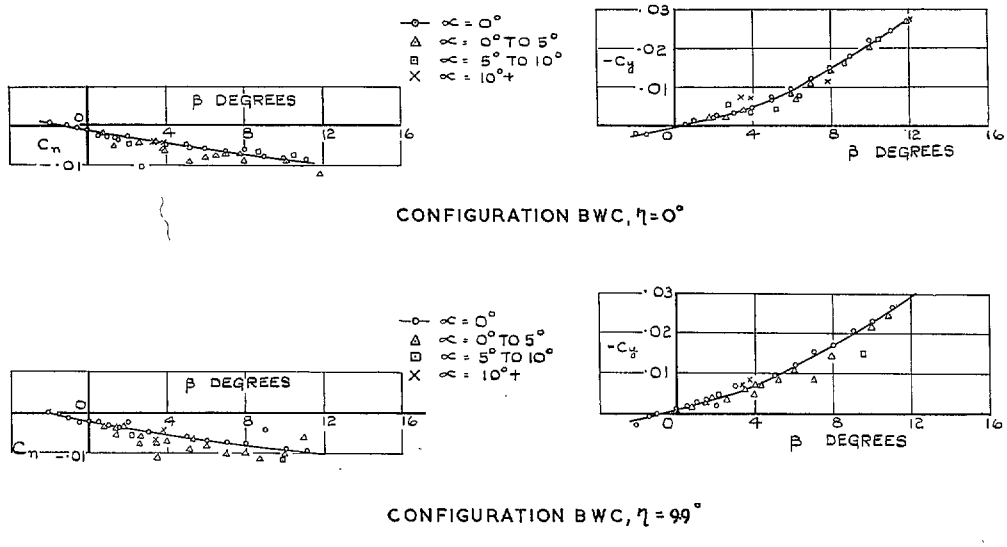

FIG. 22. Variation of $-C_y$ vs. β and C_n vs. β ($\alpha \neq 0$ deg) for configurations BWC, $\eta = 0$ deg and $\eta = 9{\cdot}9$ deg, $M = 1{\cdot}40$.

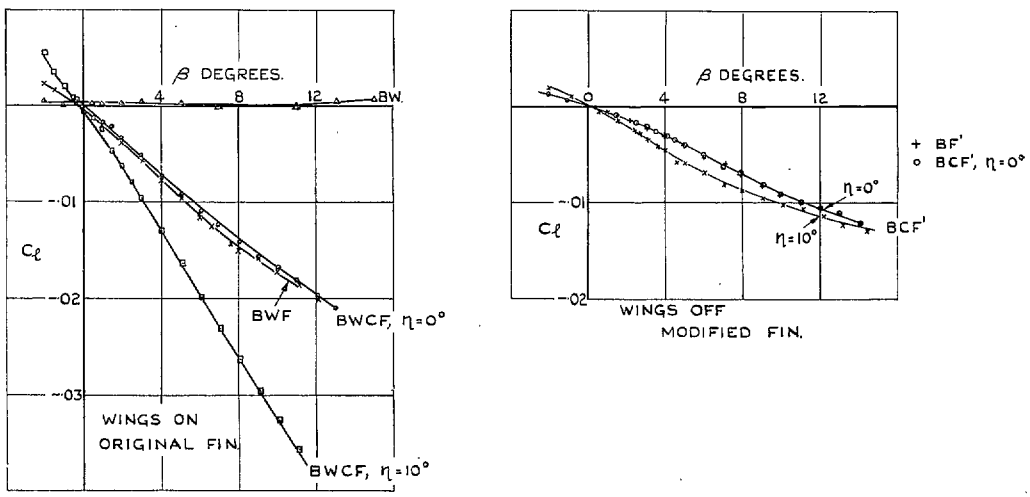

FIG. 23. C_l vs. β at $\alpha = 0$ deg for various configurations at $M = 1{\cdot}40$.

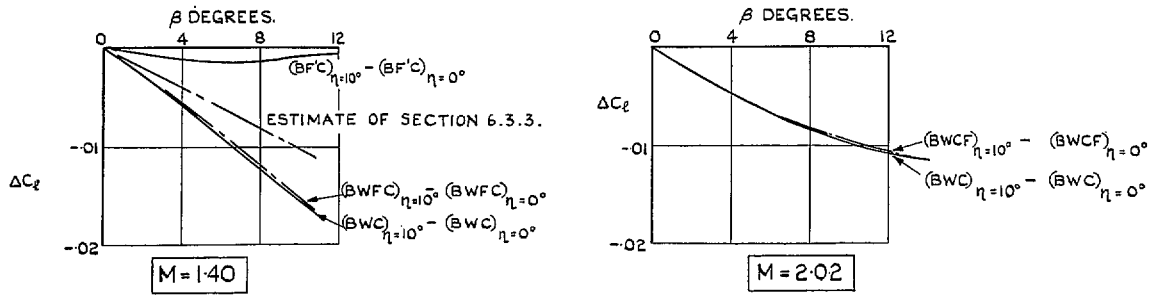

FIG. 24. Change in rolling moment due to canard control deflection, $\alpha = 0$ deg, at $M = 1{\cdot}40$ and $M = 2{\cdot}02$.

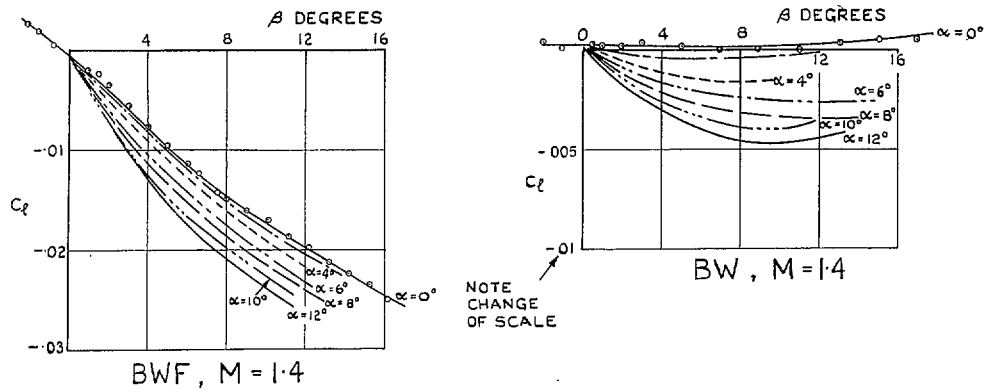

FIG. 25. Effect of α on C_l vs. β for configurations BWF and BW at $M = 1{\cdot}40$.

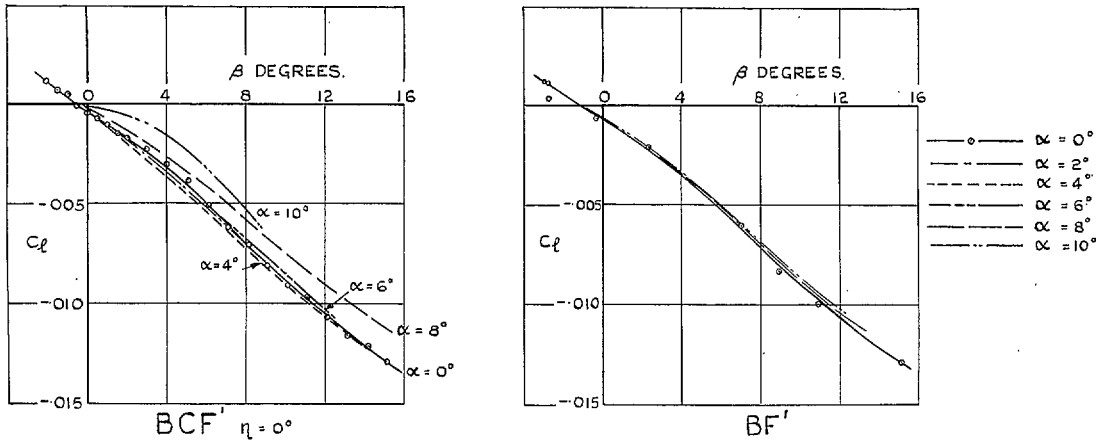

FIG. 26. Effect of α on C_l vs. β for configurations BCF', $\eta = 0$ deg and BF' at $M = 1{\cdot}40$.

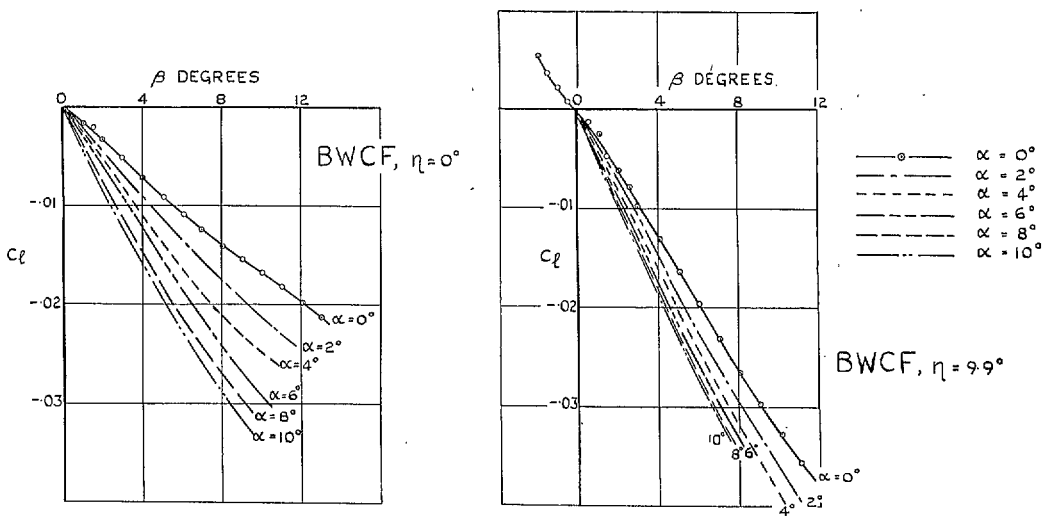

FIG. 27. Effect of α on C_l vs. β for configurations $BWCF$, $\eta = 0$ deg and $\eta = 9{\cdot}9$ deg at $M = 1{\cdot}40$.

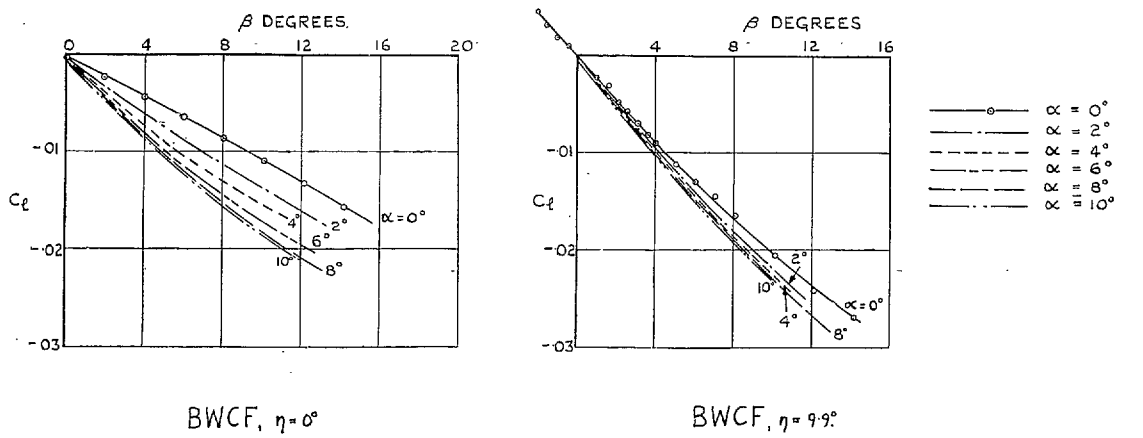

FIG. 28. Effect of α on C_l vs. β for configuration *BWCF*, $\eta = 0$ deg and $\eta = 9{\cdot}9$ deg at $M = 2{\cdot}02$.

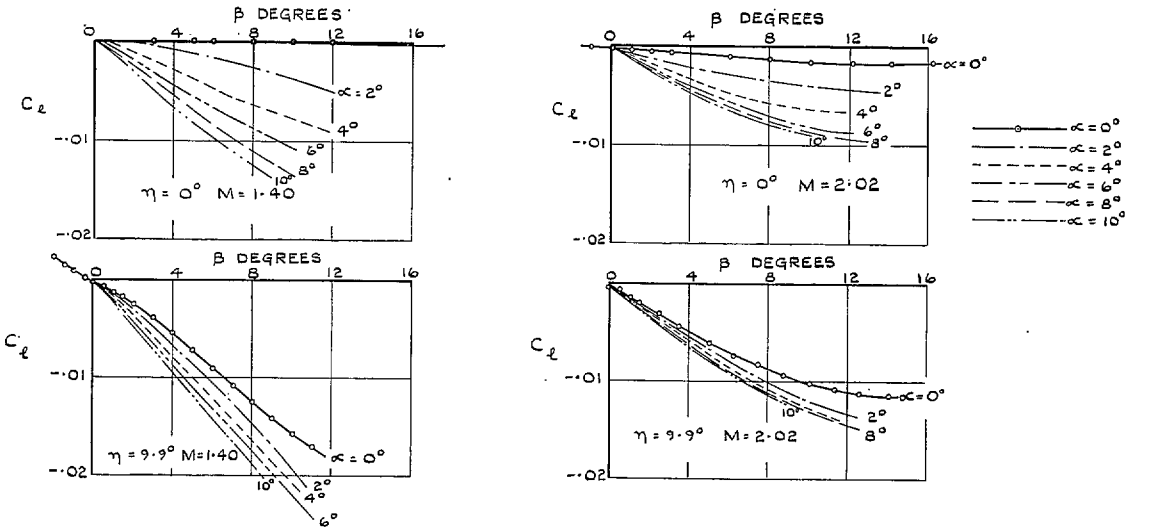

FIG. 29. Effect of α on C_l vs. β for configurations *BWC*, $\eta = 0$ deg and $\eta \simeq 10$ deg at $M = 1{\cdot}40$ and $M = 2{\cdot}02$.

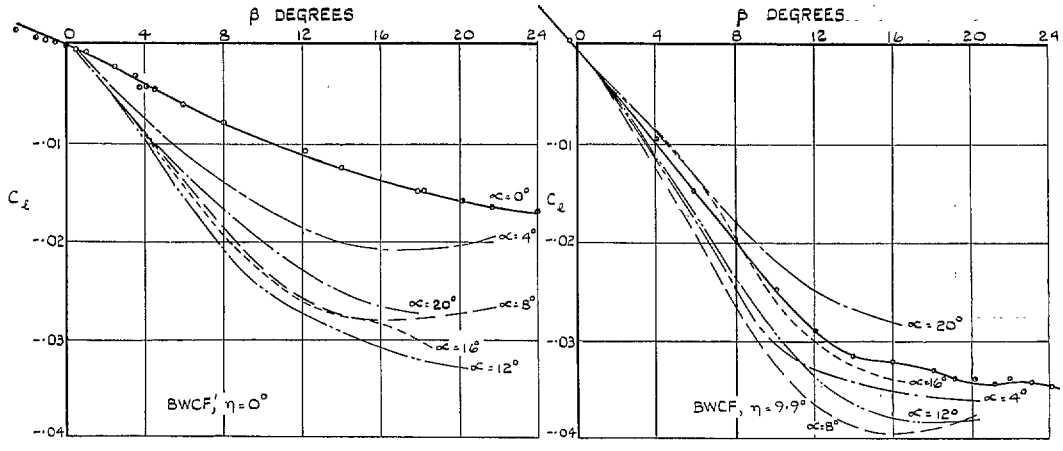

FIG. 30. Effect of large α on C_l vs. β for configurations $BWCF'$, $\eta = 0$ deg and $\eta = 9{\cdot}9$ deg at $M = 1{\cdot}40$.

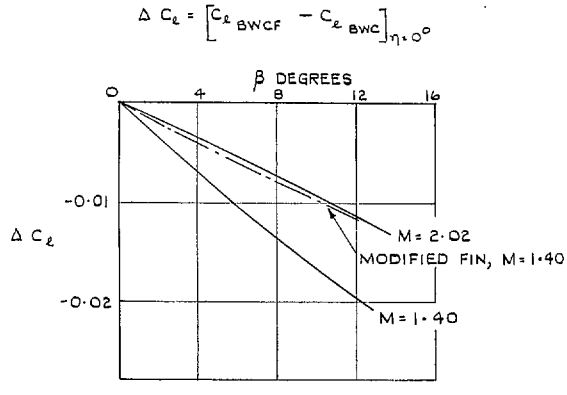

FIG. 31. ΔC_l vs. β due to fin contribution.

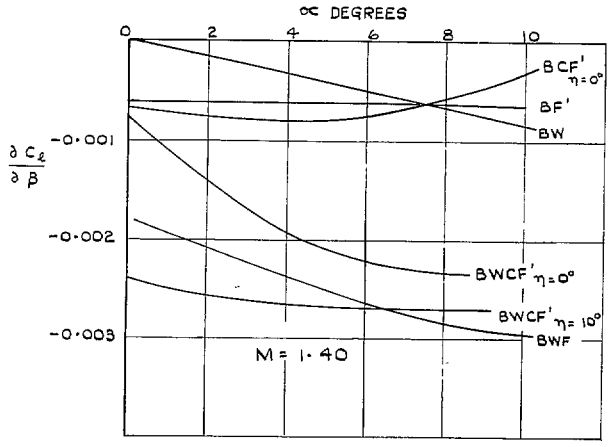

FIG. 32. Variation of $\partial C_l/\partial\beta$ with α for various configurations at $M = 1{\cdot}40$.

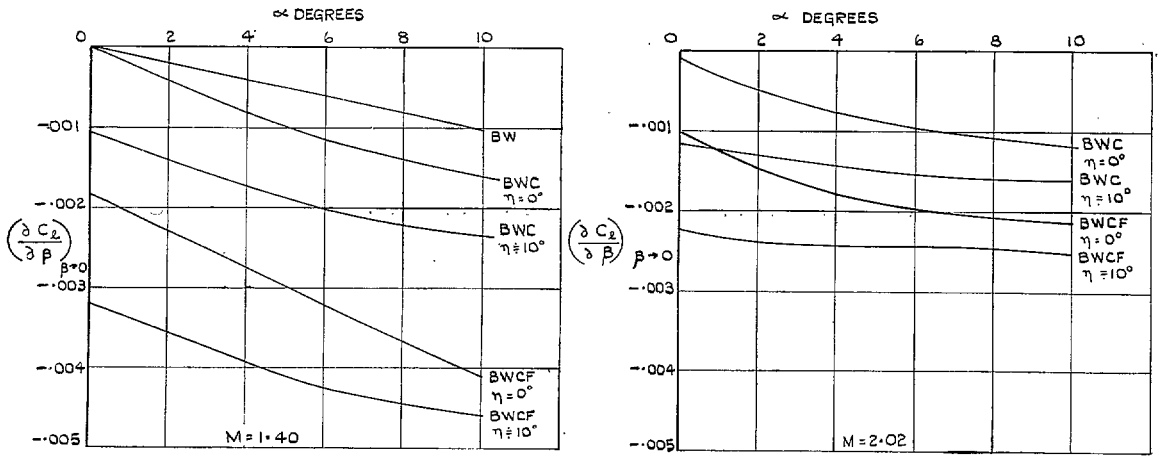

FIG. 33. Variation of $\partial C_l/\partial\beta$ with α for configurations *BWCF* and *BWC* at $M = 1{\cdot}40$ and $M = 2{\cdot}02$.

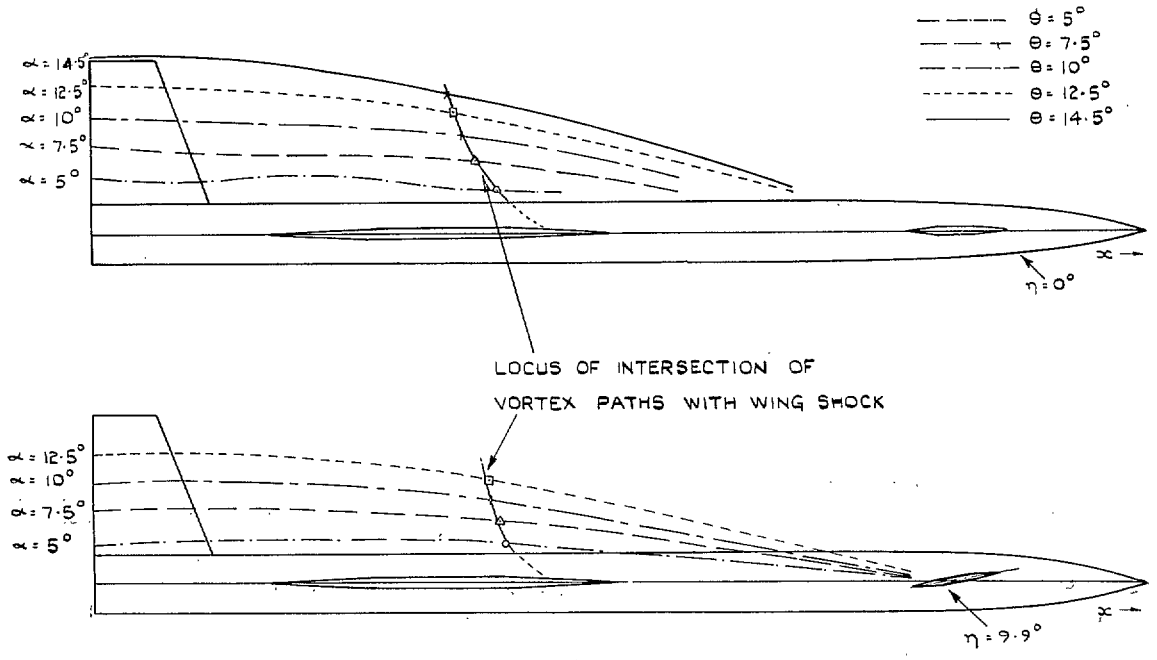

FIG. 34. Vortex paths at various α for configuration with wings on at $M = 2{\cdot}02$.

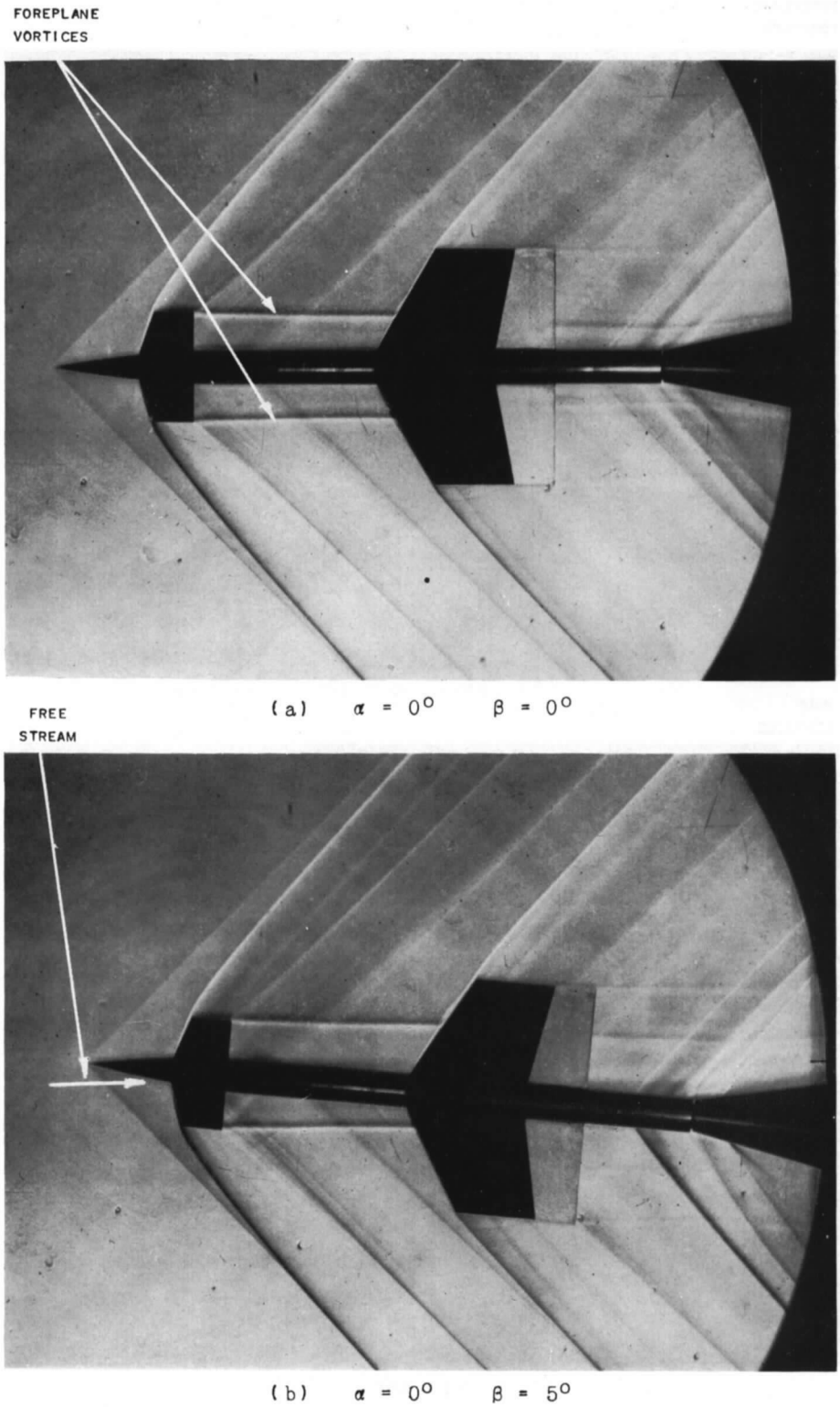

FIG. 35. Schlieren photographs of *BWC*, $\eta = 10$ deg, $\alpha = 0$ deg, plan view at $M = 1{\cdot}40$.

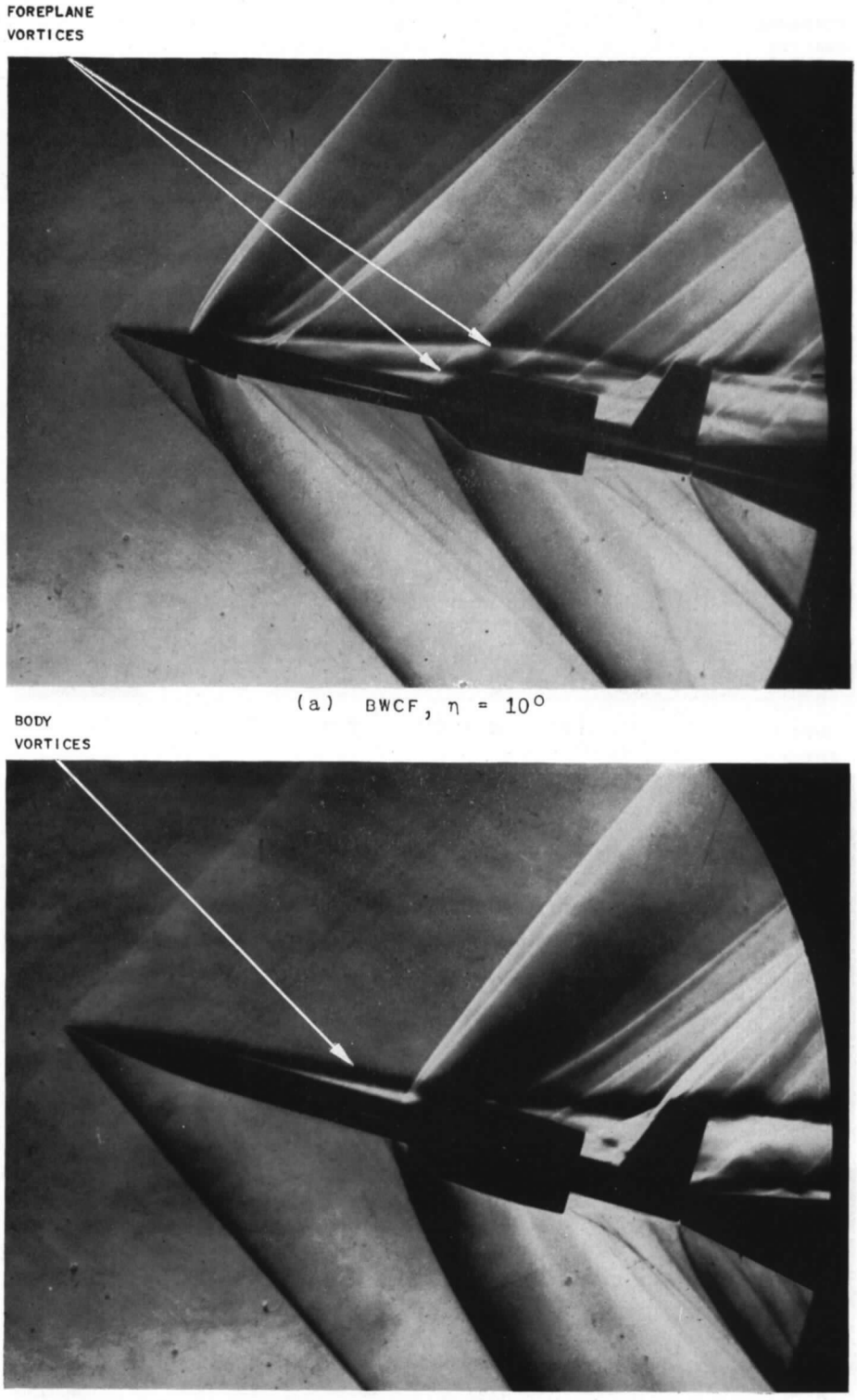

FIG. 36. Schlieren photographs *BWCF*, $\eta = 10$ deg and *BWF*, $\alpha \simeq 11$ deg, $\beta \simeq 9$ deg at $M = 1{\cdot}40$.

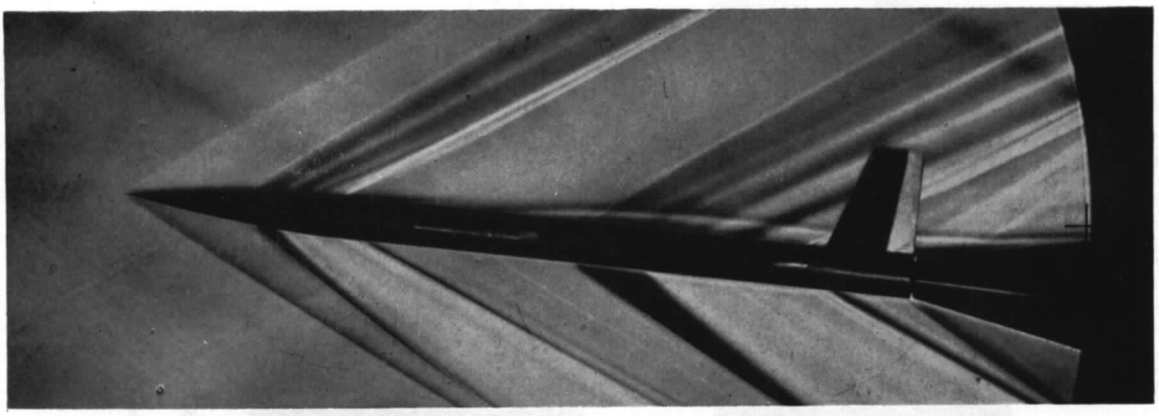

(a) $\alpha = 5^{\circ}$ $\beta = 0^{\circ}$

(b) $\alpha = 7.5^{\circ}$ $\beta = 0^{\circ}$

(c) $\alpha = 10^{\circ}$ $\beta = 0^{\circ}$

FIG. 37. Schlieren photographs *BWCF*, $\eta = 10$ deg for various α at $\beta = 0$ deg, $M = 2{\cdot}02$.

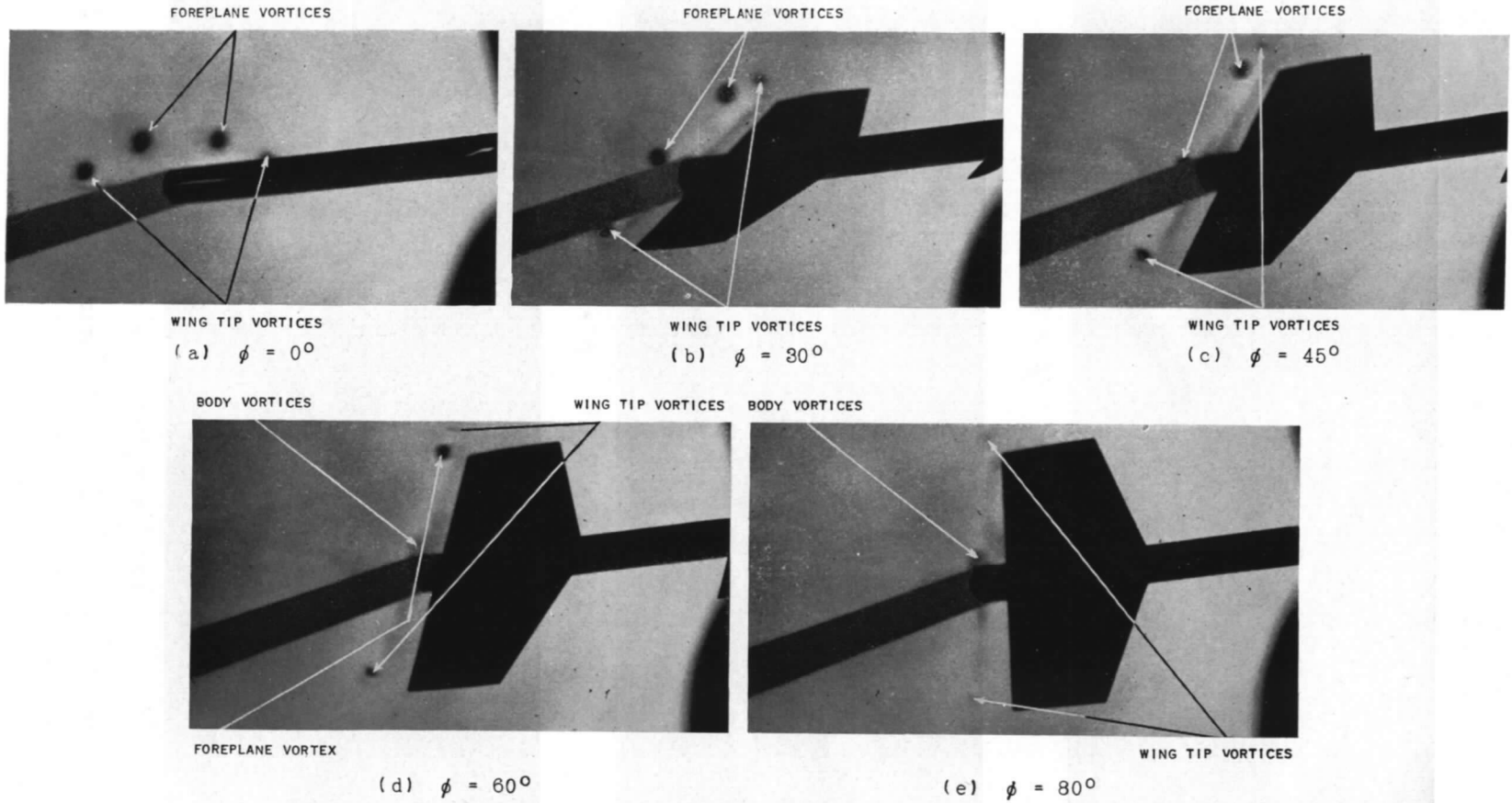

FIG. 38. Vapour screen photographs *BWCF'*, $\eta = 10$ deg, $\theta \simeq 10$ deg for various ϕ at $M = 1{\cdot}40$.

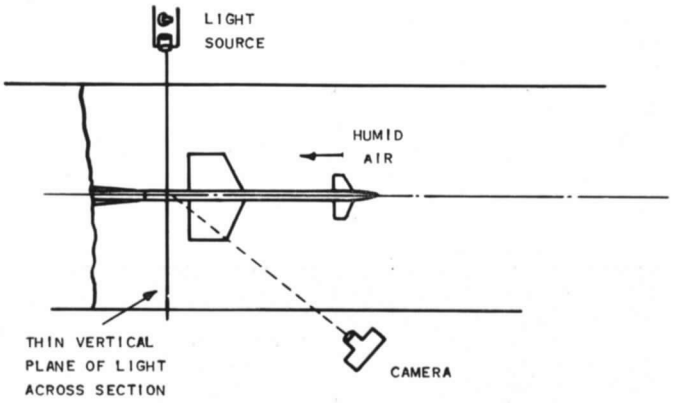

DIAGRAMMATIC LAYOUT FOR PRODUCING VAPOUR SCREEN PHOTOGRAPHS.

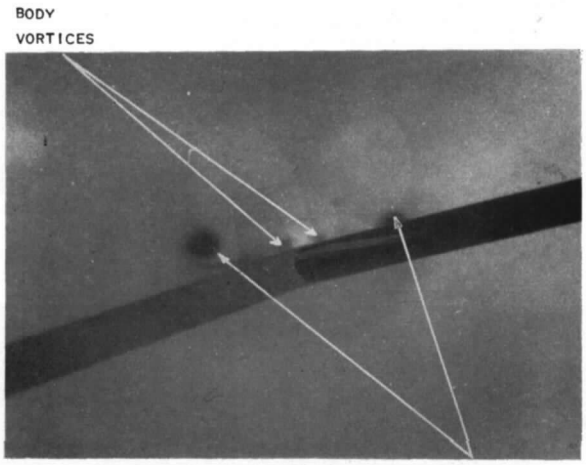

(a) $\phi = 0^{\circ}$

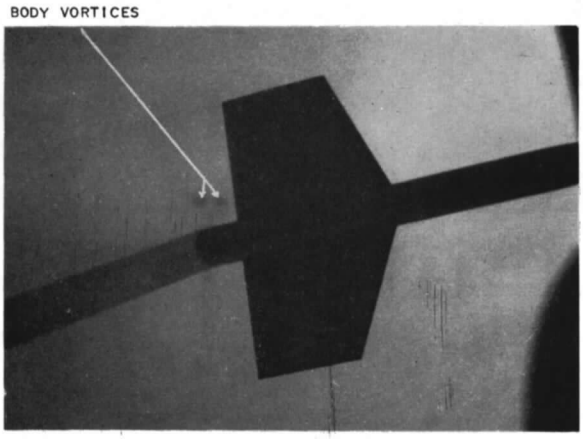

(b) $\phi = 90^{\circ}$

FIG. 39. Vapour screen photographs *BWF'*, $\theta = 10$ deg, $\phi = 0$ deg and 90 deg at $M = 1{\cdot}40$.

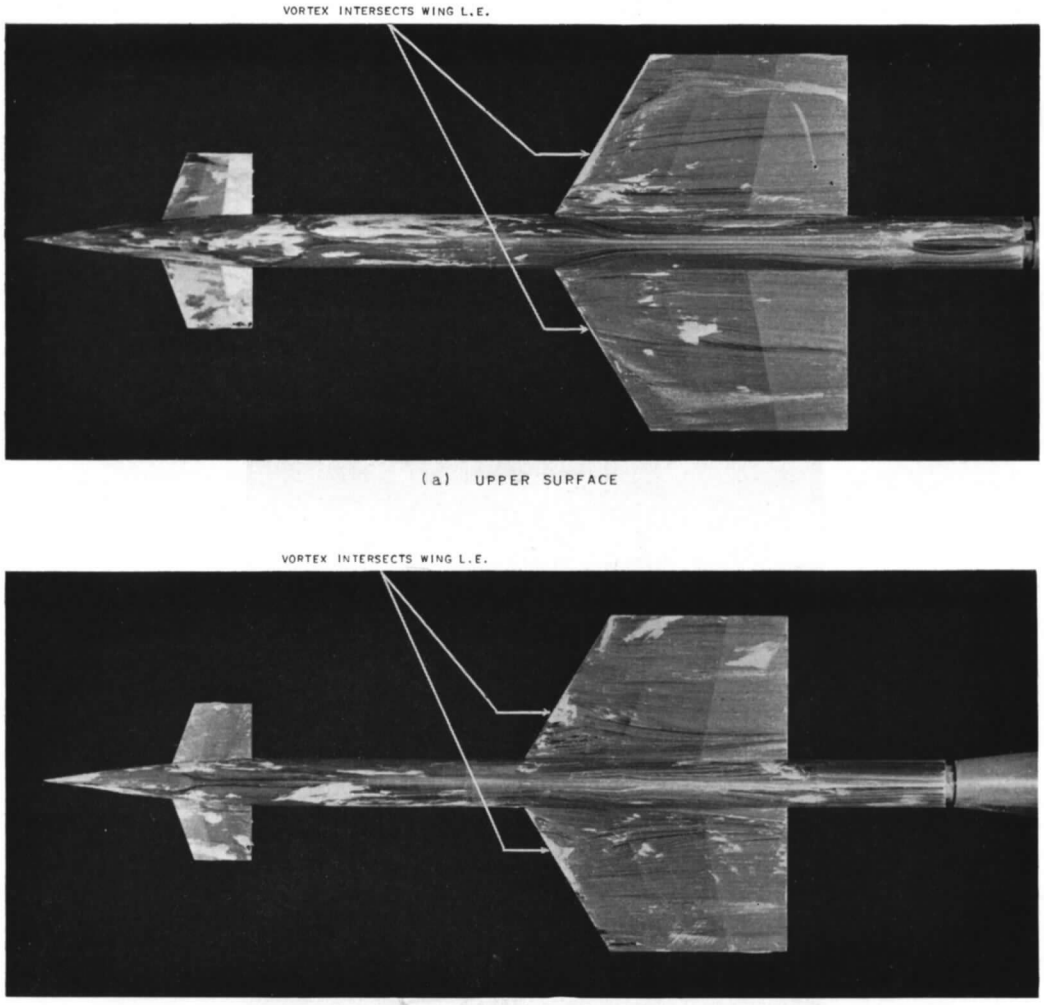

FIG. 40. Oil flow patterns $BWCF'$, $\eta = 10$ deg, $\alpha \simeq 0$ deg, $\beta = 0$ deg, $M = 1{\cdot}40$.

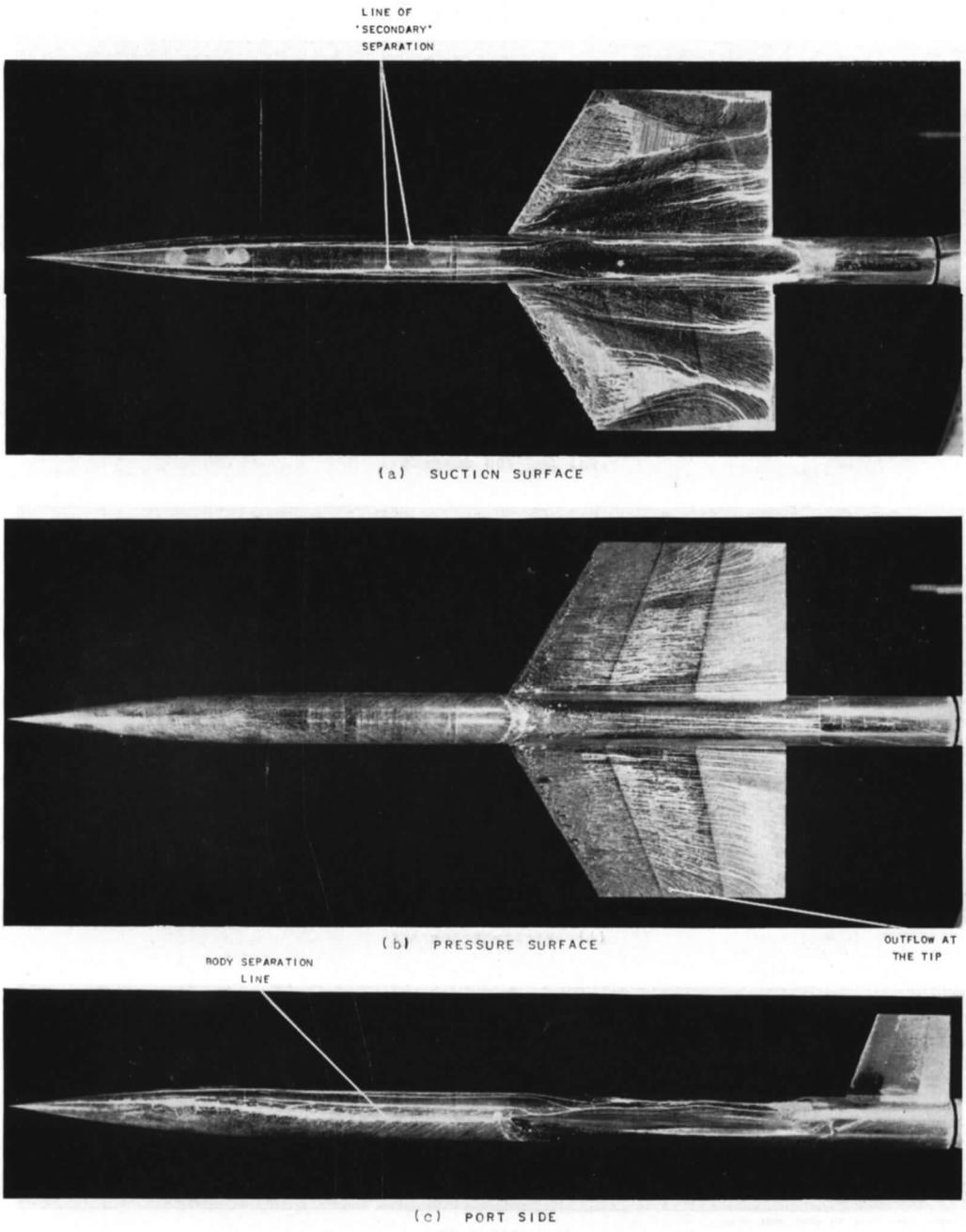

FIG. 41. Oil flow patterns BWF', $\alpha = 10$ deg, $\beta = 0$ deg, $M = 1{\cdot}40$.

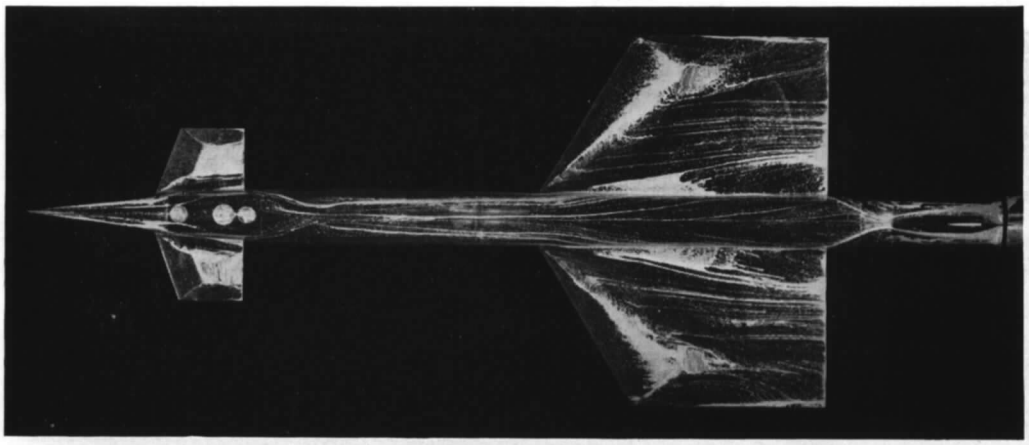

(a) SUCTION SURFACE

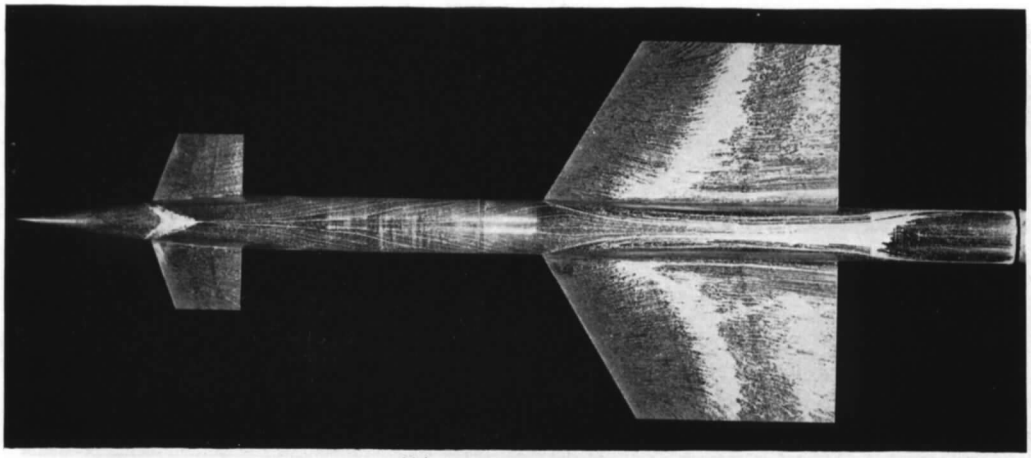

(b) PRESSURE SURFACE

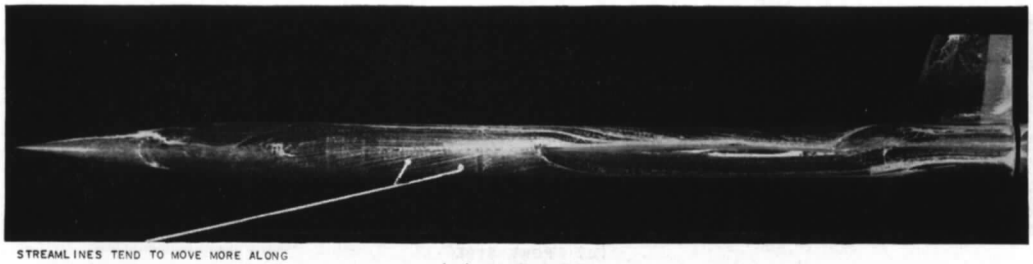

STREAMLINES TEND TO MOVE MORE ALONG THE BODY THAN WITH FOREPLANE OFF

(c) PORT SIDE

FIG. 42. Oil flow patterns $BWCF'$, $\eta = 0$ deg, $\alpha = 10$ deg, $\beta = 0$ deg, $M = 1{\cdot}40$.

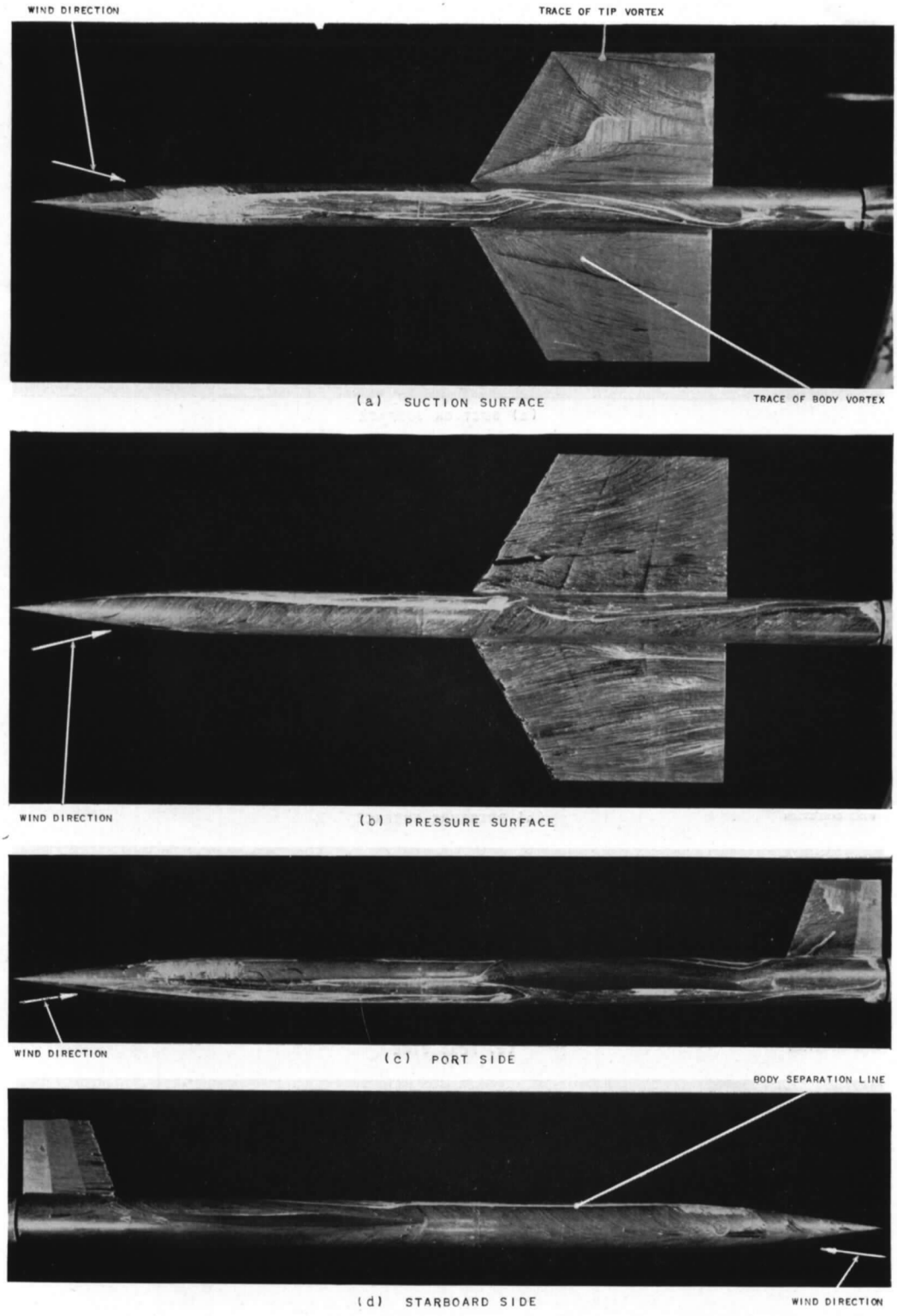

FIG. 43. Oil flow patterns BWF', $\alpha \simeq 7{\cdot}5$ deg, $\beta \simeq 13$ deg at $M = 1{\cdot}40$.

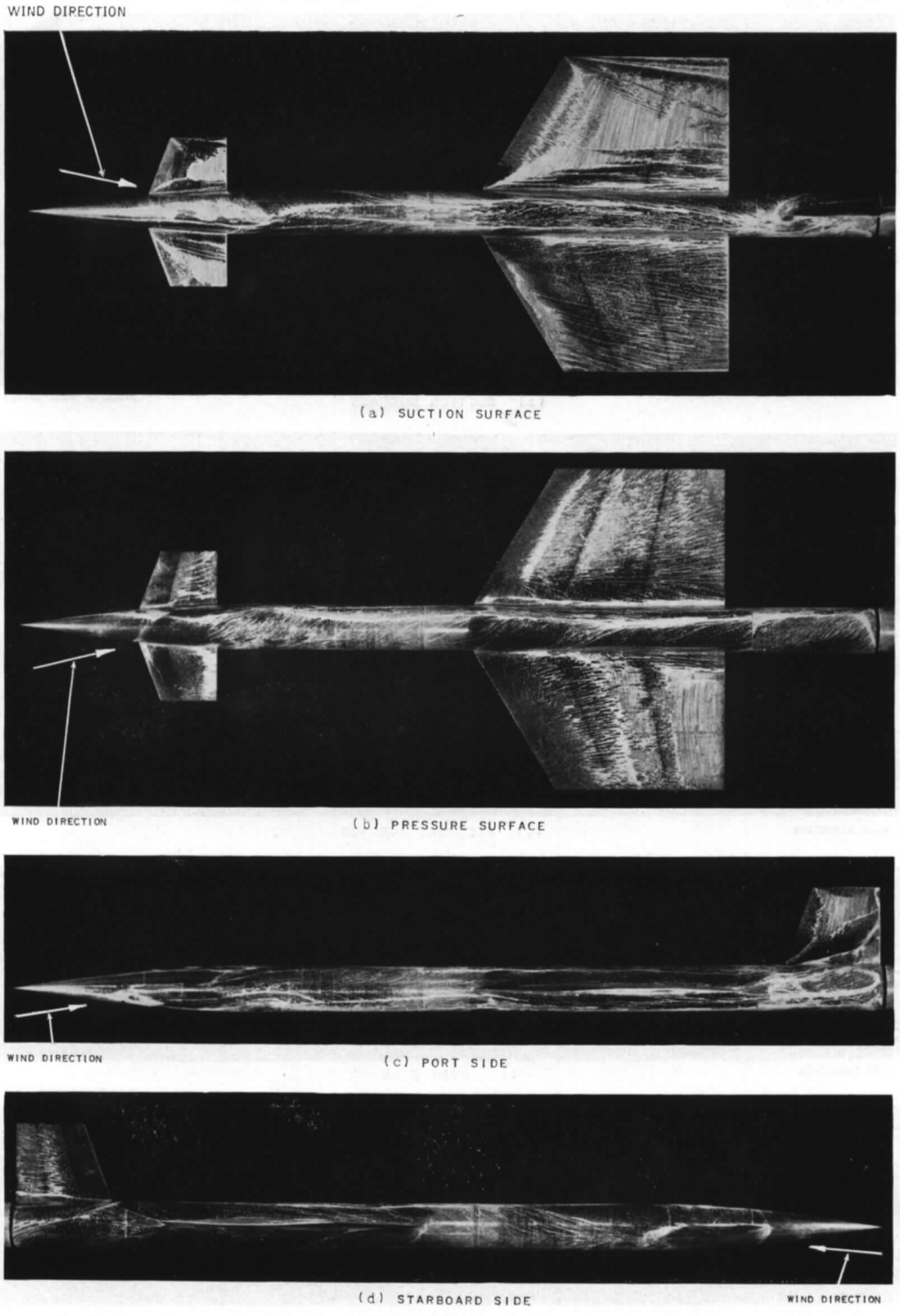

FIG. 44. Oil flow pattern *BWCF'*, $\eta = 0$ deg, $\alpha \simeq 7{\cdot}5$ deg, $\beta \simeq 13$ deg at $M = 1{\cdot}40$.

PART II

Summary. Tests were made in the R.A.E. No. 8 (9 in. × 9 in.) Supersonic Wind Tunnel to measure the overall normal and side forces, rolling, pitching and yawing moments on a typical canard aircraft layout at $M = 2{\cdot}47$. These tests are an extension of those at $M = 1{\cdot}40$ and $M = 2{\cdot}02$ recorded in Part I of this R. & M.

The foreplane lifting effectiveness, although still reduced due to the download induced on the mainplane, is greater than at the lower Mach numbers. The neutral point, $\partial C_m/\partial C_z$, is further aft at the higher Mach number and shows less variation with incidence; neither normal force nor pitching moment is affected significantly by sideslip.

There is a large negative rolling moment induced by foreplane-wing interference when positive sideslip is applied. This rolling moment increases with increase of incidence and foreplane setting.

$\partial C_n/\partial\beta$ at $\alpha = 0$ deg is considerably reduced (compared with $M = 1{\cdot}40$) and shows further reduction with increasing α, and for the moment reference chosen becomes negative for $\alpha > 7$ deg.

The tests emphasise that considerable attention will have to be given to lateral and directional characteristics at the higher Mach numbers.

---

1. *Introduction.* Some time ago, the performance requirements for a long range supersonic aircraft had stimulated interest in the tail-first or canard aircraft layout. Since little was known of the stability characteristics exhibited by such a design at supersonic speeds, wind-tunnel tests were made at Mach numbers of 1·4 and 2·02 in the R.A.E. No. 19 (18 in. × 18 in.) supersonic wind tunnel. The tests were made on a typical canard design as a preliminary to a more comprehensive investigation and measurements of the static stability characteristics were made covering conditions of combined incidence and sideslip. The results of this investigation have been analysed and presented in Ref. 1. It was subsequently decided to extend the investigation to a higher Mach number, and the model and balance were therefore transferred to the R.A.E. No. 8 (9 in. × 9 in.) Supersonic Wind Tunnel where tests were made at a Mach number of 2·47.

The present report contains the results of these tests together with some further examination of the results of the earlier investigation.

2. *Description of the Model.* The model has already been described in Ref. 1 but for convenience the outline drawing is given in Fig. 1 and the leading dimensions quoted in Table 1. It should be noted that the fin used in the present tests is the 'modified' fin of Ref. 1. Care should be taken, therefore, in comparing lateral results in this and Ref. 1 which also contains results for the model with fin before modification.

3. *Test Arrangement and Accuracy.* 3.1. *Wind Tunnel.* The R.A.E. No. 8 (9 in. × 9 in.) Supersonic Wind Tunnel is a continuous flow, non-return tunnel with a nominal Mach number range of 1·4 to 2·6 with a square working section of 9 in. side at all Mach numbers. For the present tests the stagnation pressure was constant in any run at near atmospheric pressure and the stagnation temperature regulated to near 33 deg C giving a Reynolds number of approximately $0{\cdot}25 \times 10^6$ per inch.

The air for the tunnel is drawn in over an activated alumina bed to give air of humidity of less than 0·0003 lb of water per lb of air. The tunnel has a vertical quadrant incidence gear behind the working section which enables a polar incidence, θ, of $\pm$ 25 deg to be obtained. This can be varied

from outside the tunnel by electrical control and the geometric incidence given on a digital display. At the time of test the roll setting of the model could only be varied with the tunnel stopped, the roll angle being measured optically.

3.2. *Wind-Tunnel Balance System.* The model was supported by the same flexible sting as was used for the tests reported in Ref. 1 and the rolling moment again measured by a separate strain-gauged cantilever. The output signals from the strain-gauge bridge circuits were passed to self-balancing indicator units and the results computed to final coefficient form.

3.3. *Accuracy.* As noted in Ref. 1, it is difficult to assess precisely the overall accuracy of the results but the principal factors affecting this are discussed below.

3.3.1. *Balance accuracy.* Since no strict control could be kept of the tunnel stagnation temperature, measurements of the sting temperature were made throughout the tests and the necessary corrections to the balance readings determined from a temperature calibration of the sting, were incorporated in the reduction of the results. The most likely source of error is thus probably in the reading of the indicator units. This is estimated as $\pm$ 1 division in 500 divisions with the same possibility in the wind-off readings: on this basis the accuracy of observation expressed in coefficient form is

$$C_z = \pm 0{\cdot}006 \qquad C_y = \pm 0{\cdot}001$$
$$C_m = \pm 0{\cdot}002 \qquad C_n = \pm 0{\cdot}001.$$

In practice the errors are usually well within these limits. In the case of the rolling moment there is an additional source of error due to the friction in the rolling moment balance which leads to a possible error in C_l of $\pm$ 0·0002.

3.3.2. *Accuracy of model setting.* The roll angle was measured before each run using a telescope with protractor eyepiece whilst the incidence was measured from a stop repeater giving the geometric incidence and corrected for sting deflection under load. The final angular setting in α and β is believed to be accurate within $\pm$ 3 minutes of arc. These angular measurements however are taken relative to a gravity datum and no correction has been applied for any mean flow inclination in the working section as this is believed to be small.

3.3.3. *Accuracy of control setting.* No special control setting jig was available and so it was necessary to make the setting with an optical device. The accuracy is believed to be better than $\pm$ 0·1 deg for these tests.

3.3.4. *Uniformity of flow in the working section.* The nozzles for the tunnel have been calibrated for both Mach number and flow inclination, and the mean Mach number in the test section is

$$M = 2{\cdot}47 \pm 0{\cdot}015$$

whilst the flow variations are a maximum of $\pm$ 0·2 deg.

The tunnel stagnation pressure was kept constant within $\pm$ 0·1 inch of water during each run so that the variation of kinetic pressure in the working section was negligible.

4. *Presentation and Procedure.* 4.1. *Data Presentation.* With the balance arrangement used the forces and moments were all measured either normal to or in the plane of the aircraft wings (the sting rotating with the model); this led to the adoption of a right-hand system of body axes

Oxyz, *see* Fig. 2, with the polar incidence θ and the roll angle ϕ, the angles set in the tunnel. The data has, however, been plotted as functions of the incidence angle, α, and the sideslip angle, β, defined in terms of θ and ϕ as follows

$$\alpha = \sin^{-1}(\sin\theta\cos\phi)$$

$$\beta = \sin^{-1}(\sin\theta\sin\phi).$$

It should be noted that this 'sine' definition differs slightly from that adopted for presentation of most subsonic tests and for many American tests. The differences involved in the incidence range considered are, however, barely significant.

In the reduction of moments and forces to coefficient form the reference area has been taken as that of the gross wing (8·28 sq in.); the reference length for the longitudinal pitching moment, C_m, (measured about the line joining the wing root leading edge) is the mean aerodynamic chord $\bar{\bar{c}}$ (2·40 in.) whilst that for the lateral moments C_n and C_l is the gross wing span, b (3·50 in.).

The control setting angle, η, was defined as the angle between the control chord line and the body axis Ox, and was positive in the same direction as α.

For convenience in referring to different configurations the following notation will be used throughout the report:

B	Body
W	Wing
F'	Fin—modified as detailed in Ref. 1
C	Foreplane control.

Thus $BWCF'$, $\eta = 0$ indicates the complete configuration with zero control-setting angle.

When slopes of curves are given the values are for $\alpha \to 0$ deg or $\beta \to 0$ deg unless specifically stated to the contrary. It is important to note this fact as some curves show change of slope at quite low angles of incidence or sideslip.

4.2. *Test Procedure and Scope of Tests.* The programme for these tests has been kept as limited as possible due partly to other commitments for the tunnel and also because a larger programme on canard aircraft had been planned at the time. Only configurations $BWCF'$, $\eta = 0$ and BCF', $\eta = 0$ deg have been tested over the whole range of combined α and β but various other configurations have been tested for conditions of either $\beta = 0$ deg and varying α, or $\alpha = 0$ deg and varying β.

The incidence range for some tests (e.g., $BWCF'$) was limited by the deflection of the sting causing it to touch the wind shield. The practice adopted was to test the configuration at constant values of ϕ for varying θ with closer intervals of θ near the origin up to the limiting value of θ as determined by sting deflection.

5. *Discussion of Longitudinal Results.* As in Ref. 1 the discussion will be concerned initially with results at zero sideslip and then with results for conditions of combined incidence and sideslip with further sub-divisions in each case for varying model configurations. Whilst this method of presentation gives in certain cases a rather arbitary division of the data it is believed to be the most helpful in discussing the whole investigation.

5.1. *Zero Sideslip.* 5.1.1. *Foreplane off.* The $-C_z$ vs. α and C_m vs. α, at $\beta = 0$ deg, curves for configurations B and BW are plotted in Fig. 3. The body alone (B) curves show the expected non-linear variation with incidence.

The non-linearities present in the body-wing (BW) characteristics with incidence are primarily due to the body contribution (*i.e.*, due to the body vortices), as can be seen from Fig. 4. Here the 'derived' wing results, determined by the subtraction of the BW and B results at corresponding incidences, are shown to be approximately linear functions of incidence. Estimates based on Ref. 2 are given and show similar agreement to that noted at $M = 1{\cdot}40$.

5.1.2. *Wing off.* This section is concerned with the $-C_z$ vs. α and C_m vs. α results for configurations BCF', $\eta = 0$ deg and $\eta = 10$ deg. If the 'derived' control results of Fig. 4 are compared with those for BCF' in Fig. 3, the non-linearities in the latter will again be seen to be mainly due to the body contribution. As for the 'derived' wing the 'derived' control results have been estimated using the methods of Ref. 2 and are included in Fig. 4 for comparison with the experimental values. The agreement between theory and experiment is qualitatively similar to those noted at $M = 1{\cdot}40$.

5.1.3. *Complete configuration.* Examination of Fig. 3 shows that the lift increment due to the addition or deflection of the foreplane is reduced when the wing is present. This effect is similar to that found in the tests at $M = 1{\cdot}40$[1] although at the higher Mach number the proportionate lift reduction is somewhat smaller. This reduction in foreplane effectiveness, which is attributed to the interference effects on the main wing of the velocities induced by the foreplane, is discussed in more detail in Section 5.1.4. The variation of C_m with C_z is given in Fig. 5 and the corresponding variation of $\partial C_m/\partial C_z$ with incidence is shown in Fig. 6; this is given for $\eta = 0$ since there is little significant change with η. In this latter figure the results for $M = 2{\cdot}02$ and $1{\cdot}40$ have been added for comparison. It is seen that there is a progressive rearward movement of the neutral point, $\partial C_m/\partial C_z$, at small α, with increase in Mach number, but the rearward movement with increasing incidence is much reduced as the Mach number increases. The rearward movement in the neutral point with Mach number is qualitatively in agreement with estimates based on Ref. 2 but as yet there is no satisfactory method of predicting the variation with incidence.

5.1.4. *Foreplane efficiency.* In Ref. 1 it was pointed out that when considering the interference effect of a forward surface on another larger surface mounted behind it, it is best to consider the interference force primarily as a function of the load on the forward surface. This led to the adoption of the definition of force or moment efficiency of the foreplane in the presence of the wing as follows:

$$\bar{\eta}_Z = \frac{C_{z.BWC} - C_{z.BW}}{C_{z.BC} - C_{z.B}} \qquad \bar{\eta}_M = \frac{C_{m.BWC} - C_{m.BW}}{C_{m.BC} - C_{m.B}}.$$

These definitions are retained in the present report and in Fig. 7 curves of $\bar{\eta}_Z$ and $\bar{\eta}_M$ are plotted against incidence for the case of $\eta = 0$ deg and $\eta = 10$ deg. If the curves of $\bar{\eta}_Z$ vs. α from Fig. 7 are compared with those for $M = 1{\cdot}40$ in Ref. 1 it will be seen that the foreplane lift efficiency (as defined above) is considerably increased, particularly at the smaller incidences, by increase of Mach number, which is consistent with the trends noted from the limited tests at $M = 2{\cdot}02$, also reported in Ref. 1.

Estimates have been made of the loading on a surface due to vortices using the available methods and curves of $\bar{\eta}_Z$ and $\bar{\eta}_M$, based on these estimates, are given for comparison on Fig. 7. There are three main methods available and they are considered in turn with some attempt to assess their range of application.

(*a*) *Slender-body theory.* In Ref. 3 Sacks has shown explicitly, using this theory, that the induced download is composed of two parts: one equal and opposite to that of the forward surface and the other a function of the strength and position of the vortices generated by the forward surface. For the special case of the vortices in the plane of the rear surface this theory shows that only the first part is applicable and that the induced download is equal to the foreplane load if the mainplane span exceeds that of the foreplane.

The configuration under consideration is not really slender in the sense of the theory but the theory gave a reasonable prediction (at low incidence) and at $M = 1{\cdot}40$ so may be applicable to a range of configurations which would not normally be considered slender. A serious limitation is that the theory makes no prediction of any change in $\bar{\eta}_Z$ with increase in Mach number and so, as would be expected, will be progressively less reliable at higher Mach numbers.

(*b*) *Nielsen's method.* In Ref. 2 Nielsen has given a method of predicting the induced download from the product of the lift-curve slope and the average downwash angle at the wing leading edge, suitably weighted by the local chord. The authors point out that the method may be considerably in error for a vortex passing inboard of the tips of a rectangular wing although for a triangular wing it agrees with more exact theories. As Mach number increases, however, the root and tip regions are likely to be less significant and so the method may be expected to become increasingly reliable. This method only approximates to the boundary conditions over the wing and does not adequately allow for the presence of the body. The main objection to this treatment is that it implies no upper limit to the induced download on the wing which will increase indefinitely with wing chord. Since, however, generalised charts are given in Ref. 2 the method is relatively easy and quick to apply. As can be seen from the estimate given in Fig. 7 it is tolerably accurate and at higher Mach numbers is probably of sufficient accuracy particularly when the foreplane lift is only a small percentage of the whole.

(*c*) *Influence-coefficient method.* This method is described by Alden and Schindel in Ref. 4 and is likely to be the most exact. Once again, however, the method does not completely satisfy the boundary conditions on the wing-body combination, and in this report the influence coefficients $F(t)$ have been evaluated for the gross wing, and the velocity distribution taken to be that due to two line vortices together with their associated images in the body, and the integration $\int F(t)\, w(t)\, dt$ made over the region of the net wing, where

$F(t)$	Influence coefficient
t	Spanwise station
$w(t)$	Vertical velocity at station due to the vortices and their images.

It will be seen that estimates of $\bar{\eta}_Z$ given by this method show reasonable agreement at the higher incidences.

There is a limitation in all three methods at low incidence in that no allowance is made for the interaction of the vortex and the boundary layer. A further limitation is that there is no account taken of any spanwise or vertical movement of the vortices as they pass across the wing (a feature which

has been demonstrated subsonically[5]) which could lead to a change in the chordwise loading. This latter feature is at present under investigation by pressure plotting tests at R.A.E. The position of the vortices in time and space is again not known for a real configuration in flight and thus the dynamic stability characteristics cannot be predicted because of possible lags in time of the paths of the various body and fore-plane vortices.

If consideration is now given to the estimates for $\bar{\eta}_M$ it will be seen (Fig. 7b) that the theories tend to overestimate the value of $\bar{\eta}_M$. Since there is reasonable agreement on $\bar{\eta}_Z$ this implies that the induced loading acts further forward than predicted by theory. Both strip theory and the influence-coefficient method predict the load near the centre of pressure of the net wing and, as the experiment shows the loading much nearer the leading edge, Fig. 7c, it implies a variation of chordwise loading which as noted above could be partially explained by movement of the vortices as they pass over the surface, or for lower incidences by an interaction of the free vortex with the wing boundary layer. It is hoped that the results of pressure plotting tests will give further insight into this aspect of the results.

5.2. *Combined Incidence and Sideslip.* The tests at $M = 1{\cdot}40$ on the *BWF* and *BWCF* configurations showed little variation of either C_z or C_m with sideslip. The present tests at $M = 2{\cdot}47$ do show (Fig. 8) a small increase in $-C_z$ amounting to some 7 per cent at $\beta = 10$ deg but with no corresponding change in C_m vs. α thus indicating a forward shift in neutral point position. Further results for BCF' configuration shown in Fig. 9 suggest that this variation with sideslip may be due to the load carried on the body. This is consistent with the fact that the variation is most in evidence at the higher Mach number where the contribution of the body to the overall forces is relatively greater.

6. *Discussion of Lateral Results.* It will be seen that there is a general similarity in the results at $M = 1{\cdot}40$ and $2{\cdot}02$, and certain trends with Mach number noted in Ref. 1 are generally confirmed by these present tests. The method of presentation is again similar to that of Ref. 1.

6.1. *Sideforce and Yawing Moment Results at Zero Incidence.* 6.1.1. *Foreplane off.* The $-C_y$ vs. β and C_n vs. β results for B are given in Fig. 10 together with those for BF'. The non-linearity in the BF' curves is predominantly a body effect as the derived fin curve ΔC_y vs. β [$\Delta C_y \equiv C_{y.BF'} - C_{y.B}$] is linear (not plotted) and is similar to that for [$C_{y.BCF,\eta=0} - C_{y.B}$], Fig. 11. The slopes $\partial(\Delta C_y)/\partial\beta$ and $\partial(\Delta C_n)/\partial\beta$ for the derived fin are plotted in Fig. 12 together with the estimated values. The low values obtained from the simple estimation method used in Ref. 1 (*viz.*, by assuming the fin to be effectively one half the surface produced by the reflecting of the exposed surface about the root chord), was attributed to omission of due allowance for the body upwash. The fin is now assumed to be an isolated surface extending through the body and an allowance is made using an influence-coefficient method (based on Ref. 4) for the body upwash acting over the exposed area. The method is seen to be in good agreement with the measured sideforce and yawing moment.

6.1.2. *Wing off.* It was reported in Ref. 1 that at $M = 1{\cdot}4$ there was an increase in $-\partial C_y/\partial\beta$ of about 30 per cent when the control was deflected 10 deg, however, the present tests at $M = 2{\cdot}47$ show only some 5 per cent increase (*see* Fig. 11). This compares with an estimate, using the theory of Ref. 1, of an increase of 15 per cent; the small increment being due to the reduction of control lift coefficient with increase in Mach number. The rolling moment increments, predicted by the

same theory, are greater than those measured. This would suggest, perhaps not surprisingly, that the simplified theory is inadequate in predicting the correct distribution of loading between the fin and the adjacent body section. It should however be noted that the changes occurring in the rolling moment due to foreplane interference with the fin are only about 25 per cent of the changes experienced when the wing is present (*see* Section 6.3.2.).

Some tests were made on configuration BC, $\eta = 10$ deg and these showed little difference in the C_y vs. β curve from that obtained for the body alone under conditions of pure sideslip (*see* Fig. 10).

6.1.3. *Complete configuration.* With the wing present the influence of the foreplane deflection, η, on the sideforce and yawing moments is still small (Fig. 10). In view of the small interaction with the wing absent (6.1.2) this is not surprising, although even where this is not so, *e.g.*, at $M = 1{\cdot}40^1$, the introduction of the wing largely nullifies the effect of the foreplane vortices on the fin effectiveness.

6.2. *Sideforce and Yawing Moment Results with Combined Incidence and Sideslip.* 6.2.1. *Wing off.* The principal source of interest in this section is the results for configuration BCF', $\eta = 0$ which are plotted against β for constant values of α in Fig. 13. A similar feature to that noted at $M = 1{\cdot}40^1$ is the change in $-\partial C_y/\partial\beta$ with increase of incidence, although the magnitude of the change, compared with the value at zero incidence, is proportionately less than that noted at $M = 1{\cdot}40$, the reductions are quite significant and the implications for a complete aircraft are noted in Section 6.2.2.

When the $\partial C_y/\partial\beta$ results at $M = 1{\cdot}40$ became available a simple strip theory was evolved in Ref. 1 to attempt to predict the changes. This method has again been used for the results in $M = 2{\cdot}47$ and the resulting curve plotted in Fig. 14 for comparison with the experimental data. Due to the simplifying assumption of the theory it was considered worthwhile to attempt a more precise estimate of the effect of the foreplane vortices on the fin characteristics in sideslip. The method was as follows, the gross fin (extended through the body) is considered as an isolated surface and the influence coefficients, based on Ref. 4, evaluated for this surface. The side velocity distribution $A(t)$ due to the trailing vortices was then evaluated together with $B(t)$, due to the two image vortices taken to simulate correct boundary conditions on the body. The product $F(t)(A+B)(t)$ was then integrated over the area of the net fin. This did not give very good agreement with experiment partly because the image vortex is located near a free edge and does not correctly simulate the loading. The velocity field due to the image vortices, $B(t)$, was therefore omitted and the integration $\int F(t)A(t)\,dt$ made over the net fin. This gave an underestimate and it was suggested that by integrating over the area of the gross fin a more representative result would be obtained, since it would make some allowance for load on the body. Reference to Fig. 14, where the results of similar computations at $M = 1{\cdot}40$ are included, shows that this latter method does in fact give the best agreement with the experimental results. For consistency the vortex spacing used was that given by Ref. 2. In practice, due to the presence of the body, the foreplane vortex spacing is likely to be increased above this value. In general this would give a reduction of the vortex effect on the fin loading and so is a possible source of error in the method of estimation.

Since the estimates all indicated changes in $\partial C_y/\partial\beta$ less than those measured experimentally it was thought that the foreplane vortices might have some effect on the fuselage loading. The configuration BC, $\eta = 0$ deg was therefore tested for a range of θ and ϕ and values of ΔC_y and ΔC_n evaluated for $(BC-B)$. The numerical differences are small and their significance is marginal but

there is enough evidence to suggest that there is a small effect of the foreplane vortices on the fuselage in such a way as to supplement the effect of the vortices on the fin.

An attempt was made to predict any effect of foreplane vortices on a fuselage by assuming a pair to stream back from the tips of the foreplane in a free stream direction, and to consider the magnitude of the lateral force due to the change in spacing between each vortex and the image in the body as the orientation of the vortex with respect to the body varied with both α and β. In this particular configuration the method showed only a very small effect of the vortices on the body.

6.2.2. *Complete configuration.* Comparison of the C_y vs. β curves of Figs. 13 and 15 for configurations BCF', $\eta = 0$ and $BWCF'$, $\eta = 0$ respectively show that the addition of the wing has little effect on these curves. This is contrary to the result at $M = 1{\cdot}40$ where it was noted that the addition of the wing led to a marked decrease in the effect of incidence on the C_y vs. β curve. This was attributed primarily to the 'cancellation' effect of the wing on the vortices passing over it by the production of vorticity (due to the induced download) of sign opposite to that of the foreplane vortices. It is difficult to apply this argument quantitatively due to uncertainties in predicting the form of the vorticity from the wing, but as the Mach number increases the induced download is reduced (as evidenced by the increased $\bar{\eta}_Z$, *see* Section 5.1.4), so any 'cancellation' effect might be expected to decrease with increase of Mach number.

It was also pointed out in Ref. 1 that the shock wave from the wing leading edge causes the vortex to move in such a way that at a given incidence it passes nearer the fin root than if no wing were present and this was shown (as a basis of simple strip theory) to give a reduction in the effect of the foreplane vortices on the C_y vs. β curves. As Mach number increases the downward movement of the vortices, at a given incidence, is reduced, hence the wing effect due to this cause is also reduced.

Another factor which is likely to become of increasing significance as Mach number increases is the direct effect of the wing flow field. Over the expansion surface there is likely to be a reduction of effective $\frac{1}{2}\rho V^2$, which means that, at a positive incidence, a fin in the top of the body will be acting in this region of lower energy air and so may experience a loss in effectiveness with increasing incidence. This latter effect from the wing is likely to oppose the two other alleviating factors of the wing on the fore-plane vortices at higher incidences and so at the higher Mach numbers it will be more difficult to predict the fin contribution to the directional stability.

If the corresponding C_n vs. β curves of Figs. 13 and 15 are examined it will be seen that for the complete configuration there is a greater effect of α (at low β) on the C_n vs. β curves and, with the moment references chosen, for $\alpha > 6$ deg the value of $\partial C_n/\partial\beta$ is less than zero indicating negative weather-cock stability.

From these results it will be seen that the difficulty of providing adequate directional stability on aircraft at high supersonic speeds is likely to be aggravated by the adoption of a canard design.

6.3. *Rolling Moment Results at Zero Incidence.* 6.3.1. *Wing off.* Configurations BCF', $\eta = 0$ and BF' were both tested, and at $\alpha = 0$ deg showed no significant difference in the C_l vs. β curves (Fig. 16). The derived fin contribution to the rolling moment will of course be equal to that of BF' since the body itself makes no direct contribution to C_l. The value of $\partial C_l/\partial\beta$ due to the derived fin has been obtained and has been plotted in Fig. 12 for comparison with an estimate based on the same influence-coefficient method used for ΔC_n and ΔC_y as given in 6.1.1. Whilst there is very satisfactory agreement between experiment and theory using this method for this particular

configuration there is still need for a quicker and simpler method of obtaining the fin-body interference effects.

Reference to Fig. 16 (or Fig. 11 for derived curves) indicates that the slope of C_l vs. β curve for BCF', $\eta = 10$ deg is approximately 25 per cent greater than that for BCF' $\eta = 0$ deg. This compares with an estimated change of 20 per cent by the method of Ref. 1. The C_l results thus show values greater than theory whilst the ΔC_y and ΔC_n results are less than theory. This apparent discrepancy may be due to some effect of loading on the body but no positive evidence is available to support this suggestion.

6.3.2. *Complete configuration.* The C_l vs. β results for $BWCF'$, $\eta = 0$ are plotted in Fig. 16 where it will be seen that the slope of the C_l vs. β curve is lower than that for BCF', $\eta = 0$. It is difficult to give any precise explanation of this feature but it is possible that the finite wing thickness may introduce an interference effect. As the magnitude of the change is small, however, and of relatively little significance, no effort has been given to finding an explanation.

The much more significant result, which is similar to that noted at $M = 1{\cdot}40$, is the effect of deflecting the foreplane with wings present. Fig. 16 indicates the magnitude of this change for $\eta = 10$ deg, which is perhaps even more clearly seen in Fig. 11 where the incremental value of C_l due to foreplane deflection is compared with the fin contribution to C_l. The induced load due to $\eta = 10$ deg produces a value of $\partial C_l/\partial\beta$ greater than that of the fin alone. In Ref. 1 a simple method of estimating this induced rolling moment was given assuming the induced download to move across the wing with sideslip to give:

$$\frac{\partial \Delta C_l}{\partial \beta} = -\Delta C_z(1-\bar{\eta}_Z)\frac{l_c}{b}$$

where

ΔC_z Lift on the foreplane due to $\eta = 10$ deg

$\bar{\eta}_Z$ Normal-force efficiency of the foreplane

l_c Moment arm from the foreplane centre of pressure to the effective centre of pressure of the induced download (*see* Fig. 7c).

It was pointed out that this simplified approach was not adequate since it gave too low a value of $\partial \Delta C_l/\partial\beta$. It was therefore concluded that there must also be a redistribution of loading to give the required induced rolling moment. The evidence from the results at $M = 2{\cdot}47$ gives added support to this as an estimate based on the simple formula above gives a value little over 50 per cent of that measured. A more refined approach is required and the method most readily available is that employing influence coefficients as detailed by Alden and Schindel in Ref. 4. Since at $\beta = 0$ the velocity distribution $w(t)$ will be symmetric above the centre-line there will be no net rolling moment and it was necessary to evaluate $dw(t)/d\beta$ to find $dC_l/d\beta$. As was pointed out in Section 5.1.4 the method is unlikely to give agreement with the experiment at zero or small incidences because of the interaction of the vortices with the boundary layer.

6.4. *Rolling Moment Results for Combined Incidence and Sideslip.* 6.4.1. *Wing off.* The principal results considered are for configuration BCF', $\eta = 0$. These results are plotted in Fig. 18 as curves of C_l vs. β at constant α with the corresponding curves of $\partial C_l/\partial\beta$ at $\beta \to 0$ deg given in Fig. 17. It can be seen that for small values of β there is only a small effect of α on C_l. The general trend is consistent with that noted at $M = 1{\cdot}40$[1] although the magnitude of the changes with α,

particularly for $\alpha > 6$ deg, are much smaller. Adopting a similar approach to that chosen in 6.2.1 for estimating the effect of the foreplane vortices on the fin contribution to $\partial C_y/\partial\beta$, but using the appropriate rolling moment influence coefficients, estimates have been made for the variation of the fin contribution to rolling moment in the presence of the foreplane vortices. These estimates are shown in Fig. 19 (together with those for $M = 1{\cdot}40$) and the experimental values plotted for comparison. The function $R(t)A(t)$ (where $A(t)$ is the side velocity distribution due to the foreplane vortices) was integrated over the area of the net fin and that of the gross fin. For $\partial C_y/\partial\beta$ it was noted that the latter method gave the better agreement with experiment, whereas for C_l it appears to be less satisfactory.

A third approach was also made which included the effect of the velocity field $B(t)$ of the image vortices in the body (included to satisfy the boundary conditions at the body surface). It was pointed out in 6.2.1 that the latter approach did not give very good agreement with experiment partly because the theory does not adequately deal with a vortex near a free edge. For the case of the rolling moment, however, this method appears to give best agreement with experiment (*see* Fig. 19) which might be expected since any effects near the root are relatively insignificant as compared with loadings near the tip in producing rolling moments. It is not possible at present to explain satisfactorily the marked decrease in effect of α on $\partial C_l/\partial\beta$ at $\alpha < 6$ deg at $M = 2{\cdot}47$ as compared with theory especially as agreement is reasonable at $M = 1{\cdot}40$.

6.4.2. *Complete configuration.* One of the most significant results noted in Ref. 1 was the rolling moment in sideslip due to the induced loading produced by the foreplane vortices. This same feature is still very evident at $M = 2{\cdot}47$ as indicated by the curves of $C_l$vs. β in Fig. 18 and the corresponding curves of $\partial C_l/\partial\beta$ vs. α in Fig. 17. Attention is drawn to the large increase in $-\partial C_l/\partial\beta$ with increase of α which amounts to some 150 per cent at $\alpha = 10$ deg compared with the value at $\alpha = 0$ deg.

The results for BCF, $\eta = 0$ deg show that little of this change in $\partial C_l/\partial\beta$ can be attributed to vortex-fin interference and must therefore be associated with the foreplane-wing combination. The wing itself will make some contribution to this at incidence but the contribution is difficult to assess. Gross interpolation on the computed curves of Ref. 6 indicates that for plan-form as used in these tests the wing contribution to $\partial C_l/\partial\beta$ will decrease with increase of Mach number. There is thus a large value of $\partial C_l/\partial\beta$ due to the induced loading on the wing from the foreplane vortices which as $\alpha = 10$ deg is of the same order as that due to the fin.

It should be pointed out that the increased values of $-\partial C_l/\partial\beta$ measured at incidence may have considerable significance on the lateral behaviour of the aircraft, particularly when taken in conjunction with the reduced values of $\partial C_n/\partial\beta$ at the higher Mach number, and it is recommended that calculations be made to determine the significance of these derivatives.

Time did not permit tests to be made on $BWCF'$, $\eta = 10$ deg for varying α and β, but the results at $\alpha = 0$ deg indicate that foreplane deflection is likely to increase $|\partial C_l/\partial\beta|$ still further as was demonstrated at $M = 1{\cdot}40$.

7. *Conclusions.* The main feature arising from the tests at $M = 2{\cdot}47$ are summarised below, together with some more general observations which arise from considering these results in conjunction with those reported in Ref. 1. Whilst these results may be typical for a canard layout care should be taken in generalising the results until further insight is gained into the mechanism of some of the phenomena observed. Altogether, configurations of the kind tested here present a

host of interference problems, which have never been experienced before in such complexity. It is thought that the more important effects have now been recognised and most of these could be identified in the present set of experiments. But a considerable effort would be needed if it were ever required to provide adequate methods for estimating the aerodynamic characteristics of such layouts in any given case, including their static and dynamic stability characteristics.

(1) At $M = 2{\cdot}47$, due to the download induced on the wing by the foreplane vortices, the lift effectiveness of the foreplane is approximately $0{\cdot}55$ at $\alpha = 0$ deg rising to over $0{\cdot}75$ at $\alpha = 10$ deg. These values are not greatly influenced by foreplane setting and are considerably higher than the values measured at $M = 1{\cdot}40$. They support the tentative conclusion advanced in Ref. 1 that foreplane lift effectiveness, $\bar{\eta}_Z$, increases with Mach number.

(2) Similar to the result noted at $M = 1{\cdot}40$ the effective centre of pressure of the induced download at $M = 2{\cdot}47$ is well ahead of that for the wing alone in uniform flow and is almost constant with incidence and foreplane setting. With the moment reference chosen the moment effectiveness is only slightly over $1{\cdot}0$ and hence is lower than that measured at $M = 1{\cdot}40$.

(3) The neutral point ($\partial C_m/\partial C_z$) position moves slightly aft ($0{\cdot}04\bar{c}$) with increase of incidence up to 12 deg. This movement with incidence is however less than half that noted at $M = 1{\cdot}40$. There is also a consistent rearward movement of the neutral point (at $\alpha = 0$ deg) with increasing Mach number, amounting to $0{\cdot}06\bar{c}$ from $M = 1{\cdot}40$ to $2{\cdot}47$.

(4) Sideslip causes no significant change in the variation of either normal force or pitching moment with incidence. This result is thus true throughout the supersonic speed range of the tests.

(5) The value of $\partial C_n/\partial\beta$ at $M = 2{\cdot}47$ shows the expected decrease with increase of Mach number and the estimate for the fin contribution, using an improved method, shows good agreement with experiment over the Mach number range tested.

(6) At $M = 2{\cdot}47$ for $BWCF'$, $\eta = 0$ deg there is a more marked decrease in $\partial C_n/\partial\beta$ with increase in α than noted at $M = 1{\cdot}40$ such that for $\alpha > 7$ deg there is (for the reference position chosen) a negative value of $\partial C_n/\partial\beta$. In contrast with the results at $M = 1{\cdot}40$ this decrease in $\partial C_n/\partial\beta$ is greater than that noted for configuration BCF', $\eta = 0$ deg. These results emphasise the difficulty of obtaining adequate static directional stability at the higher Mach numbers which is aggravated by the presence of the foreplane.

(7) The relatively large induced rolling moments arising from the foreplane-wing interference[1] are still present at $M = 2{\cdot}47$ and are of such a magnitude (when considered in relation to the low value of $\partial C_n/\partial\beta$) that careful consideration should be given to their possible effect on the lateral stability characteristics.

LIST OF SYMBOLS

The various configurations are denoted by the following letters used in combination.

B	Body
C	Foreplane control surface
F'	Modified fin (0·75 area of original net fin of Ref. 1)
W	Wing

If used as a subscript to a coefficient it denotes the force or moment on that particular configuration.

$Oxyz$	Right-hand system of axes fixed in the aircraft
$Ox_0y_0z_0$	Right-hand system of axes fixed in the tunnel with Ox_0 along the direction of the relative wind
$A(t)$	Side velocity distribution at the fin due to the trailing vortex
$B(t)$	Side velocity distribution at the fin due to the image of the trailing vortex
b	Gross span = 3·50 inches
c	Local chord
$\bar{\bar{c}}$	Aerodynamic mean chord $\int_{-b/2}^{b/2} \frac{c^2 dy}{S_w} = 2{\cdot}40$ in.
C_y	Side-force coefficient
$=$	$\frac{Y}{qS_w}$
C_z	Normal-force coefficient
$=$	$\frac{Z}{qS_w}$
C_l	Rolling-moment coefficient (measured about Ox)
$=$	$\frac{L}{qS_wb}$
C_m	Pitching-moment coefficient (measured about wing root leading edge)
$=$	$\frac{M}{qS_w\bar{\bar{c}}}$
C_n	Yawing-moment coefficient (measured about wing root leading edge)
$=$	$\frac{N}{qS_wb}$
$F(t)$	Normal-force influence coefficient

$\bar{h}_\alpha$		Centre of pressure position
	$=$	C_m/C_z
l		Distance from foreplane hinge line to fin centre of pressure
K		Circulation due to vortex
M		Mach number
$P(t)$		Pitching-moment influence coefficient
q		Kinetic pressure
	$=$	$\frac{1}{2}\rho V^2$
$R(t)$		Rolling-moment influence coefficient
$2s$		Foreplane vortex spacing
S_w		Gross wing area
S_F		Net fin area
t		Spanwise distance
V		Free-stream velocity
$w(t)$		Downwash velocity distribution across wing due to foreplane vortex
α		Incidence of wing, $\sin^{-1}$ (sin θ cos ϕ), in degrees
β		Sideslip of wing, $\sin^{-1}$ (sin θ sin ϕ), in degrees
θ		Polar incidence, angle between Ox and Ox_0
ϕ		Roll angle, between $OxZo$ and Oxz
η		Foreplane setting angle, angle between chord line of control and Oxy
λ		Taper ratio – tip chord ÷ root chord
$\bar{\eta}_M$		Foreplane moment efficiency (*see* Section 5.1.4)
$\bar{\eta}_Z$		Foreplane force efficiency (*see* Section 5.1.4)

REFERENCES

Ref. No.	*Author*	*Title, etc.*
1	P. E. Watts and L. J. Beecham	A wind tunnel investigation of the longitudinal and lateral aerodynamic characteristics of a canard aircraft model. Tests at $M = 1{\cdot}40$ and $M = 2{\cdot}02$. Part I of this R. & M.
2	W. C. Pitts, J. N. Neilsen and G. E. Kaattari	Lift and center of pressure of wing-body-tail combinations at subsonic, transonic and supersonic speeds. N.A.C.A. Report 1307. 1957.
3	A. H. Sacks	Vortex interference on slender airplanes. N.A.C.A. Tech. Note 3525. November, 1955.
4	H. L. Alden and L. H. Schindel	The lift, rolling moment and pitching moment on wings in non-uniform supersonic flow. *J. Ae. Sci.* Vol. 19. No. 1, p. 7. January, 1952.
5	J. P. Jones	The calculation of the paths of vortices from a system of vortex generators, and a comparison with experiment. A.R.C. C.P. 361. March, 1955.
6	W. L. Sherman and K. Margolis	Theoretical calculations of the effects of finite sideslip at supersonic speeds on the span loading and rolling moment for families of thin sweptback tapered wings at an angle of attack. N.A.C.A. Tech. Note 3046. November, 1953.

TABLE 1

Model details

Wing	
Plan-form	Cropped delta
Leading-edge sweep angle	30 deg
Section	Modified double wedge
Thickness/chord ratio	0·035
Leading edge and trailing edge included angle in streamwise direction	6 deg 41 min
Gross span b	3·50 in.
Root chord C_R	2·73 in.
Root chord at centre-line of body	2·87 in.
Tip chord C_T	1·86 in.
Taper ratio—gross wing λ_G	0·65
Taper ratio—net wing λ_N	0·68
Gross area	8·28 sq in.
Net area	6·89 sq in.
Aspect ratio—gross wing	1·48
Aspect ratio—net wing	1·31
Control	
Plan-form	Cropped delta
Leading edge sweep angle	20 deg
Section	Modified double wedge
Thickness/chord ratio	0·045
Leading edge and trailing edge included angle in streamwise direction	8 deg 35 min
Gross span	1·63 in.
Root chord at centre-line of body	0·88 in.
Tip chord	0·583 in.
Taper ratio—gross control	0·66
Taper ratio—net control	0·71
Gross area	1·19 sq in.
Net area	0·82 sq in.
Aspect ratio—gross control	2·24
Aspect ratio—net control	1·73
Fin	
Plan-form	Cropped delta
Section	Modified double wedge
Thickness/chord ratio	0·035
Leading edge and trailing edge included angle	6 deg 41 min
Height from centre-line of body	1·078 in.
Net height	0·828 in.
Root chord	1·00
Tip chord	0·699 in.
Net area	0·702 sq in.
Net taper ratio	0·70
Body	
Overall length	9·0 in.
Diameter	0·5 in.
Length/diameter ratio	18·0
Nose shape	Modified ogive
Nose fineness ratio	5·0:1

Moment reference position is at intersection of the centre-line and the line joining the wing root leading edges (4·77 in. behind nose tip).

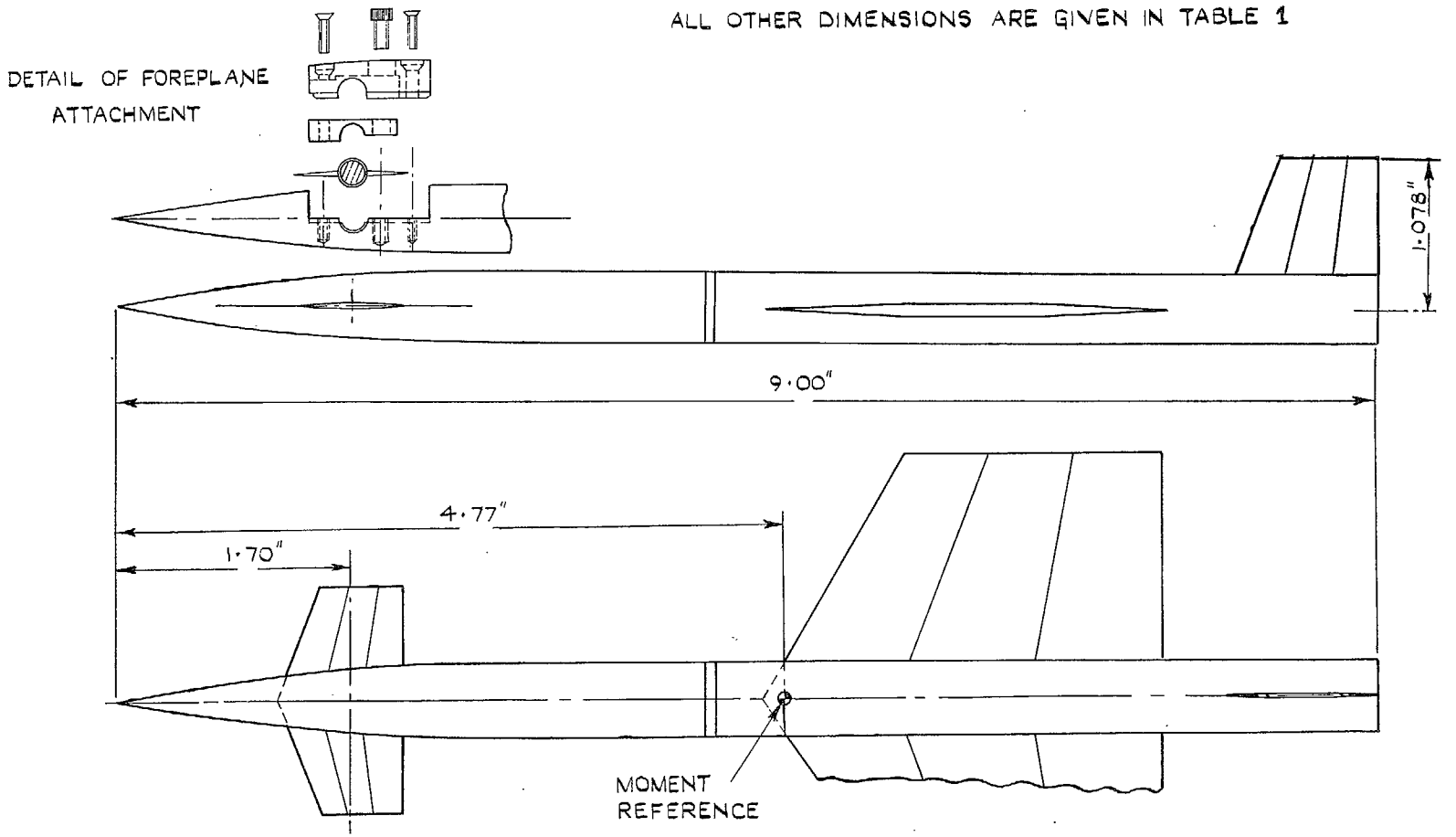

FIG. 1. Outline drawing of wind tunnel model.

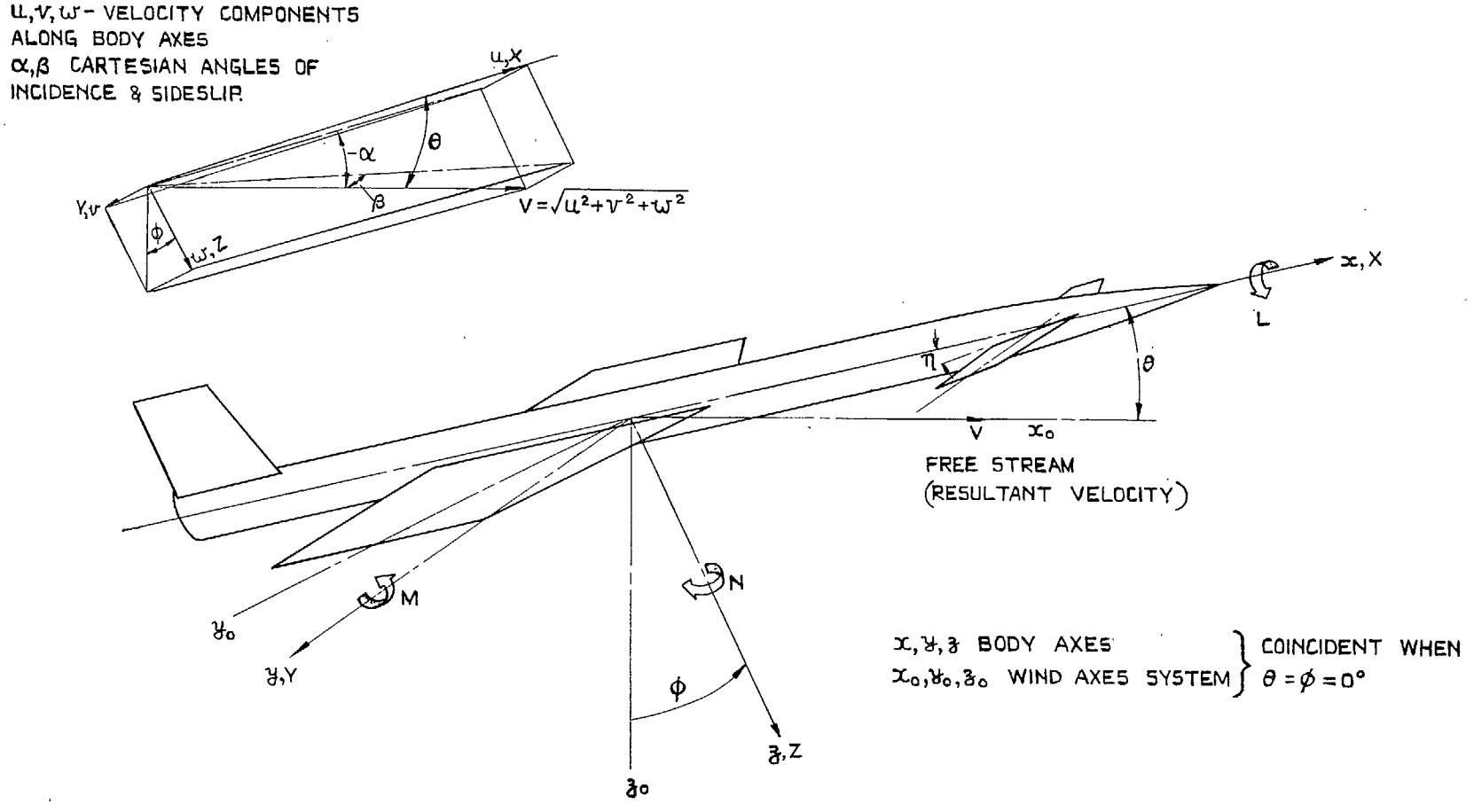

FIG. 2. Diagram showing body axes system.

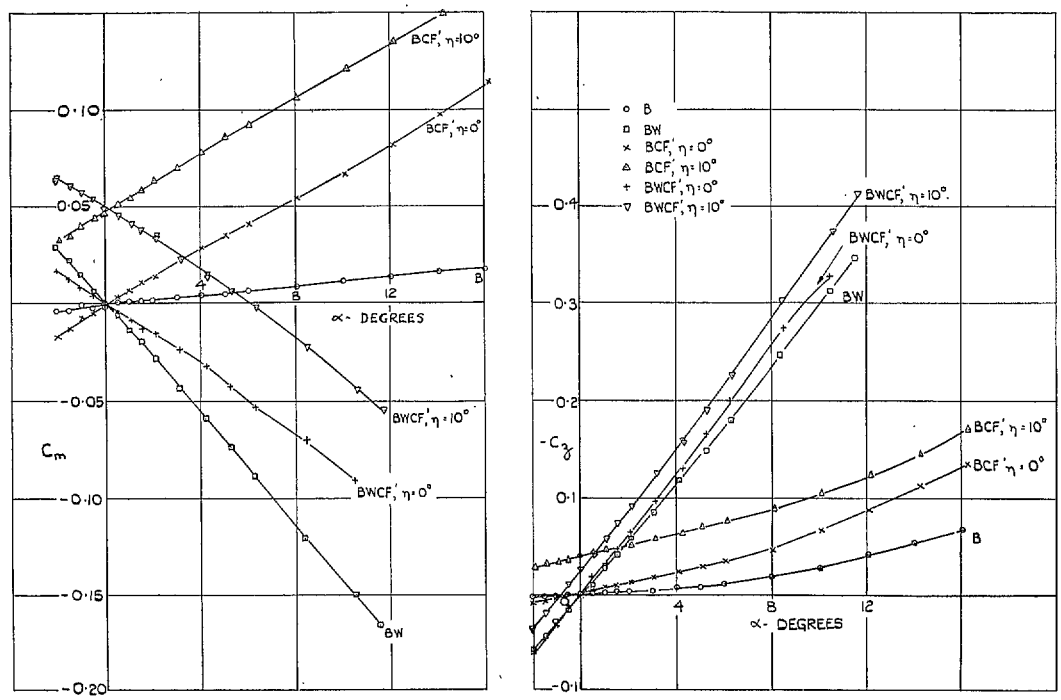

FIG. 3. Variation of C_m with α and $-C_z$ with α at $\beta = 0$ deg for various configurations at $M = 2{\cdot}47$.

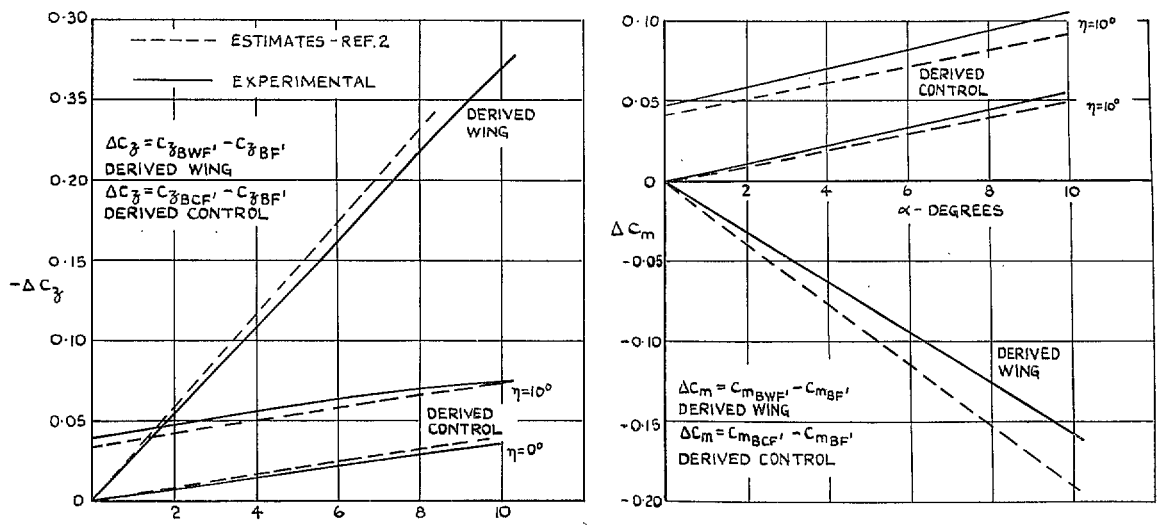

FIG. 4. Variation of $\Delta(-C_z)$ and ΔC_m vs. α for derived wing and derived control.

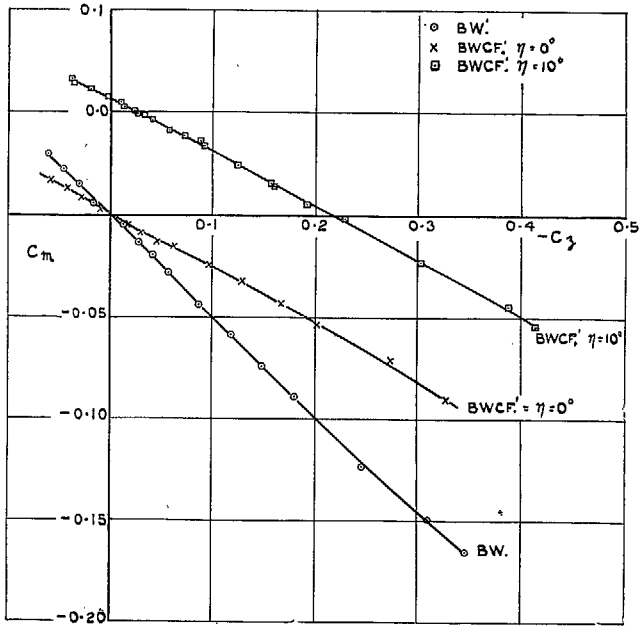

FIG. 5. Variation of C_m vs. $-C_z$ at $\beta = 0$ deg for configurations $BWCF'$, $\eta = 0$ deg, $BWCF'$, $\eta = 10$ deg and BW, at $M = 2{\cdot}47$.

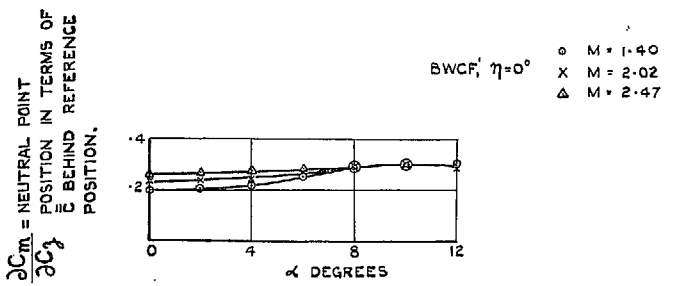

FIG. 6. Variation of $\partial C_m/\partial C_z$ vs. α for configuration $BWCF'$, $\eta = 0$ deg at $M = 1{\cdot}40$, $M = 2{\cdot}02$, and $M = 2{\cdot}47$.

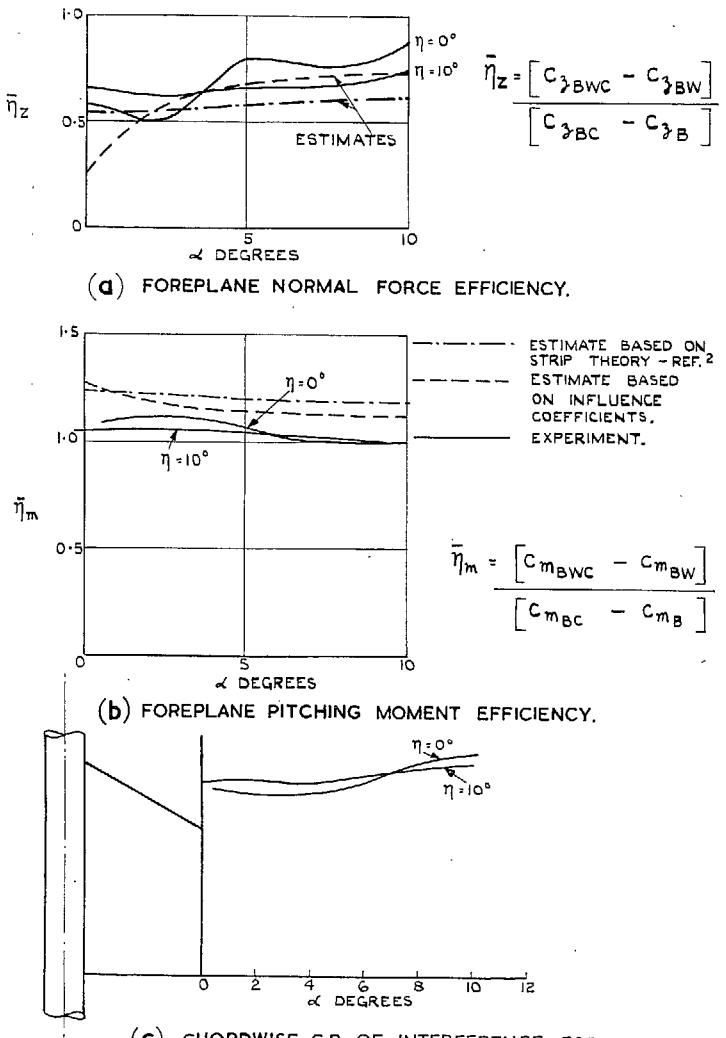

FIG. 7a to c. Interference effects between foreplane and wing at $M = 2{\cdot}47$.

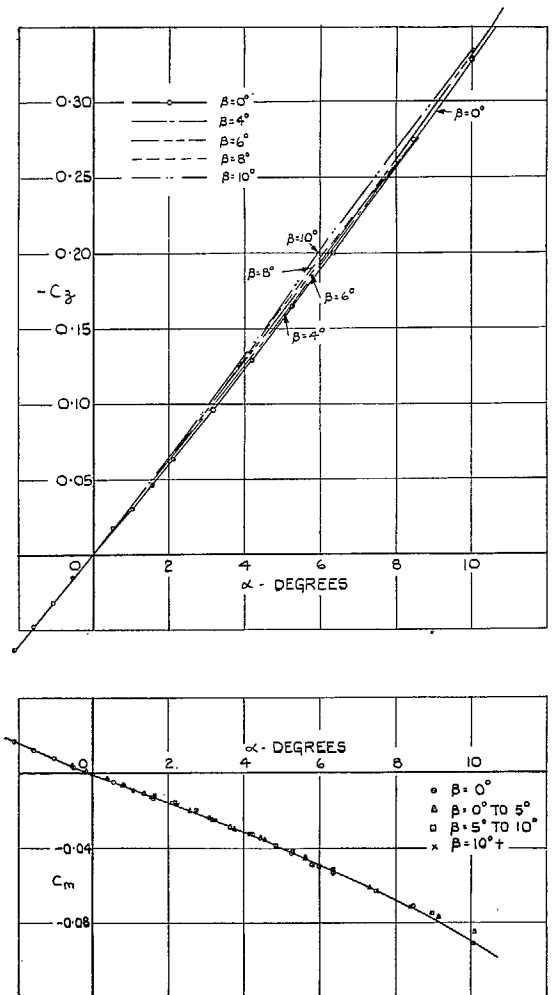

FIG. 8. Effect of β on $-C_z$ vs. α and C_m vs. α for configuration $BWCF'$, $\eta = 0$ deg at $M = 2{\cdot}47$.

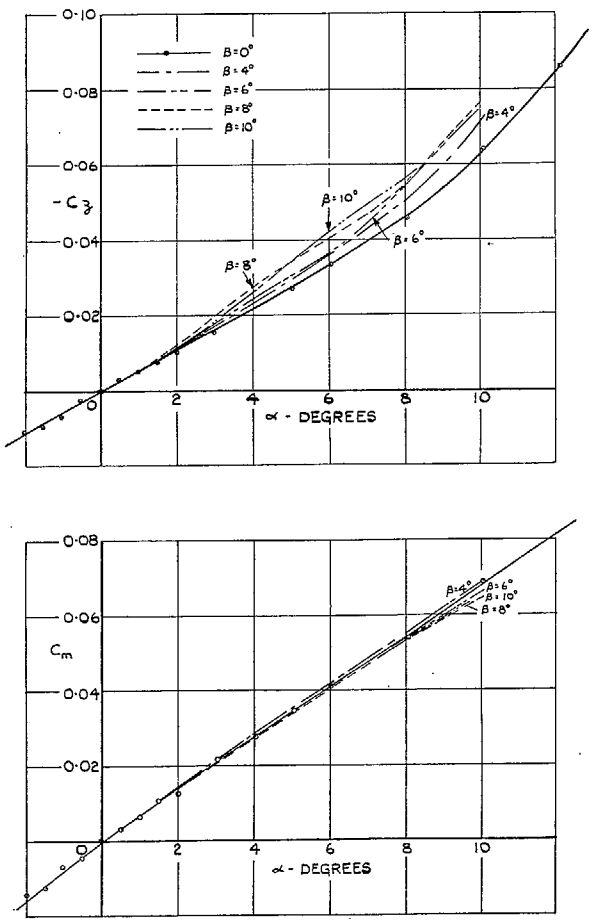

FIG. 9. Effect of β on $-C_z$ vs. α and C_m vs. α for configuration BCF', $\eta = 0$ deg at $M = 2{\cdot}47$.

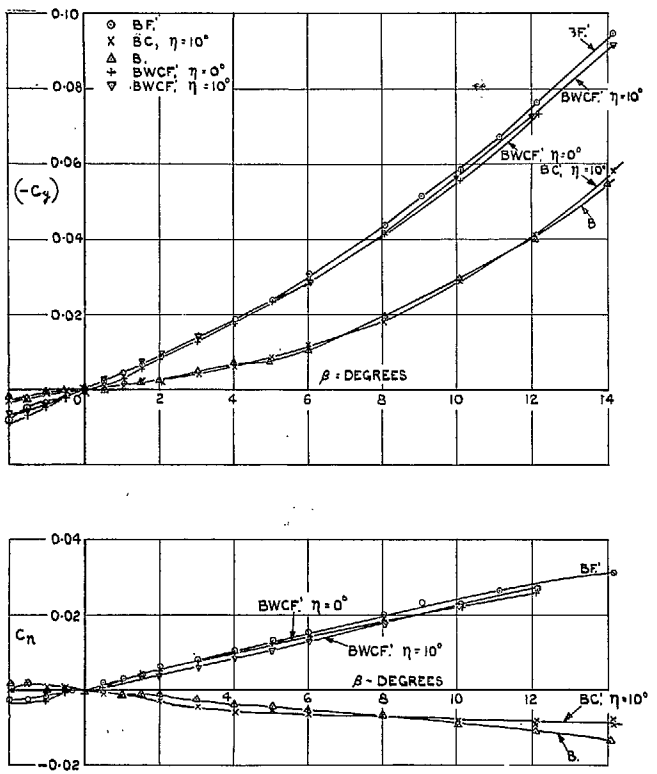

FIG. 10. Variation of $-C_y$ vs. β and C_n vs. β at $\alpha = 0$ deg for various configurations at $M = 2{\cdot}47$.

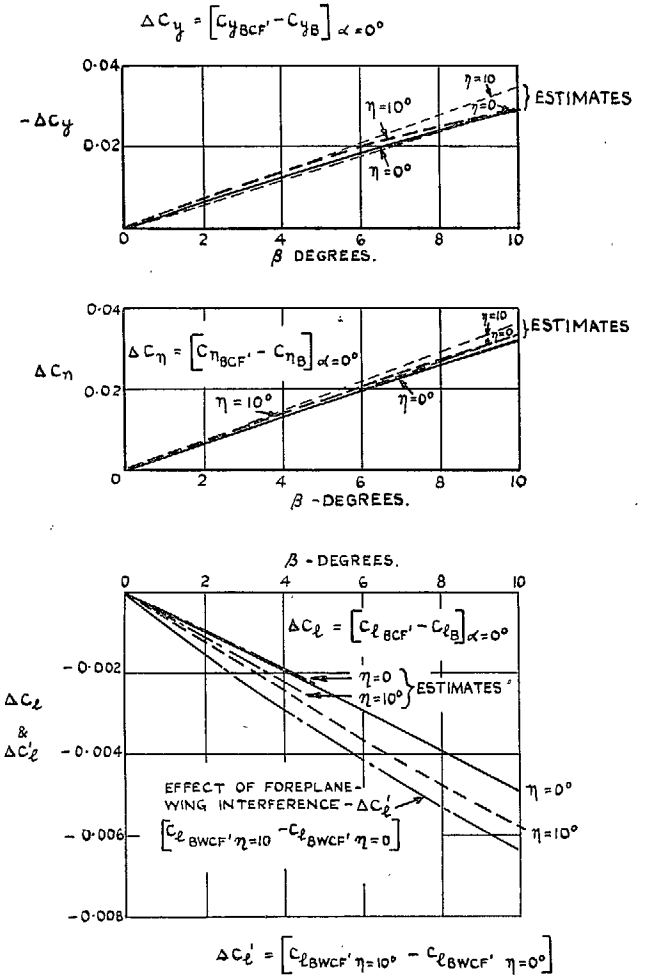

FIG. 11. Fin contribution to lateral forces and moments at $\alpha = 0$ deg for $M = 2{\cdot}47$.

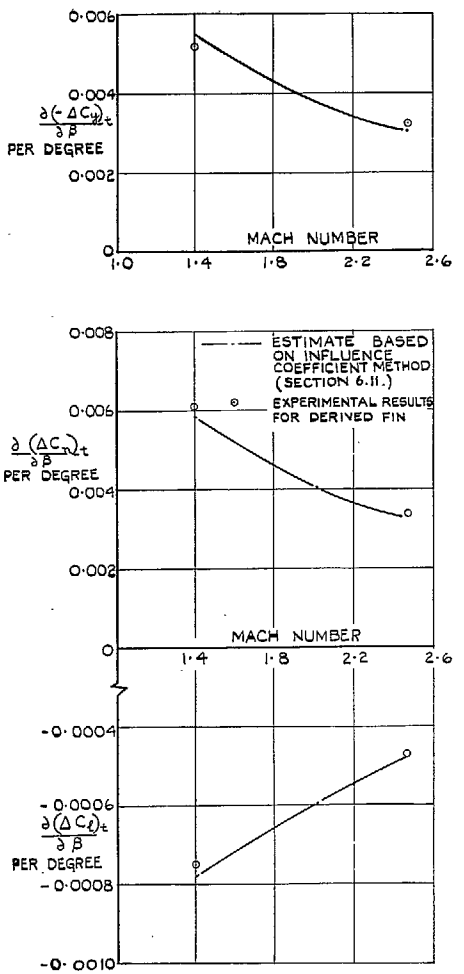

FIG. 12. Comparison of theory and experiment for fin contributions to sideslip derivatives at $\alpha = 0$ deg.

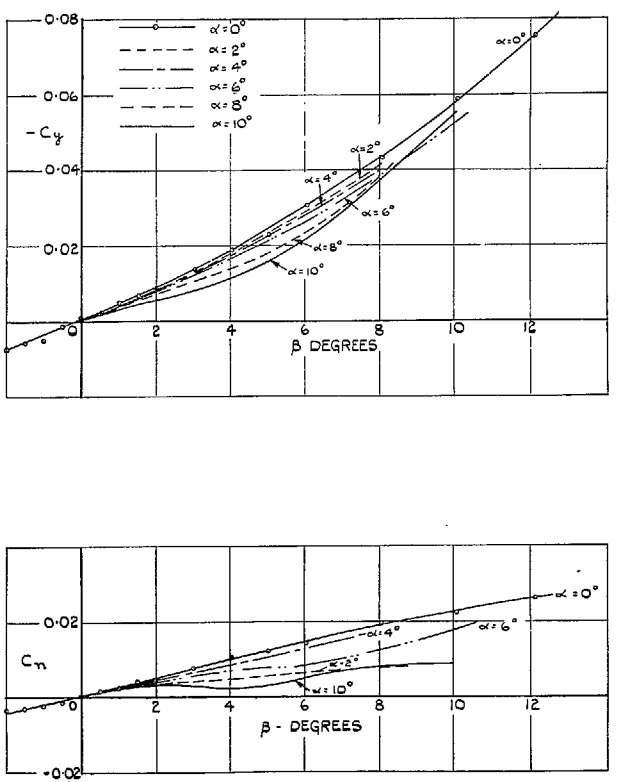

FIG. 13. Effect of α on $-C_y$ vs. β and C_n vs. β for configuration BCF', $\eta = 0$ deg at $M = 2{\cdot}47$.

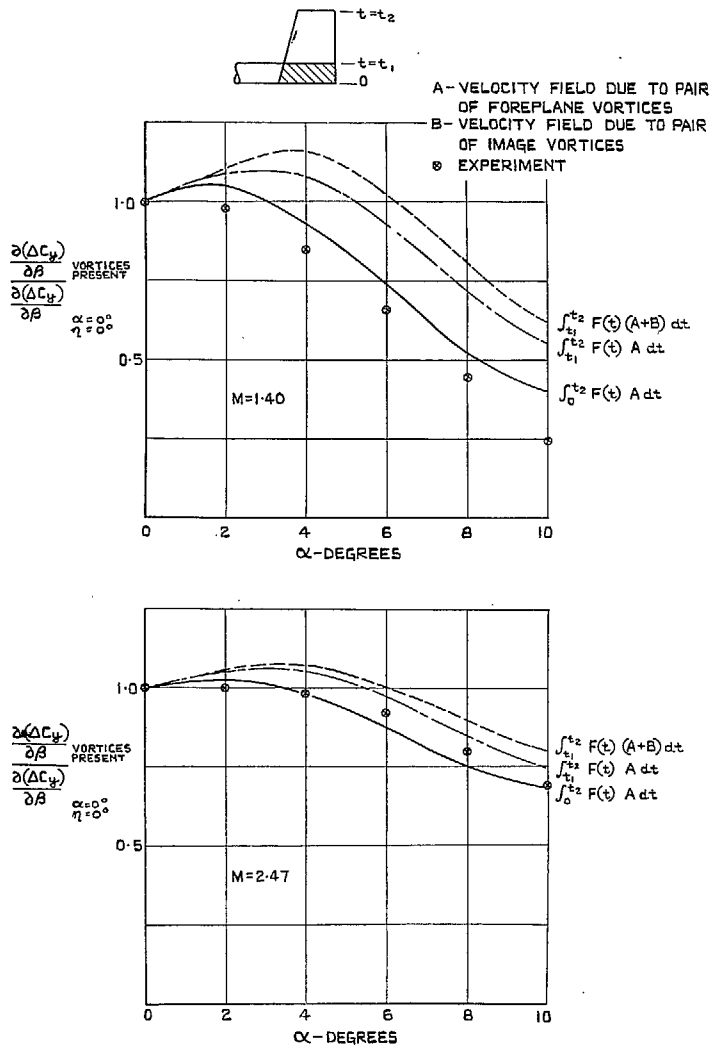

FIG. 14. Effect of foreplane vortices on derived fin contribution to $\partial C_y/\partial\beta$ for BCF', $\eta = 0$ deg.

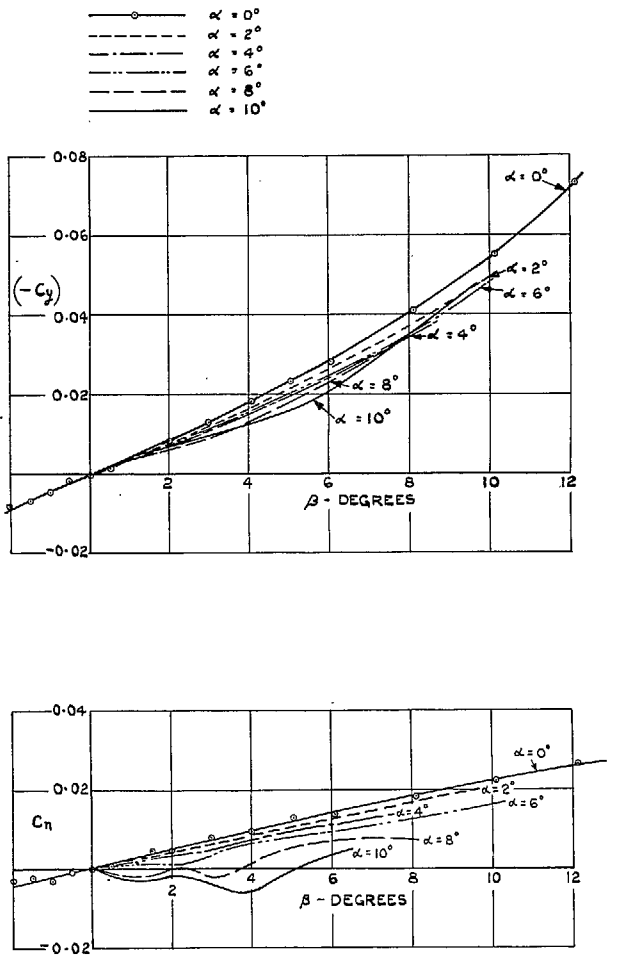

FIG. 15. Effect of α on $-C_y$ vs. β and C_n vs. β for configuration $BWCF'$, $\eta = 0$ deg at $M = 2{\cdot}47$.

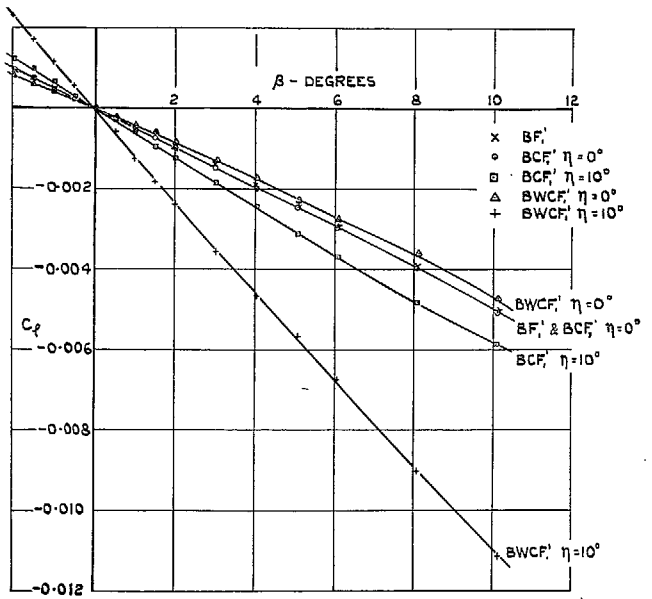

FIG. 16. C_l vs. β at $\alpha = 0$ deg for various configurations at $M = 2{\cdot}47$.

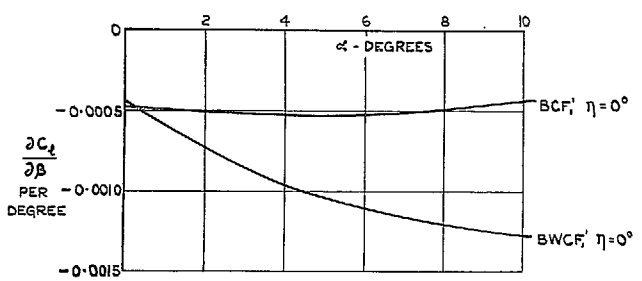

FIG. 17. $\partial C_l/\partial\beta$ vs. α for configurations $BWCF'$, $\eta = 0$ deg and BCF', $\eta = 0$ deg at $M = 2{\cdot}47$.

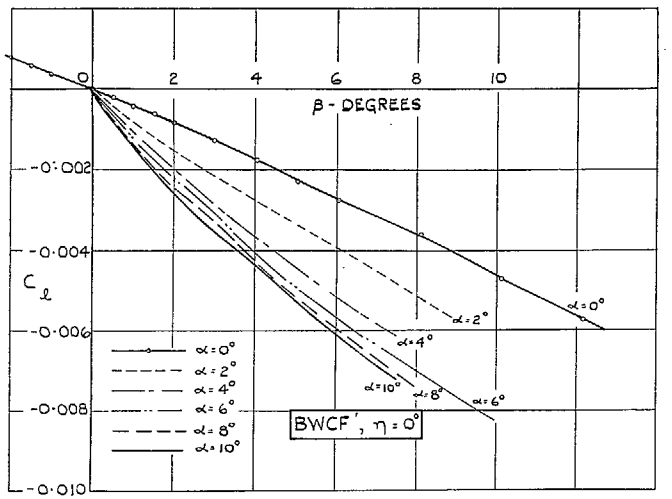

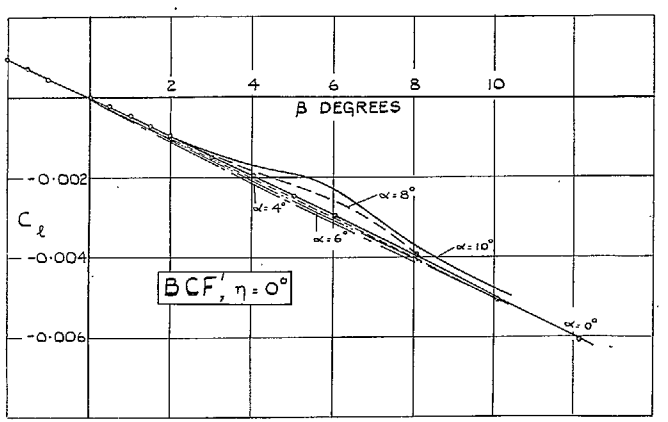

FIG. 18. C_l vs. β for various α for configurations $BWCF'$, $\eta = 0$ deg and BCF', $\eta = 0$ deg at $M = 2{\cdot}47$.

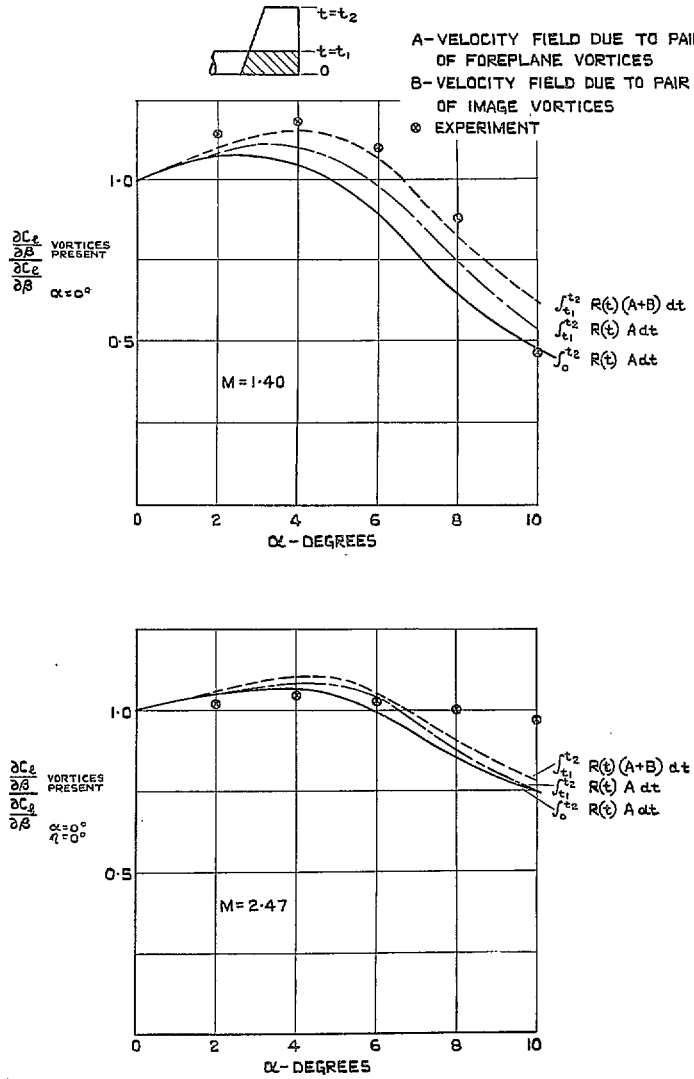

FIG. 19. Effect of foreplane vortices on fin contribution to $\partial C_l/\partial\beta$ for BCF', $\eta = 0$ deg.

(82849) Wt. 67/1876 K.5 3/62 Hw.

Publications of the Aeronautical Research Council

ANNUAL TECHNICAL REPORTS OF THE AERONAUTICAL RESEARCH COUNCIL (BOUND VOLUMES)

1941 Aero and Hydrodynamics, Aerofoils, Airscrews, Engines, Flutter, Stability and Control, Structures. 63*s.* (post 2*s.* 3*d.*)

1942 Vol. I. Aero and Hydrodynamics, Aerofoils, Airscrews, Engines. 75*s.* (post 2*s.* 3*d.*)
Vol. II. Noise, Parachutes, Stability and Control, Structures, Vibration, Wind Tunnels. 47*s.* 6*d.* (post 1*s.* 9*d.*)

1943 Vol. I. Aerodynamics, Aerofoils, Airscrews. 80*s.* (post 2*s.*)
Vol. II. Engines, Flutter, Materials, Parachutes, Performance, Stability and Control, Structures. 90*s.* (post 2*s.* 3*d.*)

1944 Vol. I. Aero and Hydrodynamics, Aerofoils, Aircraft, Airscrews, Controls. 84*s.* (post 2*s.* 6*d.*)
Vol. II. Flutter and Vibration, Materials, Miscellaneous, Navigation, Parachutes, Performance, Plates and Panels, Stability, Structures, Test Equipment, Wind Tunnels. 84*s.* (post 2*s.* 6*d.*)

1945 Vol. I. Aero and Hydrodynamics, Aerofoils. 130*s.* (post 3*s.*)
Vol. II. Aircraft, Airscrews, Controls. 130*s.* (post 3*s.*)
Vol. III. Flutter and Vibration, Instruments, Miscellaneous, Parachutes, Plates and Panels, Propulsion. 130*s.* (post 2*s.* 9*d.*)
Vol. IV. Stability, Structures, Wind Tunnels, Wind Tunnel Technique. 130*s.* (post 2*s.* 9*d.*)

1946 Vol. I. Accidents, Aerodynamics, Aerofoils and Hydrofoils. 168*s.* (post 3*s.* 3*d.*)
Vol. II. Airscrews, Cabin Cooling, Chemical Hazards, Controls, Flames, Flutter, Helicopters, Instruments and Instrumentation, Interference, Jets, Miscellaneous, Parachutes. 168s. (post 2*s.* 9*d.*)
Vol. III. Performance, Propulsion, Seaplanes, Stability, Structures, Wind Tunnels. 168*s.* (post 3*s.*)

1947 Vol. I. Aerodynamics, Aerofoils, Aircraft. 168*s.* (post 3*s.* 3*d.*)
Vol. II. Airscrews and Rotors, Controls, Flutter, Materials, Miscellaneous, Parachutes, Propulsion, Seaplanes, Stability, Structures, Take-off and Landing. 168*s.* (post 3*s.* 3*d.*)

Special Volumes

Vol. I. Aero and Hydrodynamics, Aerofoils, Controls, Flutter, Kites, Parachutes, Performance, Propulsion, Stability. 126*s.* (post 2*s.* 6*d.*)
Vol. II. Aero and Hydrodynamics, Aerofoils, Airscrews, Controls, Flutter, Materials, Miscellaneous, Parachutes, Propulsion, Stability, Structures. 147*s.* (post 2*s.* 6*d.*)
Vol. III. Aero and Hydrodynamics, Aerofoils, Airscrews, Controls, Flutter, Kites, Miscellaneous, Parachutes, Propulsion, Seaplanes, Stability, Structures, Test Equipment. 189*s.* (post 3*s.* 3*d.*)

Reviews of the Aeronautical Research Council

1939–48 3*s.* (post 5*d.*) 1949–54 5*s.* (post 5*d.*)

Index to all Reports and Memoranda published in the Annual Technical Reports

1909–1947 R. & M. 2600 6*s.* (post 2*d.*)

Indexes to the Reports and Memoranda of the Aeronautical Research Council

Between Nos. 2351–2449	R. & M. No. 2450 2*s.* (post 2*d.*)
Between Nos. 2451–2549	R. & M. No. 2550 2*s.* 6*d.* (post 2*d.*)
Between Nos. 2551–2649	R. & M. No. 2650 2*s.* 6*d.* (post 2*d.*)
Between Nos. 2651–2749	R. & M. No. 2750 2*s.* 6*d.* (post 2*d.*)
Between Nos. 2751–2849	R. & M. No. 2850 2*s.* 6*d.* (post 2*d.*)
Between Nos. 2851–2949	R. & M. No. 2950 3*s.* (post 2*d.*)
Between Nos. 2951–3049	R. & M. No. 3050 3*s.* 6*d.* (post 2*d.*)

HER MAJESTY'S STATIONERY OFFICE

from the addresses overleaf

Printed and published by
HER MAJESTY'S STATIONERY OFFICE

To be purchased from
York House, Kingsway, London W.C.2
423 Oxford Street, London W.1
13A Castle Street, Edinburgh 2
109 St. Mary Street, Cardiff
39 King Street, Manchester 2
50 Fairfax Street, Bristol 1
35 Smallbrook, Ringway, Birmingham 5
80 Chichester Street, Belfast 1
or through any bookseller

Printed in England

S.O. Code No. 23-3226